7. PUBLICATIONS & MANUSCRIPTS

7.1. Limited Proteolysis-Coupled Mass Spectrometry Identifies Phosphatidylinositol 4,5 Bisphosphate Effectors in Human Nuclear Proteome

Martin Sztacho, Barbora Šalovská, Jakub Červenka, Can Balaban, Peter Hoboth and Pavel Hozák

Cells. 2021, 10(1), 68; doi:10.3390/cells10010068

IF: 7.666 (2021)

C.B. prepared the nuclear fractions for the PIP2 pull-down assays and revised the manuscript.

cells

Article

Limited Proteolysis-Coupled Mass Spectrometry Identifies Phosphatidylinositol 4,5-Bisphosphate Effectors in Human Nuclear Proteome

Martin Sztacho [1,†], Barbora Šalovská [2,†], Jakub Červenka [3], Can Balaban [1], Peter Hoboth [1] and Pavel Hozák [1,4,5,*]

[1] Department of Biology of the Cell Nucleus, Institute of Molecular Genetics of the Czech Academy of Sciences, Vídeňská 1083, 142 20 Prague, Czech Republic; martin.sztacho@img.cas.cz (M.S.); can.balaban@img.cas.cz (C.B.); peter.hoboth@img.cas.cz (P.H.)
[2] Laboratory of Genome Integrity, Institute of Molecular Genetics of the Czech Academy of Sciences, Vídeňská 1083, 142 20 Prague, Czech Republic; barbora.salovska@img.cas.cz
[3] Laboratory of Applied Proteome Analyses, Institute of Animal Physiology and Genetics of the Czech Academy of Sciences, Rumburská 89, 277 21 Liběchov, Czech Republic; jakub.cervenka@natur.cuni.cz
[4] Microscopy Centre, Institute of Molecular Genetics of the Czech Academy of Sciences, Vídeňská 1083, 142 20 Prague, Czech Republic
[5] Division BIOCEV, Laboratory of Epigenetics of the Cell Nucleus, Institute of Molecular Genetics of the Czech Academy of Sciences, Průmyslová 595, 252 50 Vestec, Czech Republic
* Correspondence: hozak@img.cas.cz; Tel.: +420-296-442-219
† These authors contributed equally to this work.

Abstract: Specific nuclear sub-compartments that are regions of fundamental processes such as gene expression or DNA repair, contain phosphoinositides (PIPs). PIPs thus potentially represent signals for the localization of specific proteins into different nuclear functional domains. We performed limited proteolysis followed by label-free quantitative mass spectrometry and identified nuclear protein effectors of the most abundant PIP—phosphatidylinositol 4,5-bisphosphate (PIP2). We identified 515 proteins with PIP2-binding capacity of which 191 'exposed' proteins represent a direct PIP2 interactors and 324 'hidden' proteins, where PIP2 binding was increased upon trypsin treatment. Gene ontology analysis revealed that 'exposed' proteins are involved in the gene expression as regulators of Pol II, mRNA splicing, and cell cycle. They localize mainly to non-membrane bound organelles—nuclear speckles and nucleolus and are connected to the actin nucleoskeleton. 'Hidden' proteins are linked to the gene expression, RNA splicing and transport, cell cycle regulation, and response to heat or viral infection. These proteins localize to the nuclear envelope, nuclear pore complex, or chromatin. Bioinformatic analysis of peptides bound in both groups revealed that PIP2-binding motifs are in general hydrophilic. Our data provide an insight into the molecular mechanism of nuclear PIP2 protein interaction and advance the methodology applicable for further studies of PIPs or other protein ligands.

Keywords: nucleus; limited proteolysis; mass spectrometry; phosphoinositides; phosphatidylinositol 4,5-bisphosphate

Citation: Sztacho, M.; Šalovská, B.; Červenka, J.; Balaban, C.; Hoboth, P.; Hozák, P. Limited Proteolysis-Coupled Mass Spectrometry Identifies Phosphatidylinositol 4,5-Bisphosphate Effectors in Human Nuclear Proteome. *Cells* **2021**, *10*, 68.https://doi.org/10.3390/cells10010068

Received: 18 November 2020
Accepted: 29 December 2020
Published: 4 January 2021

1. Introduction

The maintenance of genome stability, genome expression, and its inheritance are amongst the main functions of the eukaryotic nucleus. In order to fulfil these functions, the nucleus shows unique, functionally compartmentalized architecture [1]. Nuclear phosphatidylinositol phosphates (PIPs) contribute to the spatial compartmentalization of the nucleus [2–4]. PIPs are known regulators of various processes such as membrane architecture and cytoskeletal dynamics, vesicular trafficking, signal transduction, or bone resorption [5,6]. The most abundant phosphatidylinositol 4,5-bisphosphate (PIP2) localizes

in the distinct nuclear sub-compartments—nuclear speckles, nucleoli, and nucleoplasmic foci—nuclear lipid islets [2]. In a study of Lewis and co-workers, more than 300 PIP2-interacting proteins involved in chromatin remodeling or RNA processing were identified [7]. PIP2 is also involved in both RNA polymerase I and RNA polymerase II mediated transcription [2,8]. Several nuclear proteins which are linked to the regulation of RNA transcription and mRNA processing have direct PIP2-binding capacity [4,9]. Various limited proteolysis followed by quantitative mass spectrometry (LiP-qMS) approaches have been successfully used for the determination of tertiary structure or conformational changes of proteins [10,11]. The LiP experimental approach uses the effect of ligand in the sample containing the ligand binding proteins. The addition of the ligand into the reaction causes binding of interactors and masks protein binding sites or induces conformational change that affects the accessibility of protease cleavage sites. Nuclear proteins rarely contain the canonical PIPs-binding domains, such as PH, FYVE, or PX domains. Instead, polybasic stretches containing lysine and arginine amino acid residues (K/R motifs) mediate the PIP2 binding [7]. Here we used LiP-qMS to identify the nuclear proteins, which directly bind to PIP2. We took the advantage of the trypsin protease activity, which specifically cleaves the peptide bond at the C-terminus of lysine and arginine residues, and developed LiP-based experimental pipeline using covalently conjugated PIP2 agarose beads followed by qMS to identify the proteins that interact with PIP2. We refer to this experimental pipeline as Phosphoinositide phosphates-based Limited Proteolysis quantitative mass spectrometry (PIPsLiP-qMS). This novel two-step approach allowed us to identify PIP2-interactome of the nuclear proteome and provides data discriminating two different types of PIP2-binding regions. Our approach provides information about structural features of the PIP2–protein interaction on a nuclear proteome scale and a methodological pipeline for further evaluation of other nuclear PIPs interactors and thus determination of their possible functions.

2. Materials and Methods

2.1. Cell Culture, Antibodies, and Lipid-Conjugated Beads

HeLa cells were cultured in suspension in DMEM media supplemented with 10% fetal bovine serum in spinner flasks at 37 °C 10% CO_2 atmosphere for 5 days. Antibodies used in this study: anti-GAPDH (Abcam, Cambridge, UK, ab8245), anti-lamin A (Abcam, Cambridge, UK, ab8990), anti-CWC25 (Sigma-Aldrich, St. Louis, MO, USA, HPA062997), anti-MPRIP antibody (Sigma-Aldrich, St. Louis, MO, USA, HPA022901). IRDye® 800 CW Donkey anti-Rabbit IgG (LI-COR Biosciences, Lincoln, NE, USA, 926-32213), IRDye® 800 CW Donkey anti-Mouse IgG (LI-COR Biosciences, Lincoln, NE, USA, 926-32212), PIP2- conjugated agarose beads (Echelon Biosciences Inc., Salt Lake City, UT, USA, P-B045A-2), blocked control agarose beads (Echelon Biosciences Inc., Salt Lake City, UT, USA, P-B000).

2.2. Nuclear Lysate Preparation

One liter of HeLa suspension culture was spun at 1300 g at 4 °C for 15 min. Pellet was resuspended in 7 mL of B buffer (50 mM Hepes pH 7.4, 150 mM NaCl, 1 mM DTT) and subjected to Dounce homogenization (20 strokes). Cell nuclei were sedimented by 1800x *g* centrifugation at 4 °C for 5 min. Supernatant was collected as cytoplasmic fraction. Nuclear pellet was washed 4 times in 10 mL of B buffer. Clean nuclear pellet was sonicated in Soniprep 150 (MSE) bench top sonicator (1 s on, 1 s off for 30 cycles at power 10 amplitude microns). Sonicated lysate was spun down at 13,000 g at 4 °C for 15 min. Supernatant was collected as nuclear lysate. Protein concentration was determined by Pierce™ BCA Protein Assay (Thermo Fisher Scientific, Waltham, MA, USA, 23227) according to the manufacturer's protocol.

2.3. Trypsin Inhibition Assay

Five micrograms of bovine serum albumin (BSA; New England Biolabs, Ipswich, MA, USA, B9001S) were diluted in 19 µL of B buffer (50 mM Hepes pH 7.4, 150 mM NaCl, 1 mM

DTT). One microliter of trypsin (0.5 µg) (Promega, Madison, WI, USA, V5111) was added to the reaction and incubated at RT for one minute. After one-minute incubation, one microliter of protease inhibitor (cOmplete™, Roche, Basel, Switzerland, 05056489001) was added or reaction was boiled at 100 °C. Protein samples were immediately vortexed and incubated at 4 °C for 60 min to ensure the stability of the reaction.

2.4. PIPsLiP-qMS Experiment

Three liters of HeLa suspension culture were used for nuclear lysate preparation. One milliliter of nuclear lysate with protein concentration of 2.5 mg/mL was used per condition. Eighty microliters of washed PIP2-conjugated agarose beads or control beads respectively, were added into the respective reaction and incubated at 4 °C for 1 h rotating to allow PIP2–protein interaction. After this step, 0.5 µg of trypsin (Promega, Madison, WI, USA, V5111) was added (1:5000 trypsin:total protein ratio), mixed well, and incubated at RT for 1 min. After the incubation, we added 1.4 µL of broad spectrum protease inhibitors (cOmplete™, Roche, Basel, Switzerland, 05056489001) into the reaction, mixed well, and placed on ice. The control beads sample was centrifuged at 300x *g* at 4 °C for 2 min. Supernatant was transferred into a new tube and 80 µL of fresh PIP2-conjugated beads were added into the reaction and the sample was incubated rotating at 4 °C for 1 h. Finally, beads were spun down and washed twice in 1 mL of B buffer and subjected to sample preparation for qMS measurement. PIPsLiP was performed in three independent replicates.

2.5. Protein Digestion

Beads were resuspended in 100 mM triethylammonium bicarbonate (TEAB) containing 2% sodium deoxycholate (SDC). Proteins were eluted and cysteines were reduced in one step by heating with 10 mM final concentration of Tris-(2-carboxyethyl)phosphine (TCEP; 60 °C for 30 min). Beads were removed by centrifugation and proteins in the supernatant were incubated with 10 mM final concentration of methyl methanethiosulfonate (MMTS; 10 min RT) to modify reduced cysteine residues. In-solution digestion was performed with 1 µg of trypsin at 37 °C overnight. After digestion, the samples were centrifuged and supernatants were collected and acidified with TFA to 1% final concentration. SDC was removed by ethylacetate extraction [12]. Peptides were desalted using homemade stage tips packed with C18 disks (Empore) according to Rappsilber et al. [13].

2.6. Nano Scale Chromatographic Tandem Mass Spectrometry (nLC MS2) Analysis

Nano reversed phase column (EASY Spray column, 50 cm x 75 µm ID, PepMap C18, 2 µm particles, 100 Å pore size) was used for Liquid chromatography-tandem mass spectrometry (LC-MS/MS) analysis. The mobile phase buffer A was composed of water and 0.1% formic acid. The mobile phase B was composed of acetonitrile and 0.1% formic acid. The samples were loaded onto the trap column (Acclaim PepMap 300, C18, 5 µm, 300 Å Wide Pore, 300 µm x 5 mm, 5 Cartridges) at 15 µL/min for 4 min. The loading buffer was composed of water, 2% acetonitrile, and 0.1% trifluoroacetic acid. Peptides were eluted with the mobile phase B gradient from 4% to 35% B in 60 min. Eluting peptide cations were converted to gas phase ions by electrospray ionization and analyzed on a Thermo Orbitrap Fusion (Q OT qIT, Thermo Fisher Scientific, Waltham, MA, USA). Survey scans of peptide precursors from 350 to 1400 m/z were performed at 120 K resolution (at 200 m/z) with a 5×10^5 ion count target. Tandem MS was performed by isolation at 1.5 Th with the quadrupole, HCD fragmentation with normalized collision energy of 30, and rapid scan MS analysis in the ion trap. The MS/MS ion count target was set to 10^4, and the max injection time was 35 ms. Only those precursors with charge state 2–6 were sampled for MS/MS. The dynamic exclusion duration was set to 45 s with a 10 ppm tolerance around the selected precursor and its isotopes. Monoisotopic precursor selection was turned on. The instrument was run in top speed mode with 2 s cycles [14].

2.7. Raw Data Processing

Raw data files acquired by LC-MS/MS were processed with MaxQuant v1.6.11.0 [15]. Peak lists were searched against the human SwissProt database (May 2020) using Andromeda search engine [16]. Minimum peptide length was set to seven amino acids, and two missed cleavages were allowed. Dithiomethylation of cysteine was set as a fixed modification while oxidation of methionine and protein N-terminal acetylation were used as variable modifications. Only peptides and proteins with false discovery rate (FDR) lower than 0.01 were accepted. Protein intensities were normalized using MaxLFQ algorithm [17]. MaxQuant output data were further analyzed using Perseus v1.6.12.0 [18] and visualized in R v4.0.0 [19]. Briefly, protein groups identified at the 0.01 FDR level were further filtered to remove potential contaminants, decoys, and proteins identified based on modified peptides only. The resulting matrix was filtered based on the number of missing values (at least three valid values in at least one of the groups), and after log2 transformation, missing values were imputed from normal distribution (width = 0.3 times standard deviation (SD) and shift = 1.8 times SD of the original distribution).

2.8. Statistical Analysis

The samples were categorized in two groups—in the first group, LiP was performed in the presence of the PIP2-beads (to protect 'exposed'-PIP2-binding motifs; PIP2-LiP) while in the second group, LiP was performed in the presence of blank beads, and the supernatant was incubated with PIP2-beads (to reveal 'hidden' PIP2-binding motifs; LiP-PIP2). Student's *t*-test was performed with an additional fold-change cut-off ($p < 0.05$; fold change > 2) to compare differentially enriched proteins between these groups and to identify the most significant hits. Additional false discovery rate (FDR) correction for multiple hypothesis testing was performed (permutation-based FDR 0.05 or 0.1; Perseus v1.6.12.0) and reported in the supplementary files.

2.9. Gene Ontology Enrichment

Gene ontology annotation (gene ontology biological process and gene ontology cellular compartment, GOBP and GOCC, resp.) was performed in Perseus, and statistical significance of GOBP and GOCC terms enrichment in the 'exposed' and 'hidden' groups was evaluated by Fisher's exact test using all quantified proteins as a background reference set. The complementary GO search for mRNA processing and RNA splicing factors in 'exposed' protein group was done using thehttps://string-db.org/interface with interaction score set as "medium confidence (0.4)". For details please refer to STRING web page [20].

2.10. Peptide Hydrophobicity Analysis

All identified peptides were assigned a grand average of hydropathy (GRAVY) value (http://www.gravy-calculator.de/index.php). Peptide distributions corresponding to 'exposed' proteins, 'hidden' proteins, and the remaining proteins were visualized, and the difference between these groups was evaluated using Kruskal–Wallis test. Pairwise comparisons were performed using pairwise Wilcoxon test with Bonferroni correction.

2.11. Data Visualization

All plots were generated using R package 'ggplot2'. The *x*-axis in the volcano plot shows log2-transformed fold change between PIP2-LiP and LiP-PIP2 groups described above; the *y*-axis shows the negative decadic logarithm of the *t*-test *p*-value. In the bubble plots, the *x*-axis shows the proportion of proteins from a GO category from all proteins in the 'exposed' or 'hidden' group; *y*-axis shows the negative decadic logarithm of *p*-value estimated using Fisher's exact test. The size of the bubble corresponds to the number of proteins. In the boxplots, the bold line indicates the median value; box borders represent the 25th and 75th percentiles, and the whiskers represent the minimum and maximum value within 1.5 times of interquartile range. Outliers out of this range are depicted using solid dots.

2.12. Bioinformatic Analyses

Sequence retrieval—Canonical protein sequences were obtained from UniProtKB [21] (release 2020_06). Search for PIPs-binding domains—the PROSITE database [22] (release 2019_11) was used for selection of protein domains previously shown to bind to PIPs resulting in 11 protein domains selected: C2; N-terminal C2 (NT-C2); DOCK-homology region (DHR)-1 and -2; epsin NH2-terminal homology (ENTH); Fab1, YOTB/ZK632.12, Vac1 and EEA1 (FYVE); GRAM-like ubiquitin-binding in EAP45 (GLUE); pleckstrin homology (PH); phosphotyrosine interaction domain (PID); phox homology (PX); and Sprouty (SPR) domain. List of all human proteins containing these domains was retrieved from Swiss-Prot [20] using the PROSITE database and compared to the list of the most significant PIP2-interactors. Search for K/R motifs—ScanProsite tool [22] was employed for searches for K/R rich motifs: [KR]-x(3,7)-K-x-[KR]-[KR], [KR]-x(3,7)-K-x-[KR], and [KR]-x(3,7)-K-x-K with match mode set as greedy with no overlaps.

2.13. PIP2-Coated Beads Pull-Down and Western Blot

PIP2-coated or control agarose beads (20 µL slurry) were incubated with 1 mg of nuclear lysate for 1 h at 4 °C. Beads were washed 3 times with buffer (50 mM Hepes pH 7.4, 150 mM NaCl, 1 mM DTT) and subjected to western blot analysis. Proteins were loaded on a 4–20% polyacrylamide gel (Bio-Rad Laboratories, Hercules, CA, USA, 4561093), separated by SDS-PAGE, and transferred on a nitrocellulose membrane (BioTrace™, Menlo Park, CA, USA, 66485). Membranes were blocked with 3% BSA in PBS for 1 h and incubated with primary antibodies and with appropriate secondary antibodies conjugated to IRDye. The signal was detected by Odyssey Infrared Imaging System (LI-COR Biosciences, Lincoln, NE, USA).

3. Results

3.1. Rationale and Experimental Workflow of PIPsLiP-qMS Experiment

We developed a novel experimental workflow PIPsLiP-qMS in order to understand molecular processes with involvement of nuclear PIP2. Heat inactivation of trypsin is a necessary step in LiP-qMS. However, this treatment has denaturing effect on all proteins in the sample. Therefore, such approach is not suitable for experiments where additional steps demand proteins in a native conformation. In our experimental set-up, with non-denaturing conditions, we preserve proteins structural folds that are important for recognition and binding of PIP2. The PIP2 pull-down step decreases the complexity of the sample analyzed by qMS. The sample treatment by trypsin is done in the complete nuclear proteome. However, the analysis of only PIP2-bound protein fraction is ensured by pull-down of PIP2-conjugated beads. In order to block trypsin catalyzed cleavage with high efficacy, we used protease inhibitor mix (Roche; see Material Methods), which irreversibly and reversibly inhibits a broad spectrum of proteases. We tested the efficacy of this inhibitor mix to block trypsin cleavage and compared it to the efficacy of heat inactivation standardly used in LiP-MS experiments. We tested the efficacy of trypsin inhibition on BSA cleavage assay (Figure1A).

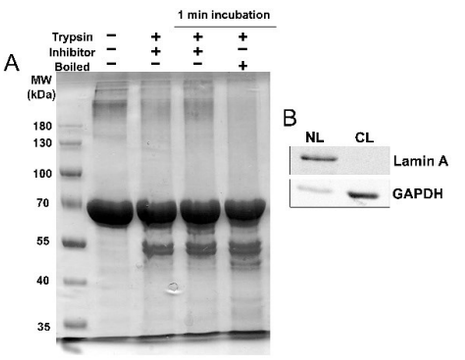

Figure 1. *Cont.*

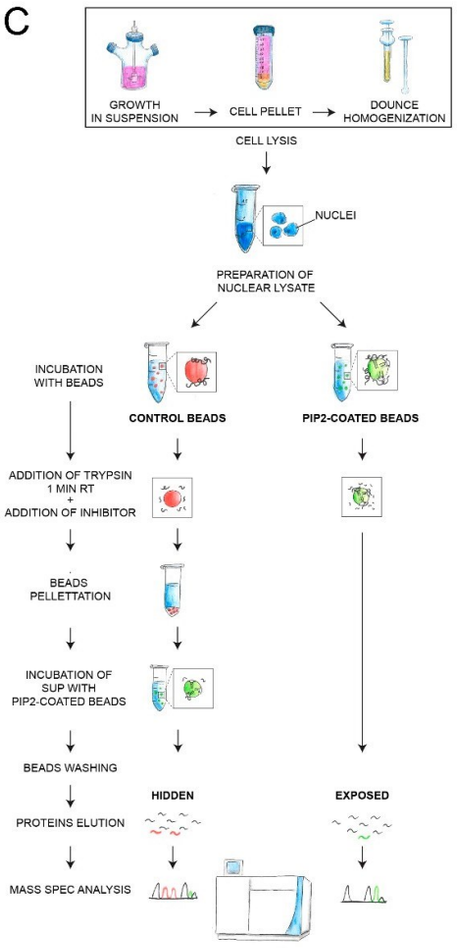

Figure 1. (**A**) Comparison of the trypsin cleavage block efficacy between inhibitor mix and heat inactivation. Bovine serum albumin (BSA) and its cleavage products were Coomassie Brilliant Blue-stained in polyacrylamide gel. First lane (from left) contains only BSA. In second lane, the inhibitors were added to the sample prior to trypsin digestion. Third lane contains a reaction where inhibitors were added after 1 min of trypsin incubation. In fourth lane, the sample was boiled after 1 min of trypsin incubation. All reactions were incubated at 4 °C for additional 1 h to ensure the stability of the trypsin inactivation. (**B**) Western blot (WB) analysis showing the purity of limited proteolysis (LiP) protein lysate starting material. NL—Nuclear lysate, CL—cytoplasmic lysate. WB shows immunodetected nuclear marker lamin A and the cytoplasmic marker GAPDH. (**C**) Scheme of the Phosphoinositide Phosphates based Limited Proteolysis quantitative Mass Spectrometry (PIPsLiP-qMS) experimental workflow. HeLa cells were grown in suspension into high densities followed by centrifugation and Dounce homogenization. The separation of nuclei from cytoplasm was done by centrifugation. Isolated nuclei were sonicated and lysates were prepared. Nuclear lysates were used as starting material in subsequent steps. Phosphatidylinositol 4,5-bisphosphate (PIP2)-coated beads or control beads were added into the nuclear lysate. The control beads served as free surface which might bind proteins non-specifically and thus protect them from trypsin cleavage. In the next step, trypsin was added into both reactions and then it was inhibited after 1 min of incubation at RT. Inactivation was done under non-denaturing conditions (inhibitors), therefore, PIP2-binding capacities of proteins remain persistent. Control beads were collected by centrifugation and discarded from the control sample. The supernatant was transferred into a clean tube and fresh PIP2-coveredbeads were added and incubated at 4 °C for 1 h. Capacity of proteins to bind PIP2 in this step should be diminished, since the binding sites were not protected by the ligand during LiP. Thus, lower amounts of these proteins will co-precipitate together with PIP2-covered beads. Washed PIP2-beads from both samples were collected; proteins were eluted and subjected to sample preparation for quantitative mass spectrometry analysis.

BSA cleavage assay revealed that BSA was partially cleaved by trypsin into fragments in all tested conditions. The cleavage occurred at the most accessible sites of BSA. The inhibitors were not able to protect all cleavage sites before reaching full inhibition of trypsin even when inhibitors were added prior to trypsin. Addition of inhibitors to the reaction prior to the addition of trypsin had similar cleavage patterns as the addition of inhibitors after 1 min incubation at RT. More cleavage products at lower molecular weights (approx. 45–60 kDa) and ~25–37 kDa appeared in reaction after heat inactivation, whereas these fragment were almost absent in both reactions with added inhibitors. Based on this, we suggest that the inhibitor mix blocks trypsin cleavage even more efficiently than the heat inactivation. The inhibition (both inhibitors and heat) was effective 1 h after the treatment, which is a necessary pre-condition for subsequent PIP2 pull-down. In the LiP-MS experiment, analysis of complex proteomes remains a challenging task. To overcome this hurdle, in PIPsLiP-qMS we used two steps to decrease the complexity of the analyzed samples. First, for the cell material fractionation, we employed an approach for cell nuclear lysate preparation. It is necessary for the subsequent qMS analysis to have highly concentrated starting material. Our protocol leads to the preparation of highly concentrated nuclear lysates with low cross-contamination. We confirmed the purity of our preparations by Western blot analysis of the nuclear and cytoplasmic markers, lamin A, and GAPDH, respectively (Figure1B). Second, the covalent ligand conjugation to the agarose beads enabled us to perform the pull-down after trypsin inactivation step (Figure1C) and thus further decrease the complexity of the samples analyzed by qMS.

3.2. The Identification of PIP2-Effectors in Nuclear Proteome by Label-Free qMS

The qMS-based comparison of the abundance of PIP2-bound proteins between both samples allowed us to identify individual proteins which were associated with PIP2-binding. Our PIPsLiP-qMS experimental approach identified 515 proteins of which PIP2 significantly changed their susceptibility to trypsin cleavage. Such changes might be due to direct PIP2-binding and thus masking cleavage site or indirect due to the conformational change which in turn exposes or hides trypsin recognition site. Therefore, these proteins can be divided into two groups. In the first group, the addition of PIP2 led to the protection of proteins from trypsin cleavage and thus their PIP2-coprecipitation was increased. This group includes direct interactors and also the proteins which do not have any PIP2-binding capacity, but their conformation is indirectly changed through interactions with components of the PIP2-binding protein complexes. We refer to this group of 191 proteins as ‘exposed’. In this set of proteins, PIP2 potentiates the formation of a complex or an indirect conformational change leading to cleavage protection by burying of trypsin cleavage sites. The second protein group, that we refer to as ‘hidden’, contains proteins that showed increased PIP2-binding upon trypsin treatment. The ‘hidden’ group includes 324 proteins in which trypsin cleavage promotes the PIP2-binding sites accessibility. We discriminated between ‘exposed’ and ‘hidden’ PIP2-interactors by further analyzing the significant PIP2-effectors in nuclear proteome and set the minimal change of protein abundance to 2-fold (Figure2and Supplementary Table S1).

Taken together, here we identified the nuclear PIP2-interacting proteins and proteins whose PIP2 interactions change their conformation. We further refer to the proteins from both groups as nuclear PIP2-effectors. We further aimed to identify processes in which these proteins participate and their sub-nuclear localization.

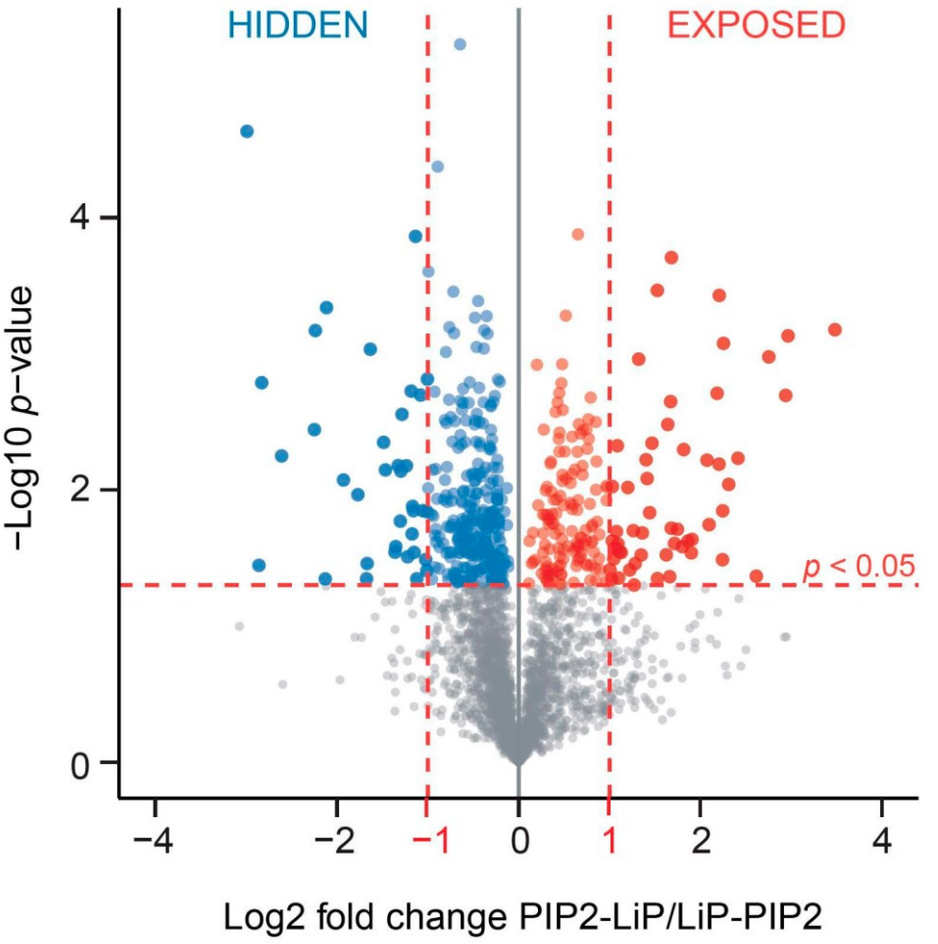

Figure 2. The PIP2-binding proteins differentially identified by PIPsLiP-qMS in HeLa nuclear proteome. LiP was performed in the presence of the PIP2-beads (to protect 'exposed' PIP2-binding motifs; PIP2-LiP) or in the presence of blank beads, and then the partially digested supernatant was incubated with PIP2-beads (to reveal 'hidden' PIP2-binding motifs; LiP-PIP2). Student's *t*-test was performed with an additional fold-change cut-off >2 (indicated by vertical red lines) to identify the most significant hits. The blue dots mark proteins enriched in LiP-PIP2 group, while red dots indicate proteins enriched in the PIP2-LiP group.

3.3. PIP2-Effectors in Human Nuclear Proteome Are Mainly Linked to Regulation of GeneExpression

Gene ontology (GO) over-representation analysis of 'exposed' and 'hidden' proteins provided insight into the function of PIP2 in the cell nucleus. In this analysis, we identified biological processes where 'exposed' and 'hidden' PIP2-effector proteins participate (Figure3A and Supplementary Table S2; GOBP).

Moreover, GO analysis provided us with the information about the localization of the processes into the various nuclear sub-compartments (Figure3B and Supplementary Table S2; GOCC). PIP2-effector localization overlaps with already known nuclear PIP2 pools—nuclear speckles, nucleoli, non-membrane bound organelles, and also cytoskeleton. The 'exposed' protein group is linked with regulation of polymerase II mediated transcription, mRNA processing, and actin organization, whereas 'hidden' group of proteins belongs to later stages of gene expression such as mRNA transport, RNA localization, or peripheral processes connected to the nuclear envelope or nuclear protein import. Therefore, 'exposed' and 'hidden' proteins have different sub-nuclear localizations, which suggests that 'exposed' and 'hidden' proteins participate in different nuclear processes.

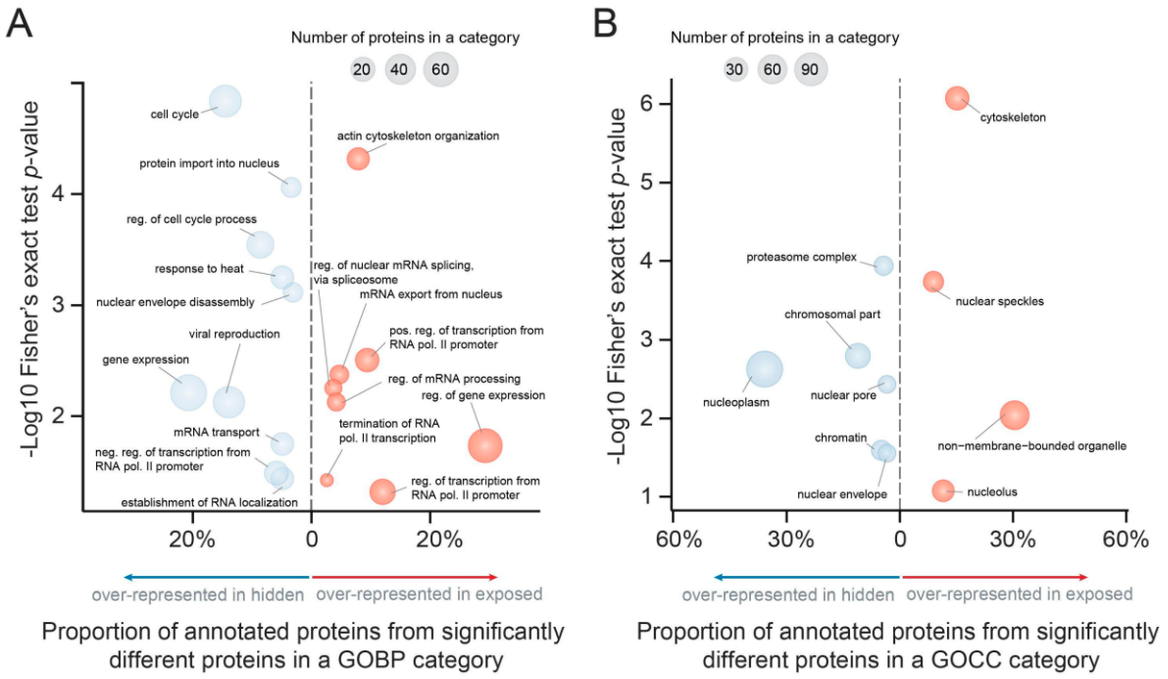

Figure 3. Gene ontology analysis of PIP2-effectors based on (**A**) biological process (GOBP) and (**B**) cellular compartment (GOCC). Bubble charts represent 'exposed' and 'hidden' proteins using all quantified proteins as a background reference set. *X*-axis shows the proportion of proteins from a gene ontology (GO) category from all proteins in the 'exposed' (red) or 'hidden' (blue) group. *Y*-axis shows the -log10 *p*-value estimated using Fisher's exact test. The size of the bubble corresponds to number of proteins.

3.4. PIP2-Binding Protects Hydrophilic Regions

Our GO analysis revealed functional and localization differences between proteins that belong to 'exposed' and 'hidden' PIP2-effectors. We further asked whether these differences are due to the variance in PIP2-binding region properties. Therefore, we performed a bioinformatic analysis of the hydropathy index of amino acid residues within peptides detected by PIPsLiP (Figure4).

This analysis revealed the difference in PIP2-binding effect on the protection of protein regions based on their hydropathy. First class of proteins showed higher degree of binding with exposed PIP2-binding regions. The peptides bound to PIP2-covered beads showed the highest hydrophilicity of their side chains. This suggests that these regions are not structural parts of hydrophobic cores of globular protein domains. On the contrary, the peptides belonging to the 'hidden' group showed lower hydrophilic properties than both 'exposed' and control protein groups. These data are in agreement with our hypothesis that 'hidden' regions are not primarily accessible to PIP2 ligand, but become accessible upon the conformational change. In summary, these data suggest that nuclear PIP2-associated effectors belong to at least two functional classes and that PIP2-binding regions are likely situated in the unstructured motifs. Importantly, the interacting motifs of 'exposed' proteins are hydrophilic, suggesting that they interact with phosphorylated head groups of PIP2 and not hydrophobic acyl group of this lipid. Therefore, we suggest that the differentially phosphorylated head groups of different PIPs represent an important signal for the functional localization of the interacting nuclear proteins.

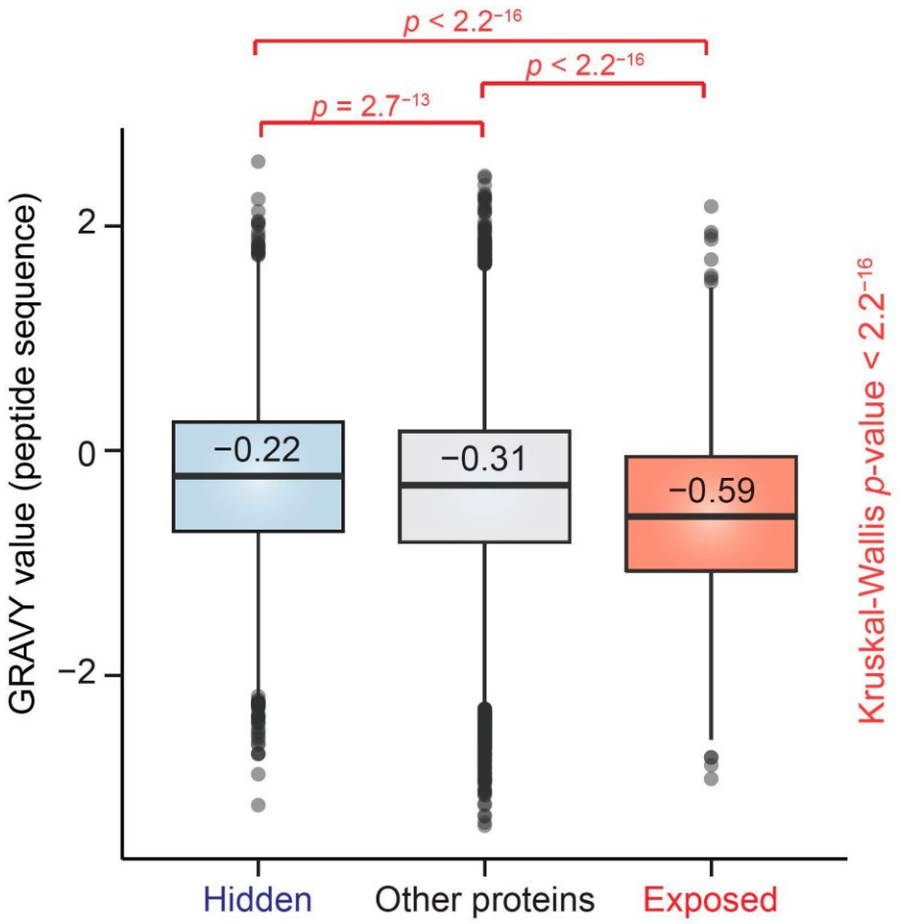

Figure 4. Hydropathy index distribution of peptides corresponding to 'exposed' and 'hidden' protein groups. GRAVY value distributions of identified peptides corresponding to 'exposed' proteins, 'hidden' proteins, and the remaining proteins from the data set ('Other proteins') are shown. The difference between these groups was evaluated using Kruskal–Wallis test. Pairwise comparisons were performed using pairwise Wilcoxon test with Bonferroni correction. The hydropathy values range from −2 to +2 for most proteins, with the positively rated proteins being more hydrophobic. The bold line and the number above the line indicate median values; box borders represent the 25th and 75th percentiles, and whiskers represent the minimum and maximum value within 1.5 times of interquartile range. Outliers out of this range are depicted using solid dots.

3.5. PIP2-Effector Proteins Contain Polybasic K/R Motifs

The majority of PIP2-associated nuclear effectors do not contain the canonical PIPs binding domains [7]. The PIPsLiP-qMS approach identified only two proteins with PIPs-binding PH domain amongst the most significant PIP2-interactors (Supplementary Table S3). The low incidence of canonical PIPs-binding domains in both 'exposed' and 'hidden' proteins is in agreement with previous observations and thus suggests that interactions between PIP2 and nuclear proteins are mediated by other regions [7]. We analyzed the abundances of polybasic K/R-rich motifs responsible for PIP2-binding. We searched for K/R motif K/R-x(3-7)-K-x-K/R-K/R and related K/R-x(3-7)-K-x-K/R and K/R-x(3-7)-K-x-K (see Section2.12. for details). Motif K/R-x(3-7)-K-x-K/R-K/R is present in 25% of 'exposed' and 24% of 'hidden' proteins. Motif K/R-x(3-7)-K-x-K/R is in 66% of 'exposed' and 57% of 'hidden' proteins. Motif K/R-x(3-7)-K-x-K is in 59% of 'exposed' and 41% of 'hidden' proteins (Supplementary Tables S4 and S5). Based on these results we assume that both, 'exposed' and 'hidden' proteins, might interact with PIP2 via these K/R motifs. Proteins without these motifs possibly have another unknown PIP2-binding motif or may interact with PIP2-binding protein complexes.

4. Discussion

PIPs are important functional regulators of mammalian nuclear processes [4]. PIPs are protein ligands with the ability to recruit and thus affect the localization, conformation, and activity of their protein effectors [4,9,23]. Therefore, it is of particular interest to identify the PIP2 nuclear effectors. Based on the PIP2-associated proteome, we can predict the molecular processes in which PIP2-effectors participate. Affinity purification in combination with MS analysis is, due to its simplicity, the method of choice for the identification of the effectors of any molecule. However, this method is often obstructed by constrains of high sample complexity, non-specific binding of proteins to bait or dynamic range of the sample, leading to relatively high degree of false positives [24]. The balance between the reduction of the protein complexity and enrichment of the target pool of proteins are the essentials for the protein extract preparation [7]. Our experimental PIPsLiP-qMS pipeline obviates the problems with dynamic range and specimen complexity, since trypsin cleavage in combination with cell fractionation and PIP2 pull-down reduce the antagonizing effect of the most abundant proteins within the sample for subsequent qMS analysis [24]. Integration of LiP with qMS provides a powerful tool to determine the boundaries of structured protein domain with an unprecedented accuracy [10]. However, the standard LiP-MS approach demands heat inactivation of the protease and therefore is not suitable for our subsequent affinity purification step, where proteins need to be in the native non-denatured state [25]. In our approach, we eliminated this obstacle by introducing protease inhibitors, which is important for the identification of the proteins in their native conformation.

In the study of Lewis and co-workers, the authors used the neomycin extraction which might not provide the entire range of PIPs-effector proteins [7]. Therefore, we developed an alternative experimental approach to expand these data and correlate both methods. The cross-correlation between results obtained by both approaches suggests that each approach leads to a different set of analyzed proteins (Supplementary Figure S1). However, the comparison of results from GO analysis provides a similar set of participating nuclear processes such as gene expression, RNA processing, and chromatin regulation [7]. This is in agreement with our previous findings that PIP2 regulates both Pol I and Pol II mediated transcription, epigenetic regulation and RNA processing [2,8,9,26]. We validated PIPsLiP-qMS approach by control pull-down experiments followed by WB detection of two chosen proteins MPRIP and CWC25 and showed that indeed both proteins have the binding capacity for PIP2 (Supplementary Figure S2). Furthermore, ~75% of identified proteins from the most significant hits are annotated as nuclear [20] or show nuclear signal detected by immunofluorescence at www.proteinatlas.org database [27,28] (Supplementary Table S6).

GO analysis of PIP2-effectors identified proteins linked to the nuclear speckles. Nuclear speckles are enriched in mRNA splicing factors and supply them to the active splicing sites [29,30]. Importantly, nuclear speckles are sites of highest PIP2 concentration in the cell nucleus [2]. Our present data support the notion of a regulatory axis between PIP2 and mRNA splicing regulation [31]. Furthermore, our PIPsLiP-qMS approach identified proteins associated with mRNA processing, mRNA splicing, and some proteins linked to PI-PLCβ1 interactome [31] (Supplementary Table S7 and Supplementary Figure S3). PI-PLCβ1 is a nuclear enzyme that catalyzes the cleavage of PIP2 and is a key factor which regulates splicing factor SRSF3 and skeletal muscle differentiation [31,32]. Therefore, we suggest that the PIP2 level at nuclear speckles regulates localization of splicing factors that bind PIP2 and thus their availability for the active splicing events [33]. In this model, PIP2 levels at nuclear speckles would represent an important determinant of the mRNA splicing rate in eukaryotic cell.

GO of PIP2-enriched 'exposed' proteins show significant increase of the regulators of Pol II transcription, gene expression, and RNA processing, whereas 'hidden' proteins belong to the nuclear pore complex and RNA export and therefore could regulate later stages of the gene expression. In agreement with this, our bioinformatics search from the GOCC database revealed proteins based on particular sub-cellular localization and indicated that 'hidden' proteins localize to the nuclear periphery. PIPsLiP-qMS provided data

which link 'exposed' PIP2-effectors and actin cytoskeleton. The growing body of evidence supports the key role of actin and cytoskeleton-related proteins in the establishment of nuclear architecture competent for gene expression [34,35]. Our laboratory identified first nuclear actin motor protein nuclear myosin 1 (NM1), which functions as Pol II transcription factor [36–38]. The importance of actin in the activity of Pol I and Pol II has also been documented [37,39]. Therefore, the presented PIPsLiP-qMS identification of the PIP2-effectors associated with actin cytoskeleton is in agreement with the previous studies that showed involvement of nucleoskeleton in the regulation of gene expression [37–41]. Moreover, the novel PIP2-binding actin- and cytoskeleton-related proteins identified here are interesting candidates for further studies.

GO analysis of PIP2-effectors further identified proteins linked to proteasome, heat response, and nucleoli localization. Heat shock induced protein aggregates or misfolded proteins are directed to nucleoli [42,43]. The degradation of protein aggregates is in general mediated by proteasomal or autophagy processes [44–46]. Ubiquitinated and heat shock proteins form aggresomes within the nucleolus [43,47] Proteins sensitive to heat shock denaturation, which are enriched for disordered regions, can be refolded within the nucleolus [42]. Nucleolar aggresomes contain proteins such as fibrillarin, ubiquitin, or autophagy factor LC3 [48,49]. In yeast, a starvation-mediated autophagy specifically removes some nucleolar factors [50]. Our PIPsLiP approach identified key regulator of autophagy serine-threonine kinase mammalian target of rapamycin (mTOR) as a PIP2-effector protein. mTOR localizes to nucleolus and is implicated in nucleolar processes such as RNA polymerase I and III -mediated transcription [51,52]. Moreover, the nucleolar protein nucleophosmin is involved in non-canonical autophagy when Pol I is inhibited [53]. PIP2 is a nucleolar factor affecting the activity of nucleolar proteins such as Pol I and fibrillarin [8,26]. When ubiquitin proteasome system is inhibited, the fibrillarin colocalizes in nucleolar aggregates with ubiquitin and LC3 [49]. The nucleolus thus represents a regulatory hub for protein quality control through ubiquitin proteasome system and autophagy signaling. Therefore, our data that identified nucleolar PIP2-interactors are in agreement with the previous notion of the nucleolar involvement in the regulation of autophagy.

GO analysis also identified viral infection response proteins. Viruses often hijack the transcription regulatory processes in order to replicate. In this regard, the recent work of Prof. Akgül laboratory represents the interesting connection of nuclear PIP2 levels increase upon HPV infection [54]. Our GO data presented here are in accordance with Akgül and coworkers, suggesting that PIP2-dependent nuclear pathway might represent promising candidate for regulation of viral infection surveillance. Therefore, the involvement of 'hidden' proteins in the later stages of gene expression and acting downstream of the 'exposed' group points to their effector role in the mRNA export, response to heat or viral replication. Furthermore, based on their localization, it seems that they act in different sites of the nucleus than 'exposed' group of proteins, indicating the mobility of PIP2-associated effectors from the sites of their primary action to other sub-nuclear compartments.

PIPsLiP-qMS data analysis further describes the hydropathy properties of regions responsible for the PIP2 interaction. Our hydropathy data show that PIP2-binding motifs are presumably situated in the regions with increased hydrophilicity. Our subsequent bioinformatics search found polybasic K/R motifs in a substantial portion of PIPsLiP-qMSidentified proteins.

In summary, we developed the PIPsLiP-qMS experimental pipeline which enabled the identification of nuclear PIP2-effectors. Data provided here determine the nuclear PIP2-effectors which uniquely belong to two protein groups representing regulators of such processes as gene expression, Pol II transcription, and mRNA splicing. These protein groups show different sub-nuclear locations of their actions. Further, we discovered that the PIP2-binding motifs are hydrophilic and thus presumably interact with inositol head group. The PIPsLiP-qMS thus represents a promising approach for identification of ligand–effector interactions and further determination of specific binding motifs. Standard affinity-based

MS approaches do not allow for the characterization of protein topography at the site of ligand-protein association. In contrast, the proteolytic cleavage which preferentially occurs at accessible, unstructured, and flexible regions of native proteins, allows for the discrimination and definition of these regions, since globular domains are typically resistant to proteolysis [11]. Therefore, PIPsLiP-qMS provides novel information about the topology, organization, and conformational changes of proteins associated with PIP2 binding. Moreover, the combination of other proteases may provide a better dissection of ligand binding sequences in future studies, e.g., non-specific proteinase K which would enable a more general view of the exposed regions. This experimental pipeline is theoretically applicable for any other ligand which is covalently linked to beads. Our high-throughput PIPsLiP-qMS approach provides a powerful, label-free tool to study protein–lipid interactions and to elucidate the molecular functions of nuclear PIPs and their effectors.

Supplementary Materials: The following files are available online athttps://www.mdpi.com/2073-4409/10/1/68/s1, Table S1: Summary of all protein groups identified in this study; Table S2: Selected results from the gene ontology overrepresentation analysis; Table S3: The PIP2-binding domain-containing proteins identified by bioinformatics analysis; Table S4: The summary of bioinformatics analysis of PIP2-binding motifs in 'exposed' protein group; Table S5: The summary of bioinformatics analysis of PIP2-binding motifs in 'hidden' protein group; Table S6: Summary of the most significant hits from the 'exposed' and 'hidden' proteins including the information about protein nuclear localization; Table S7: The list of proteins annotated in GOBP as mRNA splicing, mRNA processing factors, and protein linked to nuclear speckles; Figure S1: The Venn diagram representing the overlap of data provided by PIPsLiP-qMS with data presented in [7]; Figure S2: The verification of PIP2- binding capacity of MPRIP and CWC25; Figure S3: The Gene ontology analysis of 'Exposed' proteingroup using STRING.

Author Contributions: Conceptualization, M.S. and J.Č.; Data curation, M.S., B.Š. and J.Č.; Formal analysis, M.S., B.Š. and J.Č.; Funding acquisition, P.H. (Pavel Hozák); Investigation, M.S., B.Š. and P.H. (Pavel Hozák); Methodology, M.S., B.Š., J.Č., P.H. (Peter Hoboth), C.B. and P.H. (Pavel Hozák); Project administration, M.S. and P.H. (Pavel Hozák); Resources, P.H. (Pavel Hozák); Supervision, P.H. (Pavel Hozák); Validation, M.S., B.Š., J.Č., P.H. (Peter Hoboth), C.B. and P.H. (Pavel Hozák); Visualization, M.S., B.Š. and P.H. (Pavel Hozák); Writing—original draft, M.S., B.Š., J.Č., P.H. (Peter Hoboth) and P.H. (Pavel Hozák); Writing—review & editing, M.S., B.Š., J.Č., P.H. (Peter Hoboth), C.B. and P.H. (Pavel Hozák); All authors have read and agreed to the published version of the manuscript.

Funding: This work was funded by the Grant Agency of the Czech Republic (Grant Nos. 19-05608S and 18-19714S); by the Czech Academy of Sciences (Grant No. JSPS-20-06); by the Institutional Research Concept of the Institute of Molecular Genetics (Grant No. RVO: 68378050); by the MEYS CR (COST Inter-excellence internship LTC19048 and LTC20024) and the project: BIOCEV—Biotechnology and Biomedicine Centre of the Academy of Sciences and Charles University (CZ.1.05/1.1.00/02.0109), from the European Regional Development Fund. The Microscopy Centre was supported by the MEYS CR (LM2018129 Czech-BioImaging) and by the European Regional Development Fund-Project "Modernization and support of research activities of the national infrastructure for biological and medical imaging CzechBioImaging" (No. CZ.02.1.01/0.0/0.0/16_013/0001775). B.S. was supported by grant of the Czech Academy of Sciences (L200521953).

Institutional Review Board Statement: Not applicable.

Informed Consent Statement: Not applicable.

Data Availability Statement: Data is contained within the article or Supplementary Materials.

Acknowledgments: We acknowledge Karel Harant and Pavel Talacko from Laboratory of Mass Spectrometry, Biocev, Charles University, Faculty of Science for performing LC/MS analysis. Aurélia E. Lewis from the University of Bergen for providing the complete PIP2 interactome data. Pavel Kříž and Iva Jelínková for technical support and Zdeněk Hodný for proofreading of the manuscript. Dorotea Fracchiolla Art&Science, Vienna, Austriahttps://my-art-science.com/for drawing of PIPsLiP-qMS pipeline scheme.

Conflicts of Interest: The authors declare no conflict of interest.

References

1. Dundr, M.; Misteli, T. Functional architecture in the cell nucleus. *Biochem. J.* **2001**, *356*, 297–310. [CrossRef] [PubMed]
2. Sobol, M.; Krausová, A.; Yildirim, S.; Kalasová, I.; Fáberová, V.; Vrkoslav, V.; Philimonenko, V.; Marášek, P.; Pastorek, L.; Čapek, M.; et al. Nuclear phosphatidylinositol 4,5-bisphosphate islets contribute to efficient RNA polymerase II-dependent transcription. *J. Cell. Sci.* **2018**, *131*. [CrossRef] [PubMed]
3. Sztacho, M.; Sobol, M.; Balaban, C.; Eliana, S.; Lopes, E.; Hozák, P. Nuclear phosphoinositides and phase separation: Important players in nuclear compartmentalization. *Adv. Biol. Regul.* **2019**, *71*, 111–117. [CrossRef] [PubMed]
4. Castano, E.; Yildirim, S.; Fáberová, V.; Krausová, A.; Uličná, L.; Paprčková, D.; Sztacho, M.; Hozáket, P. Nuclear phosphoinositides-versatile regulators of genome functions. *Cells* **2019**, *8*, 649. [CrossRef] [PubMed]
5. Di Paolo, G.; De Camilli, P. Phosphoinositides in cell regulation and membrane dynamics. *Nature* **2006**, *443*, 651–657. [CrossRef][PubMed]
6. Sztacho, M.; Segeletz, S.; Sanchez-Fernandez, M.A.; Czupalla, C.; Niehage, C.; Hoflack, B. BAR proteins PSTPIP1/2 regulate podosome dynamics and the resorption activity of osteoclasts. *PLoS ONE* **2016**, *11*, e0164829. [CrossRef] [PubMed]
7. Lewis, A.E.; Sommer, L.; Arntzen, M.Ø.; Strahm, Y.; Morrice, N.A.; Divecha, N.; D'Santos, C.S. Identification of nuclear phosphatidylinositol 4,5-bisphosphate-interacting proteins by neomycin extraction. *Mol. Cell. Proteom.* **2011**, *10*. [CrossRef]
8. Yildirim, S.; Castano, E.; Sobol, M.; Philimonenko, V.V.; Dzijak, R.; Venit, T.; Hozák, P. Involvement of phosphatidylinositol 4,5-bisphosphate in RNA polymerase I transcription. *J. Cell. Sci.* **2013**, *126*, 2730–2739. [CrossRef] [PubMed]
9. Ulicna, L.; Kalendova, A.; Kalasova, I.; Vacik, T.; Hozák, P. PIP2 epigenetically represses rRNA genes transcription interacting with PHF8. *Biochim. Biophys. Acta Mol. Cell. Biol. Lipids* **2018**, *1863*, 266–275. [CrossRef]
10. Suh, M.J.; Pourshahian, S.; Limbach, P.A. Developing limited proteolysis and mass spectrometry for the characterization of ribosome topography. *J. Am. Soc. Mass. Spectrom.* **2007**, *18*, 1304–1317. [CrossRef]
11. Gao, X.; Bain, K.; Bonanno, J.B.; Buchanan, M.; Henderson, D.; Lorimer, D.; Marsh, C.; Reynes, J.A.; Sauder, J.M.; Schwinn, K.; et al. High–throughput limited proteolysis/mass spectrometry for protein domain elucidation. *J. Struct. Funct. Genom.* **2005**, *6*, 129–134. [CrossRef] [PubMed]
12. Masuda, T.; Tomita, M.; Ishihama, Y. Phase transfer surfactant-aided trypsin digestion for membrane proteome analysis. *J. Proteome Res.* **2008**, *7*, 731–740. [CrossRef] [PubMed]
13. Rappsilber, J.; Mann, M.; Ishihama, Y. Protocol for micro-purification, enrichment, pre-fractionation and storage of peptides for proteomics using stagetips. *Nat. Protoc.* **2007**, *2*, 1896–1906. [CrossRef] [PubMed]
14. Hebert, A.S.; Richards, A.L.; Bailey, D.J.; Ulbrich, A.; Coughlin, E.E.; Westphall, M.S.; Coon, J.J. The one hour yeast proteome. *Mol. Cell. Proteom.* **2014**, *13*, 339–347. [CrossRef]
15. Cox, J.; Mann, M. MaxQuant enables high peptide identification rates, individualized p.p.b.-range mass accuracies and proteome-wide protein quantification. *Nat. Biotechnol.* **2008**, *26*, 1367–1372. [CrossRef] [PubMed]
16. Cox, J.; Neuhauser, N.; Michalski, A.; Scheltema, R.A.; Olsen, J.V.; Mann, M. Andromeda: A peptide search engine integrated into the MaxQuant environment. *J. Proteome Res.* **2011**, *10*, 1794–1805. [CrossRef]
17. Cox, J.; Hein, M.Y.; Luber, C.A.; Paron, I.; Nagaraj, N.; Mann, M. Accurate proteome-wide label-free quantification by delayed normalization and maximal peptide ratio extraction, termed MaxLFQ. *Mol. Cell. Proteom.* **2014**, *13*, 2513–2526. [CrossRef] [PubMed]
18. Tyanova, S.; Temu, T.; Sinitcyn, P.; Carlson, A.; Hein, M.Y.; Geiger, T.; Mann, M.; Cox, J. The Perseus computational platform for comprehensive analysis of (prote)omics data. *Nat. Methods* **2016**, *13*, 731–740. [CrossRef]
19. R Core Team. *R: A Language and Environment for Statistical Computing*; R Foundation for Statistical Computing: Vienna, Austria, 2020. Available online:https://www.Rproject.org/.v4.0.0(accessed on 24 April 2020).
20. Szklarczyk, D.; Gable, A.L.; Lyon, D.; Junge, A.; Wyder, S.; Huerta-Cepas, J.; Simonovic, M.; Doncheva, N.T.; Morris, J.H.; Bork, P.; et al. STRING v11: Protein-protein association networks with increased coverage, supporting functional discovery in genome-wide experimental datasets. *Nucleic Acids Res.* **2019**. [CrossRef]
21. UniProt, C. UniProt: A worldwide hub of protein knowledge. *Nucleic Acids Res.* **2019**, *47*, 506–515. [CrossRef]
22. Sigrist, C.J.A.; de Castro, E.; Cerutti, L.; Cuche, B.A.; Hulo, N.; Bridge, A.; Bougueleret, L.; Xenarios, I. New and continuing developments at prosite. *Nucleic Acids Res.* **2013**, *41*, 344–347. [CrossRef] [PubMed]
23. Faberova, V.; Kalasová, I.; Krausová, A.; Hozák, P. Super-resolution localisation of nuclear PI(4)P and identification of its interacting proteome. *Cells* **2020**, *9*, 1191. [CrossRef] [PubMed]
24. Zubarev, R.A. The challenge of the proteome dynamic range and its implications for in-depth proteomics. *Proteomics* **2013**, *13*,723–726. [CrossRef] [PubMed]
25. Schopper, S.; Kahraman, A.; Leuenberger, P.; Feng, Y.; Piazza, I.; Müller, O.; Boersema, P.J.; Picotti, P. Measuring protein structural changes on a proteome-wide scale using limited proteolysis-coupled mass spectrometry. *Nat. Protoc.* **2017**, *12*, 2391–2410. [CrossRef]
26. Guillen-Chable, F.; Corona, U.R.; Pereira-Santana, A.; Bayona, A.; Rodríguez-Zapata, L.C.; Aquino, C.; Šebestová, L.; Vitale, N.; Hozak, P.; Castano, E. Fibrillarin ribonuclease activity is dependent on the gar domain and modulated by phospholipids. *Cells* **2020**, *9*, 1143. [CrossRef] [PubMed]
27. Uhlen, M.; Fagerberg, L.; Hallström, B.M.; Lindskog, C.; Oksvold, P.; Mardinoglu, A.; Sivertsson, A.; Kampf, C.; Sjöstedt, E.; Navani, S.; et al. Proteomics. Tissue-based map of the human proteome. *Science* **2015**, *347*, 1260419. [CrossRef] [PubMed]

28. Thul, P.J.; Akesson, L.; Wiking, M.; Mahdessian, D.; Geladaki, A.; Blal, H.A.; Alm, T.; Asplund, A.; Björk, L.; Breckels, L.M.; et al. A subcellular map of the human proteome. *Science* **2017**, *356*. [CrossRef]
29. Lamond, I.A.; Spector, D.L. Nuclear speckles: A model for nuclear organelles. *Nat. Rev. Mol. Cell. Biol.* **2003**, *4*, 605–612. [CrossRef]
30. Mintz, P.J.; Patterson, S.D.; Neuwald, A.F.; Spahr, C.S.; Spector, D.L. Purification and biochemical characterization of interchromatin granule clusters. *EMBO J.* **1999**, *18*, 4308–4320. [CrossRef]
31. Bavelloni, A.; Faenza, I.; Cioffi, G.; Piazzi, M.; Parisi, D.; Matic, I.; Maraldi, N.M.; Cocco, L. Proteomic-based analysis of nuclear signaling: PLCbeta1 affects the expression of the splicing factor SRp20 in Friend erythroleukemia cells. *Proteomics* **2006**, *6*, 5725–5734. [CrossRef]
32. Faenza, I.; Ramazzotti, G.; Bavelloni, A.; Fiume, R.; Gaboardi, G.C.; Follo, M.Y.; Gilmour, R.S.; Martelli, A.M.; Ravid, K.; Cocco, L. Inositide-dependent phospholipase C signaling mimics insulin in skeletal muscle differentiation by affecting specific regions of the cyclin D3 promoter. *Endocrinology* **2007**, *148*, 1108–1117. [CrossRef] [PubMed]
33. Hochberg-Laufer, H.; Neufeld, N.; Brody, Y.; Nadav-Eliyahu, S.; Ben-Yishay, R.; Shav-Tal, Y. Availability of splicing factors in the nucleoplasm can regulate the release of mRNA from the gene after transcription. *PLoS Genet.* **2019**, *15*, e1008459. [CrossRef]
34. Viita, T.; Kyheröinen, S.; Prajapati, B.; Virtanen, J.; Frilander, M.J.; Varjosalo, M.; Vartiainen, M.K. Nuclear actin interactome analysis links actin to KAT14 histone acetyl transferase and mRNA splicing. *J. Cell Sci.* **2019**, *132*. [CrossRef] [PubMed]
35. Yamazaki, S.; Yamamoto, K.; Harata, M. Contribution of nuclear actin to transcription regulation. *Genom. Data* **2015**, *4*, 127–129. [CrossRef]
36. Pestic-Dragovich, L.; Stojiljkovic, L.; Philimonenko, A.A.; Nowak, G.; Ke, Y.; Settlage, R.E.; Shabanowitz, J.; Hunt, D.F.; Hozak, P.; de Lanerolle, P. A myosin I isoform in the nucleus. *Science* **2000**, *290*, 337–341. [CrossRef] [PubMed]
37. Philimonenko, V.V.; Zhao, J.; Iben, S.; Dingová, H.; Kyselá, K.; Kahle, M.; Zentgraf, H.; Hofmann, W.A.; de Lanerolle, P.; Hozák, P.; et al. Nuclear actin and myosin I are required for RNA polymerase I transcription. *Nat. Cell Biol.* **2004**, *6*, 1165–1172. [CrossRef]
38. Hofmann, W.A.; Vargas, G.M.; Ramchandran, R.; Stojiljkovic, L.; Goodrich, J.A.; de Lanerolle, P. Nuclear myosin I is necessary for the formation of the first phosphodiester bond during transcription initiation by RNA polymerase II. *J. Cell. Biochem.* **2006**, *99*,1001–1009. [CrossRef]
39. Hofmann, W.A.; Stojiljkovic, L.; Fuchsova, B.; Vargas, G.M.; Mavrommatis, E.; Philimonenko, V.; Kysela, K.; Goodrich, J.A.; Lessard, J.L.; Hope, T.J.; et al. Actin is part of pre-initiation complexes and is necessary for transcription by RNA polymerase II. *Nat. Cell Biol.* **2004**, *6*, 1094–1101. [CrossRef]
40. Takahashi, Y.; Hiratsuka, S.; Machida, N.; Takahashi, D.; Matsushita, J.; Hozak, P.; Misteli, T.; Miyamoto, K.; Harata, M. Impairment of nuclear F-actin formation and its relevance to cellular phenotypes in Hutchinson-Gilford progeria syndrome. *Nucleus* **2020**, *11*, 250–263. [CrossRef]
41. Venit, T.; Semesta, K.; Farrukh, S.; Endara-Coll, M.; Havalda, R.; Hozak, P.; Percipalle, P. Nuclear myosin 1 activates p21 gene transcription in response to DNA damage through a chromatin-based mechanism. *Commun. Biol.* **2020**, *3*, 115. [CrossRef]
42. Frottin, F.; Schueder, F.; Tiwary, S.; Gupta, R.; Körner, R.; Schlichthaerle, T.; Cox, J.; Jungmann, R.; Hartl, F.U.; Hipp, M.S. The nucleolus functions as a phase-separated protein quality control compartment. *Science* **2019**, *365*, 342–347. [CrossRef] [PubMed]
43. Azkanaz, M.; López, A.R.; de Boer, B.; Huiting, W.; Angrand, P.; Vellenga, E.; Kampinga, H.H.; Bergink, S.; Martens, J.H.A.; Schuringa, J.; et al. Protein quality control in the nucleolus safeguards recovery of epigenetic regulators after heat shock. *Elife* **2019**, *8*. [CrossRef] [PubMed]
44. Zaffagnini, G.; Savova, A.; Danieli, A.; Romanov, J.; Tremel, S.; Ebner, M.; Peterbauer, T.; Sztacho, M.; Trapannone, R.; Tarafder, A.K.; et al. Phasing out the bad-How SQSTM1/p62 sequesters ubiquitinated proteins for degradation by autophagy. *Autophagy* **2018**, *14*, 1280–1282. [CrossRef] [PubMed]
45. Turco, E.; Witt, M.; Abert, C.; Bock-Bierbaum, T.; Su, M.Y.; Trapannone, R.; Sztacho, M.; Danieli, A.; Shi, X.; Fracchiolla, D.; et al. FIP200 claw domain binding to p62 promotes autophagosome formation at ubiquitin condensates. *Mol. Cell.* **2019**, *74*, 330–346.e11. [CrossRef] [PubMed]
46. Cohen-Kaplan, V.; Livneh, I.; Avni, N.; Cohen-Rosenzweig, C.; Ciechanove, A. The ubiquitin-proteasome system and autophagy: Coordinated and independent activities. *Int. J. Biochem. Cell. Biol.* **2016**, *79*, 403–418. [CrossRef] [PubMed]
47. Latonen, L.; Moore, H.M.; Bai, B.; Jäämaa, S.; Laiho, M. Proteasome inhibitors induce nucleolar aggregation of proteasome target proteins and polyadenylated RNA by altering ubiquitin availability. *Oncogene* **2011**, *30*, 790–805. [CrossRef]
48. Kraft, L.J.; Manral, P.; Dowler, J.; Kenworthy, A.K. Nuclear LC3 associates with slowly diffusing complexes that survey the nucleolus. *Traffic* **2016**, *17*, 369–399. [CrossRef]
49. Salmina, K.; Huna, A.; Inashkina, I.; Belyayev, A.; Krigerts, J.; Pastova, L.; Vazquez-Martin, A.; Erenpreisa, J. Nucleolar aggresomes mediate release of pericentric heterochromatin and nuclear destruction of genotoxically treated cancer cells. *Nucleus* **2017**, *8*,205–221. [CrossRef]
50. Mostofa, M.G.; Rahman, M.A.; Koike, N.; Yeasmin, A.M.; Islam, N.; Waliullah, T.M.; Hosoyamada, S. CLIP and cohibin separate rDNA from nucleolar proteins destined for degradation by nucleophagy. *J. Cell. Biol.* **2018**, *217*, 2675–2690. [CrossRef]
51. Iadevaia, V.; Zhang, Z.; Jan, E.; Proud, C.G. mTOR signaling regulates the processing of pre-rRNA in human cells. *Nucleic Acids Res.* **2012**, *40*, 2527–2539. [CrossRef]
52. Tsang, K.C.; Liu, H.; Zheng, X.F. mTOR binds to the promoters of RNA polymerase I- and III-transcribed genes. *Cell Cycle* **2010**, 953–957. [CrossRef] [PubMed]

53. Katagiri, N.; Kuroda, T.; Kishimoto, H.; Hayashi, Y.; Kumazawa, T.; Kimura, K. The nucleolar protein nucleophosmin is essential for autophagy induced by inhibiting Pol I transcription. *Sci. Rep.* **2015**, *5*, 8903. [CrossRef] [PubMed]
54. Marx, B.; Hufbauer, M.; Zigrino, P.; Majewski, S.; Markiefka, B.; Sachsenheimer, T.; Brügger, B.; Akgül, B. Phospholipidation of nuclear proteins by the human papillomavirus E6 oncoprotein: Implication in carcinogenesis. *Oncotarget* **2018**, *9*, 34142–34158. [CrossRef] [PubMed]

7.2. The F-Actin-Binding MPRIP Forms Phase-Separated Condensates and Associates with PI(4,5)P2 and Active RNA Polymerase II in the Cell Nucleus

Can Balaban, Martin Sztacho, Michaela Blažíková and Pavel Hozák

Cells. 2021, 10(4), 848; doi:10.3390/cells10040848

IF: 7.666 (2021)

C.B. designed and performed all of the experiments (Confocal and STED microscopy imaging, molecular cloning, generating stable cell lines, heat shock and hexanediol treatments, cellular fractionation, immunoprecipitation, pull-down assays, immunofluorescence experiments, FRAP experiments, live cell imaging, western blotting and data analysis), wrote and revised the manuscript.

cells

Article

The F-Actin-Binding MPRIP Forms Phase-Separated Condensates and Associates with PI(4,5)P2 and Active RNA Polymerase II in the Cell Nucleus

Can Balaban [1], Martin Sztacho [1], Michaela Blažíková [2] and Pavel Hozák [1,2,*]

[1] Department of Biology of the Cell Nucleus, Institute of Molecular Genetics of the Czech Academy of Sciences, v.v.i., 142 20 Prague, Czech Republic; can.balaban@img.cas.cz (C.B.); martin.sztacho@img.cas.cz (M.S.)
[2] Light Microscopy Core Facility, Institute of Molecular Genetics of the Czech Academy of Sciences, v.v.i., 142 20 Prague, Czech Republic; michaela.blazikova@img.cas.cz
* Correspondence: hozak@img.cas.cz

Abstract: Here, we provide evidence for the presence of Myosin phosphatase rho-interacting protein (MPRIP), an F-actin-binding protein, in the cell nucleus. The MPRIP protein binds to Phosphatidylinositol 4,5-bisphosphate (PIP2) and localizes to the nuclear speckles and nuclear lipid islets which are known to be involved in transcription. We identified MPRIP as a component of RNA Polymerase II/Nuclear Myosin 1 complex and showed that MPRIP forms phase-separated condensates which are able to bind nuclear F-actin fibers. Notably, the fibrous MPRIP preserves its liquid-like properties and reforms the spherical shaped condensates when F-actin is disassembled. Moreover, we show that the phase separation of MPRIP is driven by its long intrinsically disordered region at the C-terminus. We propose that the PIP2/MPRIP association might contribute to the regulation of RNAPII transcription via phase separation and nuclear actin polymerization.

Keywords: MPRIP; phase separation; PIP2; actin; nucleus

Citation: Balaban, C.; Sztacho, M.; Blažíková, M.; Hozák, P. The F-Actin-Binding MPRIP Forms Phase-Separated Condensates and Associates with PI(4,5)P2 and Active RNA Polymerase II in the Cell Nucleus. *Cells* **2021**, *10*, 848. https://doi.org/10.3390/cells10040848

Academic Editor: Michael F. Olson

Received: 5 March 2021
Accepted: 6 April 2021
Published: 8 April 2021

Publisher's Note: MDPI stays neutral with regard to jurisdictional claims in published maps and institutional affiliations.

1. Introduction

Myosin phosphatase rho-interacting protein (MPRIP) was first described as a cytoskeletal protein involved in the regulation of stress fibers [1–3]. Recently, we identified MPRIP by label-free quantitative mass spectrometry as a nuclear Phosphatidylinositol 4,5-bisphosphate (PIP2) interactor [4]. Its depletion was reported to stabilize and thus increase the number of actin stress fibers in smooth muscle cells, whereas its overexpression leads to the disassembly of stress fibers in neuronal cells [5,6]. Its binding to F-actin stress fibers is mediated by the N-terminal region which also contains two Pleckstrin Homology (PH) domains [7,8]. These PH domains possess a lipid binding site where the positively charged residues (i.e., Lysine and Arginine) enable the binding of the negatively charged inositol head group of the phosphatidylinositol phosphates (PIPs) [9].

It was shown that the PH-like domains are responsible for the localization of proteins such as Nuclear Myosin I (NM1) to nuclear PIP2 [10–12]. Recently, we proposed a model where PIP2 localizes into discrete nuclear areas where it regulates processes such as transcription and splicing [12]. Moreover, we described the importance of nanoscale, nucleoplasmic PIP2-rich structures—nuclear lipid islets (NLIs) in RNA polymerase II (RNAPII) mediated transcription and showed that their surface is in the proximity of chromatin, RNA and NM1 [12–14]. However, the precise mechanism of interplay among PIP2, NM1 and RNAPII in regulation of transcription remains elusive. Recently, it was shown that the activity of RNAPII is regulated by its propensity to phase separate [15,16]. The phase separation of RNAPII is regulated through the phosphorylation of its intrinsically disordered C-terminal domain (CTD) [17]. In the last decade, it became evident that the intrinsically disordered regions (IDRs) are responsible for the regulation of diverse

nuclear processes through functional compartmentalization into membraneless nuclear bodies [18–21]. The intermolecular multivalent interactions of IDRs lead to the formation of condensates with liquid-like properties [22–24]. The liquid–liquid phase separation (LLPS) is an entropy-driven mechanism which provides the basis for the biophysical explanation of the compartmentalization of biological processes in the dense nuclear environment [25,26].

In this study, we show that MPRIP localizes to PIP2-containing nuclear structures, forms complex with RNAPII and MYO1C-an isoform of NM1-and undergoes LLPS (liquid–liquid phase-separation) in cell nucleus while preserving its F-actin binding capacity [27,28]. Furthermore, we describe the liquid-like properties of MPRIP protein in the cell nucleus. Therefore, we hypothesized that MPRIP might represent the functional hinge in the transcriptional regulation of RNAPII compartmentalization through actin, PIP2 and NM1 interaction.

2. Material and Methods

2.1. Cell Cultures and Transfections

Human cervical carcinoma (HeLa, ATCC no. CCL2) cells and human osteosarcoma (U2OS, ATCC no. HTB96) cells were grown in Dulbecco's modified Eagle's medium (DMEM, Sigma D6429) with 10% FBS at 37 °C in a humidified 5% CO_2 atmosphere. HeLa cells in suspension were kept in minimum essential medium Eagle with Spinner modification (S-MEM, Sigma M8167) supplemented with 5% FBS at 37 °C in a humidified 5% CO_2 atmosphere. Transfections were carried out using Lipofectamine 3000 (Invitrogen, Thermo Fisher Scientific, Waltham, MA, USA) according to the manufacturer's protocol. Stable cell lines were established by sorting the transiently transfected cells and keeping them under selective media (G418, Sigma G8168). The cells were then evaluated by Westernblot and fluorescence light microscopy (Figure S6).

2.2. Constructs and Antibodies

pDEST53 GFP-MPRIP (Human Isoform 3 of MPRIP) plasmid was used for the overexpression of MPRIP in U2OS cells (Figure S6). The N-terminal (1–450th amino acid) and C-terminal (450–1000th amino acid) regions of MPRIP were amplified by PCR using pDest-53-GFP-MPRIP as a template. The N-terminal region was inserted in pEGFP-N1, while the C-terminal region was inserted in pEGFP-C1. The constructs were transiently overexpressed in U2OS cells to examine their specific localization and features. For the detailed structure of the fragment, please see Figure S3:

Anti-MPRIP antibody-HPA022901 (SigmaAldrich, St. Louis, MO, USA)
Anti-PI (4,5) P2 antibody: Z-A045, clone 2C11 (Echelon, San Jose, CA, USA)
Anti-RNAPII CTD Phospho S5 antibody-ab5131 (Abcam, Cambridge, UK)
Anti-Lamin B1 antibody—ab16048 (Abcam, Cambridge, UK)
Anti-GAPDH antibody [6C5]-ab8245 (Abcam, Cambridge, UK)
Rabbit Anti-Mouse Immunoglobulin G H&L—ab46540 (Abcam, Cambridge, UK)
Anti-MYO1C antibody was supplied by Peter G. Gillespie, Oregon Hearing Research Center and Vollum Institute [29].

2.3. Bioinformatics Analyses

Nuclear Localization Signal (NLS) prediction was done by using the online tool cNLS Mapper (Figure S1) [30]. The Clustal Omega test, analyzing the degree of the conserved domains, was performed by the tool provided by European Bioinformatics Institute (Figure S2) [31]. The IDRs of the MPRIP were predicted by the D2P2 tool; Database of Disordered Protein Predictions (Figure S3) [32].

2.4. Immunofluorescence Labelling

U2OS cells grown on high-performance cover glasses of 12 mm in diameter with restricted thickness-related tolerance (depth = 0.17 mm ± 0.005 mm) and the refractive index = 1.5255 ± 0.0015 (Marienfeld 0107222). The cells were fixed with 4% formaldehyde

for 20 min and permeabilized with 0.1% Triton X-100 for 5 min. Non-specific binding was blocked by 5% Bovine Serum Albumin (BSA). All solutions were diluted in Phosphate-Buffered Saline (PBS). Then, the cells were incubated with anti-PtdIns(4,5)P2 and anti-MPRIP antibodies, and mounted in 90% glycerol with 4% n-Propyl gallate (NPG). For the super-resolution microscopy, five 5 min washes in PBS with 0.1%Tween were made between each step.

2.5. Stimulated Emission Depletion (STED) Microscopy

The images were acquired using a Leica TCS SP8 STED 3x microscope equipped witha Leica DFC365 FX digital camera with a STED white CS 100x 1.40 NA oil objective for the optimized overlay of excitation and an STED beam (Leica Mikrosysteme Vertrieb GmbH, Wetzlar, Germany). Image capturing was performed using the Leica LASX 64-bit software package. The acquired images were deconvolved using Huygens Professional software version 19.04 (Scientific Volume Imaging, Hilversum, Netherlands), using the Classic Maximum Likelihood Estimation (CMLE) algorithm, with SNR:07 and 20 iterations. The image analysis was carried out using the Coloc 2 plugin of Fiji software. The significance of each statistical analysis was determined by a Student's t test. The randomized images for statistical tests were obtained by rotating one of the two channels 90 degrees [33]. The resolution format was taken at 1024 x 1024 and the corresponding pixel sizes were both 28 nm in x and y. A minimum of five cells were analyzed per each condition.

2.6. Nuclear Extraction and Pull-Down Assay

Nuclear lysate fraction was prepared from the suspended HeLa cells as described by Trinkle-Mulcahy [34]. Cytoplasmic fraction was obtained by Dounce homogenization (Kontes 885300-0015) on ice (30 strokes), following three cold PBS washes. The homogenate was incubated 20 min on ice in buffer 150 mM NaCl, 1% NP-40, 50 mM Tris pH 7.4, 1 mM DTT supplemented with protease inhibitors from F. Hoffmann (La Roche Ltd., Basel, Switzerland, 05056489001) followed by centrifugation at 4000x *g* at 4 °C. The nuclear pellet was sonicated at Soniprep 150 (MSE) bench top sonicator (1 sec on, 1 s off for 30 cycles at power 10 amplitude microns). Sonicated lysate was spun down at 13,000x *g* for 15 min at 4 °C. Supernatant was collected as nuclear lysate. Protein concentration was determined by Pierce™ BCA Protein Assay (Thermo Scientific, 23227) according to the manufacturer's protocol.

In pull-down experiments, 3 mg of HeLa total nuclear lysate was used for each condition. Fifty µL of PIP-coated beads slurry were added to each condition and incubated overnight in the nuclear lysate. The beads were washed five times with 1 mL of ice-cold nuclear extract buffer (150 mM NaCl, 1% NP 40, 50 mM Tris pH 7.4, 1 mM DTT, protease inhibitors from F. Hoffmann (La Roche Ltd., Basel, Switzerland, 05056489001). Two times Laemmli buffer was added to the beads, boiled for 5 min and loaded to the SDS gel followed by Western blot analysis. The PIP-coated beads were obtained from Echelon Biosciences Inc., Salt Lake City, UT, USA (Control Beads, P-B000; PI(3)P beads, P-B003A; PI(4)P beads, P-B004A; PI(5)P beads, P-B005A; PI(3,4)P2 beads, P-B034A; PI(3,5)P2 beads, P-B035A; PI(4,5)P2 beads, P-B045A; PI(3,4,5)P3 beads, P-B345A).

2.7. Co-Immunoprecipitation Assay

Nuclei from suspended HeLa cells were prepared as described previously [34]. One milligram (1 mg) of nuclear lysate was incubated with 2 µg MPRIP antibody at 4 °C overnight. The lysates were incubated with G-protein magnetic beads (Pierce™, Thermo Fischer 88848) at 4 °C for 1 h. Beads were washed 5x times by buffer (150 mM NaCl, 1.0% NP-40, 50 mM Tris pH 7.4, 1 mM DTT) and subjected to Western blot analysis.

2.8. Live-Cell Imaging Microscopy

U2OS cells expressing pDEST53-GFP-MPRIP were grown on 35 mm glass bottom dishes (# P35G-1.5-14-C, MatTek Corporation, Ashland, OR, USA). Live-cell imaging was

performed using a Leica TCS SP5 Confocal microscope equipped by an environmental chamber with CO_2 and temperature control. Image acquisition started 24 h post transfection. For the video (Video S1), the cells were recorded every 5 min for 8 h and 10 min, starting from the 12th hour after transfection. The video has a pixel size of 197 nm × 197 nm.

2.9. Hexanediol Treatment

Twenty-four hours after transfection, the cells were exposed to 25% aliphatic alcohols dissolved in PBS (1,6-Hexanediol and 2,5-Hexanediol, SigmaAldrich, St. Louis, MO, USA, Cat. No. 240117, H11904) for two minutes at room temperature. GFP signals of the nuclear droplets were recorded by Leica TCS SP8 confocal microscope for 2 min.

2.10. FRAP

Cells were transfected a day before the experiment on 35 mm coverslip bottom dishes (catalogue # P35G-1.5-14-C, MatTek Corporation, Ashland, MA, USA). Fluorescence recovery after photobleaching (FRAP) experiments were performed on Leica TCS SP8 confocal microscope with Leica HC PL APO 63x /1.40 oil CS2 objective. Scanning speed was set to 1800 Hz with bidirectional X and an imaging acquisition rate was 0.0232 s Ten pre-bleach images were captured and the photo bleach was performed for another 10 frames and finally, one thousand post-bleach images were acquired. Full-and inner-FRAPs were performed more than one hundred times. The fiber-FRAP was performed at least 50 times and ten bleaches were done for nucleoplasmic-FRAP. Solidified structures were bleached as full-FRAP experiments (n = 20).

Protein mobility within the condensate was measured by quantifying the recovery of the bleached area at the coast of the unbleached region by a custom written MATLAB script (ver. R2019b, The MathWorks, Inc., Natick, MA, USA). The recovery curves were fitted with a single and/or bi-exponential curve, using the non-linear least squares (lsqcurvefit) function. The bleached region was corrected for general bleaching during image acquisition.

We employed FRAP on the circular regions of four different sizes. Full-FRAP experiments covered the area of the whole condensate which was around 3 µm in diameter. In inner-FRAP experiments, the bleached area was a circle of 1 µm in diameter within the 3 µm condensates. Nucleoplasmic-FRAP was performed on a circular area of 6 µm in diameter. For the fiber-FRAP, the bleached are was taken as 0.5 µm in diameter. All FRAP experiments except fiber-FRAP were fitted to a single exponential curve; the fiber-FRAP was fitted to the bi-exponential curve.

2.11. Phalloidin Staining of GFP-MPRIP Expressing U2OS Cells

Cells were transfected with pDEST53-GFP-MPRIP on coverslips and fixed by 4% formaldehyde. F-actin was visualized by 1.5 µg/mL Alexa Fluor™ 568 Phalloidin (Invitrogen, Carlsbad, CA, USA, catalogue # A12380) staining following a standard indirect immunofluorescence labelling protocol. Images were acquired by the STED microscopy as mentioned in Section2.5. The resolution format was taken as 256 x 256 and the corresponding pixel sizes were both 13 nm in x and y.

3. Results

3.1. MPRIP Protein Is Present in the Cell Nucleus

The MPRIP protein was previously described as a cytoplasmic protein localizing to F-actin stress fibers [1,2,5]. It was also identified as MYO1C interactor by quantitative mass spectrometry (qMS) [35]. Therefore, this protein might represent a link between nuclear actin and the transcriptional factor NM1, suggesting a role in the RNAPII transcription process. To evaluate if MPRIP has a nuclear function, we first investigated its nuclear localization. We performed an indirect immunofluorescence (IF) labelling on U2OS cells using MPRIP-specific antibody.

The MPRIP IF labelling confirmed the previously described cytoplasmic stress fiber localization (Figure1A). Moreover, we observed that MPRIP localizes inside the nucleus, displaying a granular pattern that was dispersed in the nucleoplasm (Figure1A). In order to confirm its nuclear presence, we analyzed the fractionated lysates of HeLa cells. The Western blot (WB) analysis of nuclear and cytoplasmic fractions confirmed that MPRIP occurs in both environments (Figure1B). Lamin B and GAPDH were used as the purity controls of fractions. The nuclear fraction was devoid of GAPDH, whereas Lamin B was detected exclusively in nuclear fraction (Figure1B).

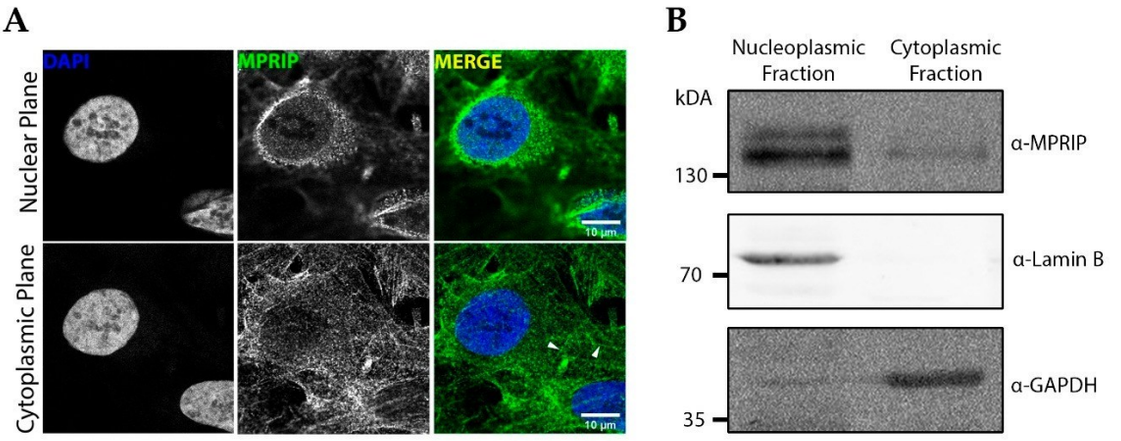

Figure 1. Myosin phosphatase rho-interacting protein (MPRIP) localizes to the cytoplasm and cell nucleus: (**A**) confocal microscopy of an immunofluorescence (IF) experiment shows the localization of endogenous MPRIP in U2OS nucleus and cytoplasmic stress fibers. Upper and lower images represent different focal planes: nuclear and cytoplasmic, respectively. Arrowheads point to the MPRIP staining on stress fibers. Scale bars represent 10 µm; (**B**) Western blot (WB) of HeLa cells fractionated to nuclear and cytoplasmic fractions with detected MPRIP, Lamin B and GAPDH by a specific antibody (*n* = 3).

This protein of ~120 kDa would require an NLS region to be targeted to the nucleus. Our bioinformatics analysis predicts a NLS region at residues 155 to 164 (Figure S1). Clustal Omega test run on eight different MPRIP sequences (three isoforms in Homo sapiens and five orthologues from other mammals) delineated that the predicted NLS region and the PH domains were highly conserved (Figure S2).

3.2. Nuclear MPRIP Interacts with PIP2 and Forms a Complex with RNAPII and MYO1C

We recently identified PIP2 as an important player in the regulation of RNAPII transcription, presumably through NM1 interaction [12]. Therefore, we next sought to determine whether PH domain-containing MPRIP has the capacity to bind PIPs [36]. We used PIP-covered beads in pull-down experiments in nuclear lysates and detected the bound MPRIP protein by WB (Figure2). These experiments showed that MPRIP interacts specifically with PI4,5P2. Thus, we asked whether MPRIP localizes to the proximity of PIP2 in the cell nucleus.

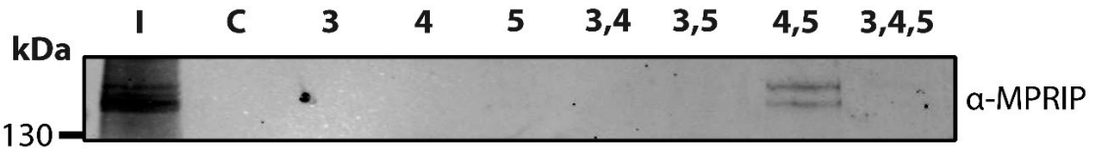

Figure 2. MPRIP specifically interacts with Phosphatidylinositol 4,5-bisphosphate (PIP2). Various PIP-coated agarose beads were used as a bait to pull-down interacting proteins from HeLa nuclear fraction. The membrane was WB analyzed with anti-MPRIP antibody. I—input 2%; C—control beads; 3—PI(3)P, 4—PI(4)P; 5—PI(5)P; 3,4—PI(3,4)P2; 3,5—PI(3,5)P2; 4,5—PI(4,5)P2; 3,4,5—PI(3,4,5)P3. *n* = 3.

We stained the U2OS cells with MPRIP-and PIP2-specific antibodies and revealed their sub-nuclear localization by STED microscopy. The nuclear PIP2 localizes to three different compartments: nuclear speckles, NLIs and nucleoli [12,37]. The statistical analysis revealed that MPRIP localizes to the proximity of the PIP2 signal in the nuclear speckles and NLIs (Figure3). Two statistical coefficients, Manders and Spearman, were determined for two different PIP2-rich compartments, where all tests scored significant differences compared to the randomized images (Figure3D,G).

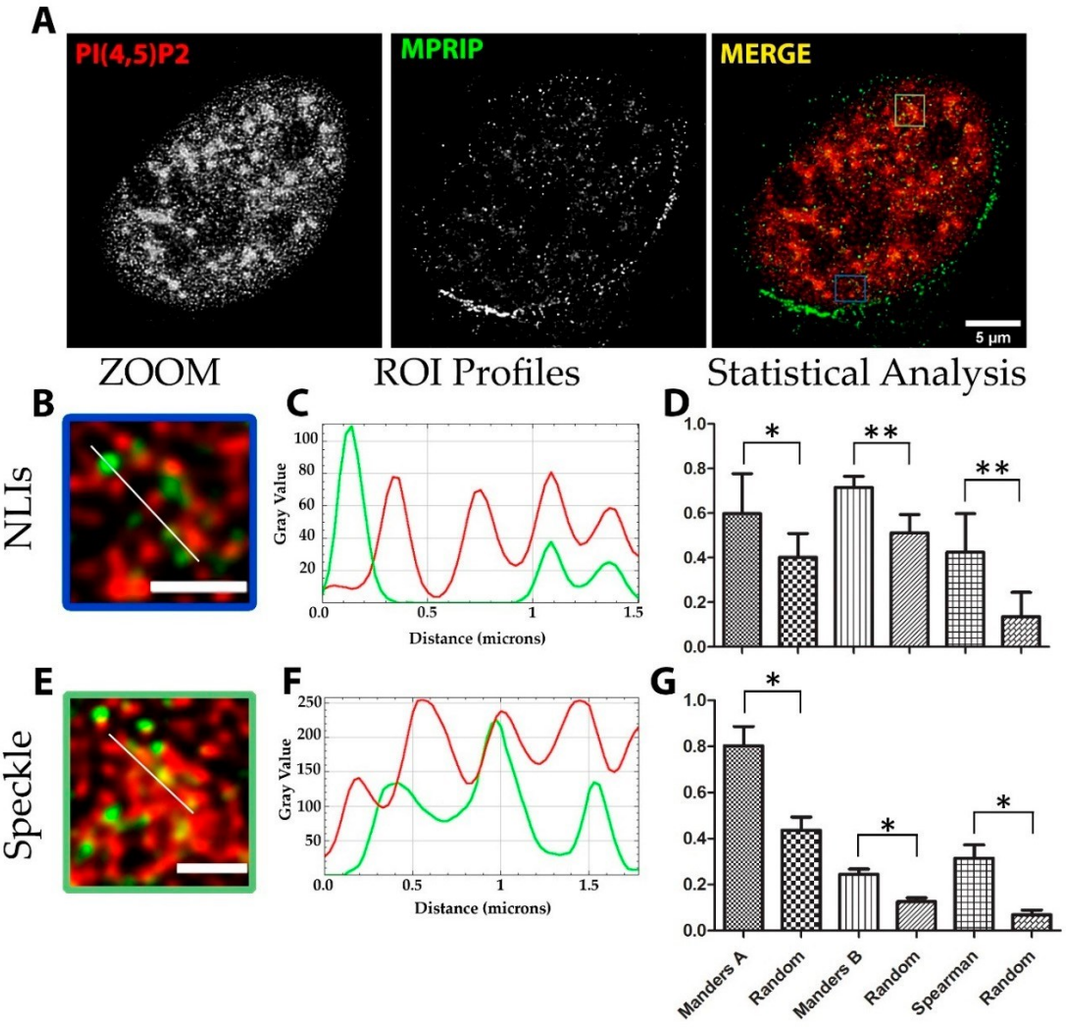

Figure 3. Super-resolution microscopy revealed that Myosin phosphatase rho-interacting protein (MPRIP) localizes in close proximity to Phosphatidylinositol 4,5-bisphosphate (PIP2) at nuclear speckles and nuclear lipid islets (NLIs): (**A**) immunofluorescence labelling experiment showing the presence of endogenous MPRIP and PIP2 in U2OS nucleus. Scale bar represents 5 µm; (**B**–**D**) zoomed view, intensity profiles and statistical analysis of the NLIs. Scale bar corresponds to 1 µm. (**E**–**G**) Zoomed view, intensity profiles and statistical analysis of the speckle-associated PIP2 pool. Scale bar correspondsto 1 µm. Intensity profiles plotted correspond to the lines on the zoomed view. (**D**,**G**) The bar graph shows the statistical Mander's and Spearman coefficients of the MPRIP and PIP2 signal. Mander's A analysis: PIP2 over MPRIP channel, and Mander's B analysis: MPRIP over PIP2 channel. Bars that are marked as Random were obtained by analyzing randomized images (see M.M.). Single asterisk * corresponds to a significance level of $p \leq 0.05$ and the double asterisks ** to $p \leq 0.007$.

Our data presented here indicate that MPRIP colocalizes with nucleoplasmic PIP2-rich NLI structures which were shown to be sites of RNAPII active transcription [12]. Therefore, we suggest that MPRIP might represent the possible link between RNAPII and transcription factor NM1, a MYO1C isoform. Therefore, we tested whether MPRIP

associates with RNAPII and MYO1C by MPRIP immunoprecipitation (IP) followed by WB (Figure4). Our data show that MPRIP is in the same complex with MYO1C and the active form of RNAPII (phosphor Ser5) which was previously shown to associate with PIP2-rich NLIs [12]. Thus, it is possible that MPRIP is involved in an ongoing transcription process that occurs at the surface of NLIs.

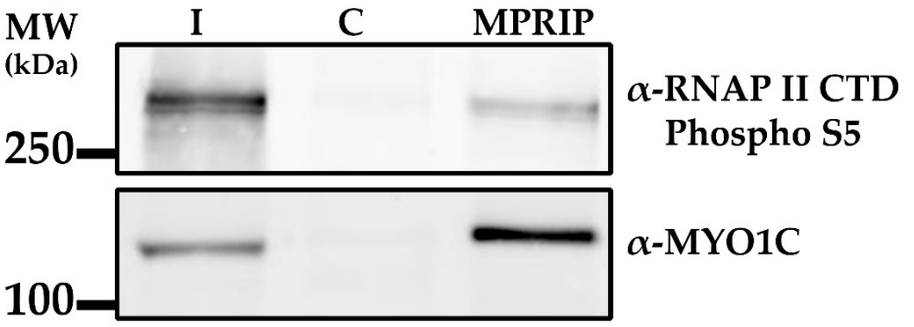

Figure 4. The immunoprecipitation assay confirms the existence of a MPRIP/RNAPII/MYO1C nuclear complex. The MPRIP immunoprecipitation was performed with HeLa nuclear lysates and the corresponding proteins were detected by Anti-RNAP II CTD Phospho S5 and anti-MYO1C antibodies. I—input 2%; C—control non-specific rabbit Immunoglobulin G. *n* = 3.

3.3. Overexpression of MPRIP Leads to Formation of Condensates and Fibrous Structures in theCell Nucleus

To further study the nuclear localizations of MPRIP, we overexpressed GFP-tagged MPRIP in human U2OS cells. Interestingly, the transfected cells showed three different phenotypes (Figure5A–C). The first and most common (~70%) phenotype recapitulates the pattern of IF labelling of endogenous MPRIP which is fine granular foci that is diffused throughout the nucleoplasm (Figure5A). The second phenotype resembles globular condensed structures in the nucleoplasm, which had 1 to 5 µm in diameter (Figure5B). The third phenotype of the MPRIP-expressing cells shows nucleoplasmic, fibrous structures that are intertwined (Figure5C).

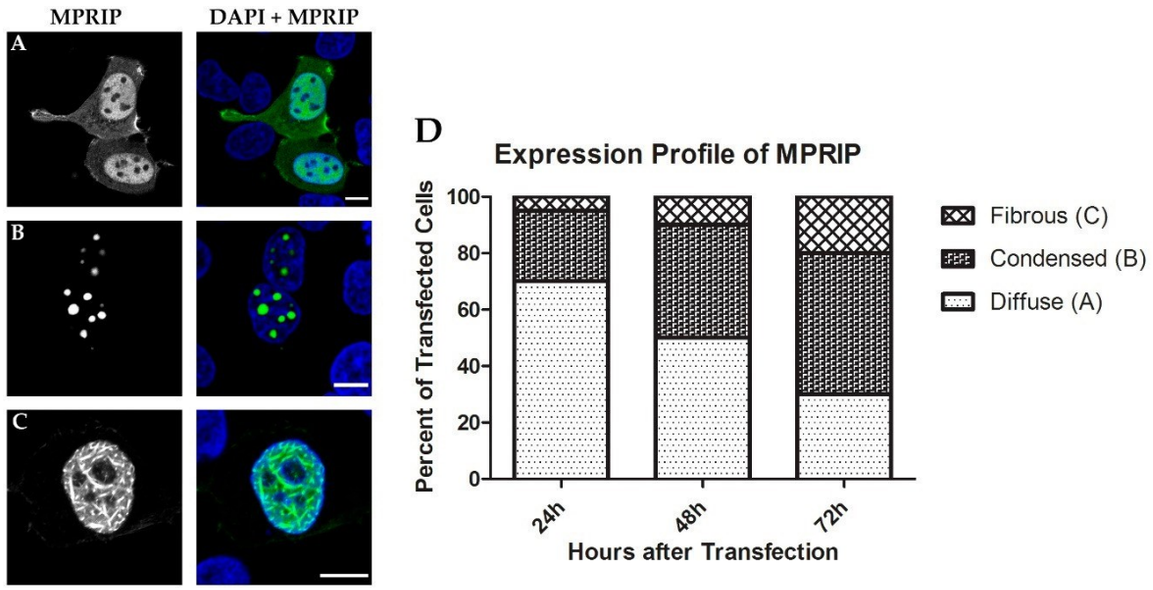

Figure 5. The overexpression of GFP-MPRIP results in three different phenotypes. Confocal microscopy of U2OS cells over-expressing GFP-MPRIP. (**A**) diffuse; (**B**) condensed; and (**C**) fibrous structures, which constitute the three different phenotypes. DAPI in blue and MPRIP in green. Scale bars correspond to 5 µm. (**D**) The graph reflects the changes in population of cells showing different phenotypes over the time post transfection.

The large globular condensates started to appear 8 h post-transfection and persisted throughout 72 h after transfection. The fibrous structures started to appear mostly at 20th hour of post transfection. Interestingly, the population of cells forming large condensates and fibrous structures increased over time after transfection, whereas the population of cells with a diffused pattern decreased (Figure5D).

3.4. Nuclear MPRIP Condensates Are Formed by Phase Separation

Our data show that the overexpression of MPRIP leads to the formation of spherical condensates. We speculated that the formation of these roundish structures might be driven by LLPS. Therefore, we utilized the aliphatic alcohol 1,6-hexanediol, which is widely used for the disruption of weak hydrophobic interactions driving phase separation [38,39]. In contrast, the derivative 2,5-Hexanediol has minimal impact on the phase separated condensates and thus serves as a negative control [40–42]. To demonstrate the LLPS ability of condensed GFP-MPRIP structures, we treated the cells with 25% of 1,6- and 2,5-Hexanediol/PBS solution for 2 min (Figure6A). The MPRIP condensates started to dissolve 10 s after the addition of 1,6-Hexanediol and disappeared completely after 2 min of incubation. On the contrary, the treatment of 2,5-Hexanediol did not lead to the complete dissolution of the condensates, even after 2 min of incubation (Figure6B).

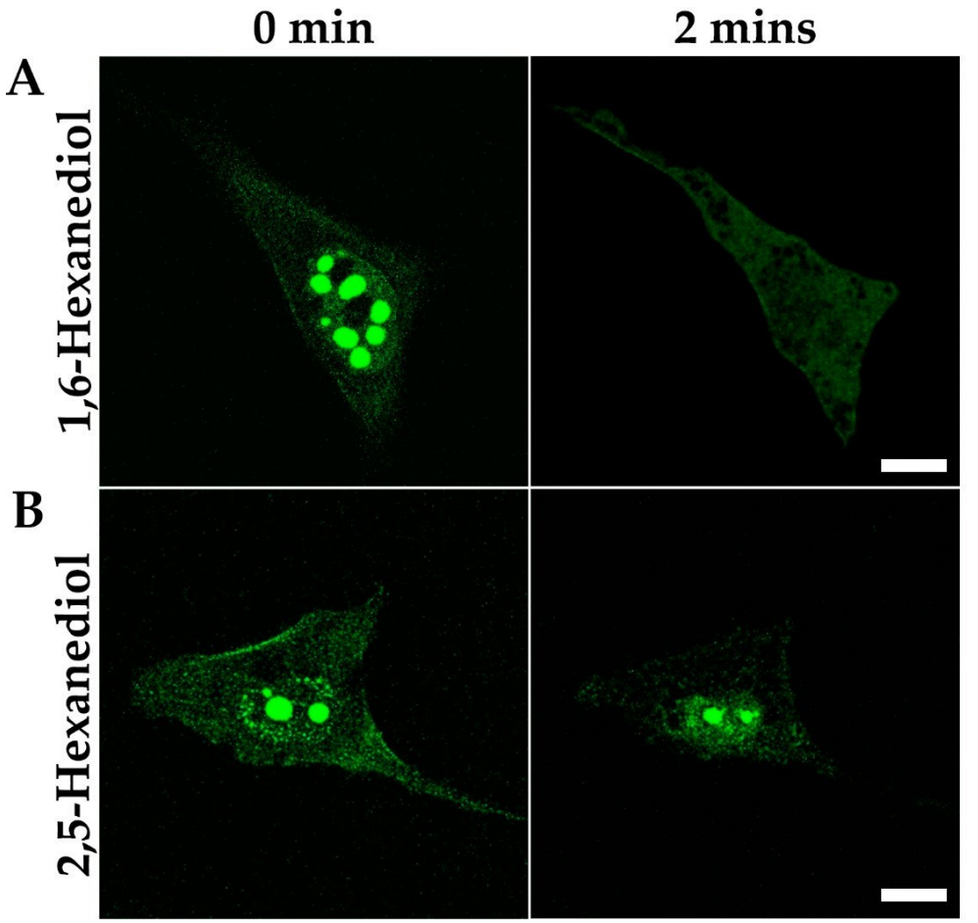

Figure 6. 1,6-Hexanediol treatment of the cells overexpressing GFP-MPRIP dissolves the condensates. Live cell imaging showing U2OS cells over-expressing GFP-MPRIP before and after 2 min of Hexanediol treatment: (**A**) the GFP-MPRIP condensates in a cell nucleus treated with 1,6-Hexanediol; (**B**) with 2,5-Hexanediol. Green is GFP-MPRIP. Scale bars correspond to 10 µm. $n = 2$.

3.5. Dynamic Liquid-Like MPRIP Condensates Are Able to Fuse, Segregate and Form Fibers

The phase-separated structures are usually spherical and they show dynamic behavior with a capacity to fuse and split [26,43]. In our live-cell imaging experiments, we observed that GFP-MPRIP condensates show dynamic motility; they fuse and form larger condensates, preserving their spherical shape (Figure7A) and finally they divide (Video S1, 0:55 to 1 h). Figure7B represents images from the video S1 that shows the ability of GFP-MPRIP condensates to transform into the fibers and then back into condensates.

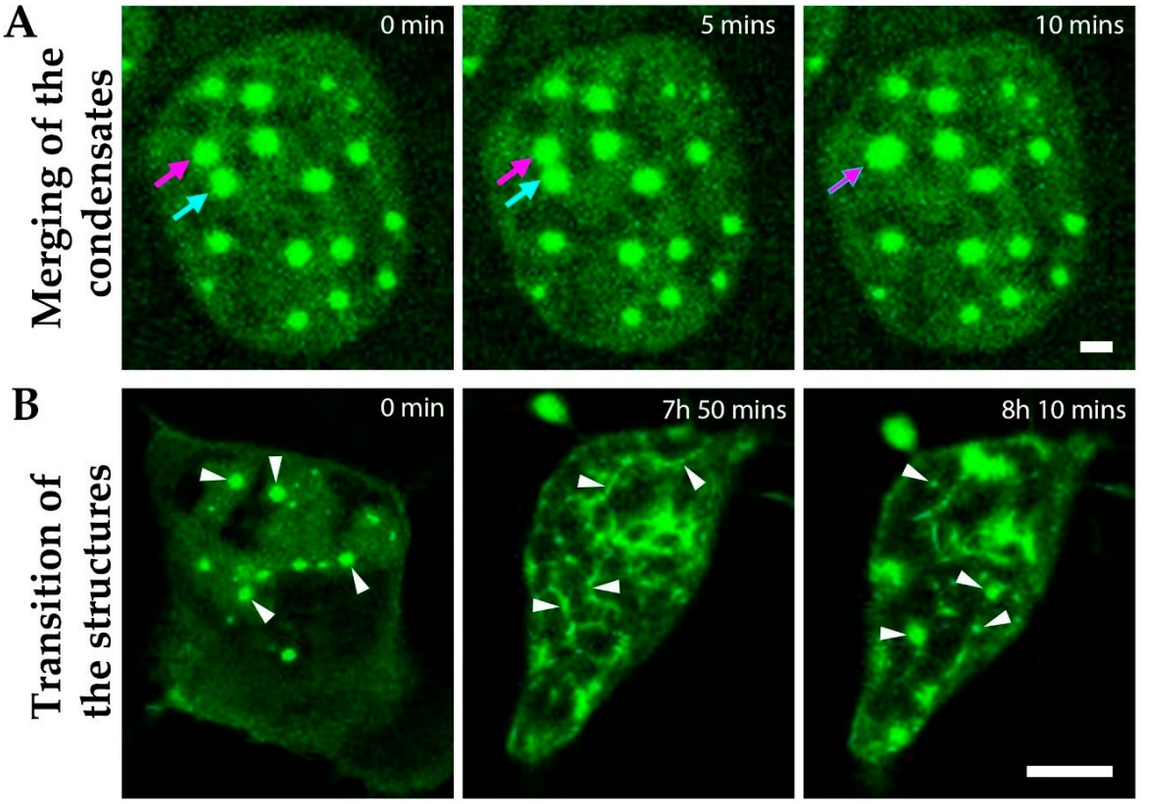

Figure 7. MPRIP condensates show typical features of liquid-like structures. Live cell imaging showing the nucleus of an U2OS cell over-expressing GFP-MPRIP. (**A**) The GFP-MPRIP condensates were visualized for 15 min. Arrows show the structures that merge during the imaging. Green is GFP-MPRIP. Scale bar represents 3 µm. (**B**) The GFP-MPRIP expressing cell was visualized for 8 h and 10 min. Arrowheads show the spherical condensates that disappear and form fibers, and then revert back into condensates over time. Imaging started at the 12th hour after transfection. The scale bar represents 10 µm.

3.6. MPRIP Condensates Show High Internal Dynamics and Rapid Molecular Interchange between Condensates and Neighboring Nucleoplasm

To further study the liquid-like properties of MPRIP condensates, we measured their molecular dynamics by FRAP experiments. For this purpose, we performed a total of five FRAP experiments corresponding to each phase and structure. We started by full-FRAP experiment in order to assess the rate of molecular exchange between nucleoplasm and MPRIP condensed structures (Figure8A). The half-time was recorded as 3.6 (±1.2) s with a diffusion coefficient D of 0.147 μ^2/s. As described by Patel et al. in 2015, we also observed a solidified, gel-like phase of the condensates [44]. This phase occurs more frequently with increasing time after transfection. In the first 24 h post transfection, the mobile fraction of the full-FRAP was ~60%, which dropped down to ~10% in 48 h post transfection (Figure8B , solidified structure).

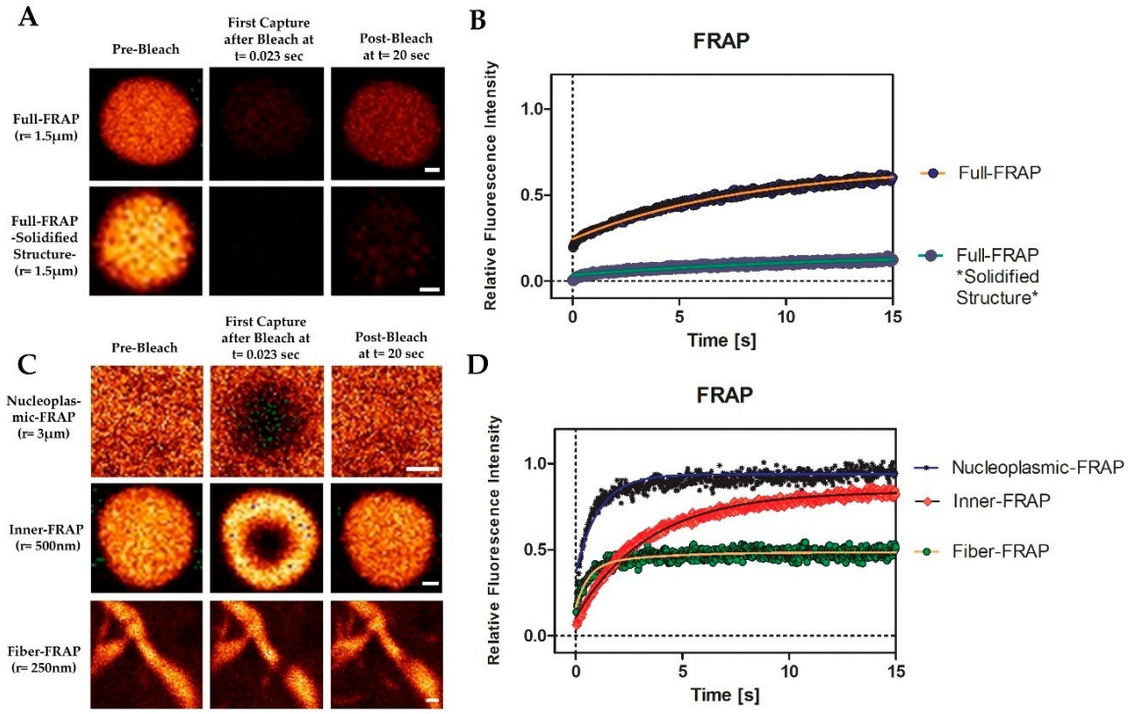

Figure 8. MRPIP nuclear condensates show dynamic liquid-like properties. (**A**) Representative images of Full-Fluorescence recovery after photobleaching (FRAP) experiments that were performed on GFP-MPRIP nuclear condensates. The lower row images correspond to a solidified structure. Imaging rate was 23 ms. Scale bars represent 0.5 µm. (**C**) Representative images of nucleoplasmic-, inner- and fiber-FRAP. r is the radius of the circular bleached area. Scale bars represent 3 µm, 0.5 µm and 0.25 µm from the top to the bottom, respectively. (**B**–**D**) The graphs represent the relative fluorescence values in time, starting with the first capture after bleaching. Each point corresponds to the corrected and normalized fluorescence values of the bleached areas of the FRAP experiments. The lines passing through the points are single exponential curves except for fiber-FRAP. The line for fiber-FRAP is a bi-exponential curve. The FRAP graph was created using one exemplary experiment for each FRAP experiment. "*" in subfigure B corresponds to a solidified structure.

In order to confirm the liquid-like properties, it was necessary to measure the inner dynamics of MRPIP condensates (Figure8C, inner-FRAP). The measured half-time of the recovery was 1.6 (±0.6) seconds with 85% mobile fraction (Figure8D). To determine the mobile fraction of the fibers, the nucleoplasmic mobile fraction needed to be measured first. This was due to the small diameter of the fiber that causes the nucleoplasm to interfere with the calculations of the fiber-FRAP. The nucleoplasm was bleached as a circle with 3 µm radius and the calculated half-time of the recovery was around 0.5 (±0.15) seconds (Figure8C) . Our data indicate that the nucleoplasmic GFP-MPRIP moves by free diffusion, which is determined by the mobile fraction ~96% (Figure8D). The fiber-FRAP was performed and the half-times were determined as follows: fast fraction = 0.2 (± 0.15) seconds and slow fraction = 1.6 s. The data show two fractions. One corresponds to the free diffusion (nucleoplasmic-FRAP) and the second corresponds to the fiber itself. The mobile fraction of the fiber-FRAP was 45% (Figure8D).

Interestingly, the inner fraction of a fiber shows the same dynamics as the inner fraction of a condensate. However, the difference in the mobile fractions (inner-FRAP: 85%, fiber-FRAP: 45%) suggests that 40% of the immobile fraction is bound to an additional factor; presumably, to nuclear actin (see below) (Figure 8D).

3.7. MPRIP Fibers Contain Nuclear F-Actin

The results of FRAP experiments prompted us to further investigate the fibrous structures which presented an immobile fraction. Since MRPIP is an F-actin binding protein, we tested whether F-actin might be responsible for the immobile fraction of the

fibrous MPRIP structures [1]. To examine this process, GFP-MPRIP was overexpressed in U2OS cells for 24 h and were subsequently stained with phalloidin. Indeed, we observed that the actin fibers labelled by phalloidin were decorated by GFP-MRPIP (Figure 9A,B). This suggests that condensed MPRIP protein retains the F-binding capacity in nuclear environment. In Figure9A, the GFP-MPRIP condensates are aligned on fibers adopting an elongated shape that extrude thin, connecting lines localizing to the phalloidin labelled fibers. Furthermore, STED microscopy was employed on the cells presenting only GFP-MPRIP fibers (without the globular condensates) to visualize the structure in more detail that determined its thickness ranging from 150 to 250 nm (Figure9B).

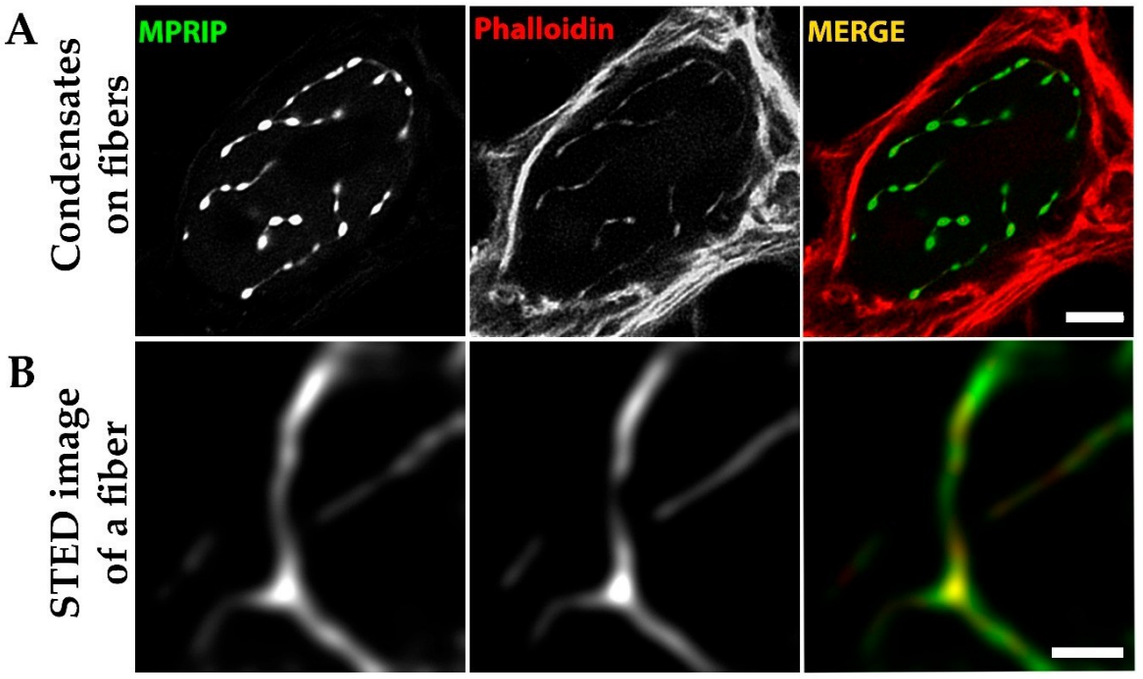

Figure 9. Phalloidin staining of the GFP-MPRIP overexpressing U2OS cells. Fixed GFP-MPRIP transfected cells were stained with phalloidin and investigated by confocal microscopy. (**A**) GFP-MPRIP condensates localized on phalloidin labelled fibers in cell nucleus. Scale bar represents 5 µm (**B**) GFP-MPRIP fibers visualized by STED microscopy. Blue is DAPI, green is GFP-MPRIP and red is the phalloidin staining. The scale bar represents 1 µm.

3.8. The C-Terminal IDR Domain Is Responsible for Phase Separation of MPRIP

To determine the regions that are responsible for MPRIP propensity for phase separation and fiber formation, we split MPRIP into two fragments. We prepared the GFP tagged constructs which comprise different domains (see Materials and Methods 2.2). The first fragment F1 consists of the N-terminal domain of MPRIP; carrying F-actin binding and the NLS region. The fragment F2 consists of the C-terminal domain, comprising a long IDR with regions that are known to interact with F-actin, regulating proteins such as PP1, MYPT1 and RhoA [8]. The fragments overexpressed in U2OS cells show a different cellular localization (Figure10). The F1 fragment contains NLS, thus mainly localizing to the nucleus. However, it also binds to the F-actin stress fibers (Figure10A). Moreover, the F1 fragment shows no sign of phase separation. The fragment F2 localizes only to the cytoplasm where it forms fibrous and globular structures reminiscent of those formed by phase separation (Figure10C). Interestingly, we also noticed that the F2 fragment was also able to bind to the F-actin cytoskeleton (Figure S5).

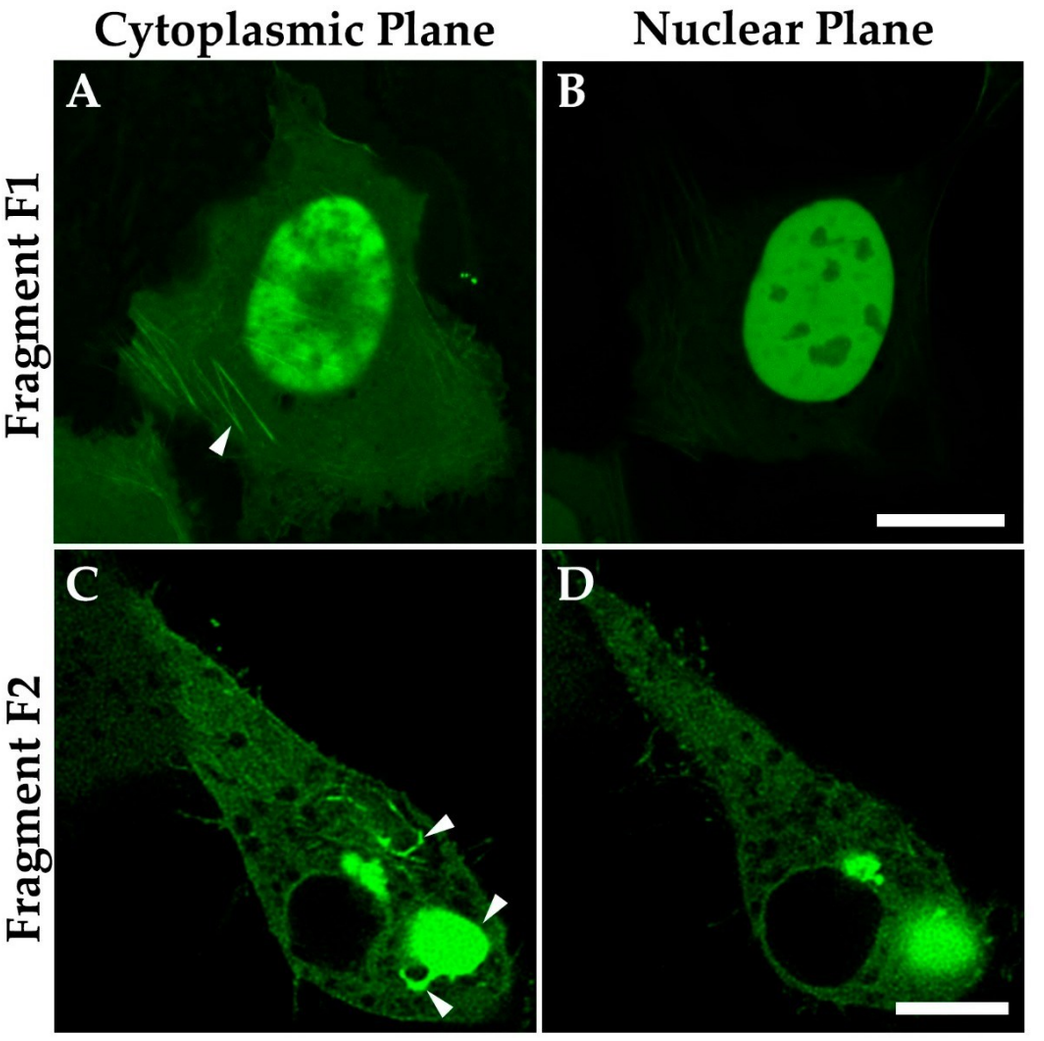

Figure 10. Confocal microscopy revealed the sub-cellular localization of the overexpressed GFP-MPRIP fragments F1 andF2. Fragment F1 localizing to (**A**) stress fibers and (**B**) to nucleus. Fragment F2 shows (**C**) globular and fibrous structures in the cytoplasm but not in the (**D**) nucleus. Scale bars represent 10 μm.

4. Discussion

PIP2, as the integral component of the cytoplasmic inner membrane leaf, is a crucial regulator of F-actin polymerization [44–46]. PIP2 regulates actin cortex, membrane tension, raft formation, endocytosis, motility and forms signaling hubs [47–50]. In the nucleus, PIP2 is an integral element of nuclear compartments which are involved in transcription, epigenetic regulation, the enzymatic activity of fibrillarin and presumably, mRNA splicing [12,13,51–54]. Recently, the nuclear PIP2 interactors were identified by an advanced quantitative mass spectrometry approach and showed that the polybasic K/R regions which are responsible for PIP2 interaction are a common feature of PIP2-effectors [4,55].

Initially, we showed that MPRIP is a nuclear protein that exists in two forms (Figure1B) which presumably represent different phosphorylation states due to a number of predicted phosphorylation sites (Figure S4). Our super-resolution microscopy followed by the statistical analysis of MPRIP spatial distribution showed that MPRIP localizes predominantly to PIP2-rich nuclear speckles and NLIs (Figure3D,G). NLIs were previously shown to be important for an active RNAPII transcription [12]. The PIP2 nuclear localization was visualized in unprecedented resolution using advanced super-resolution microscopy—direct stochastic optical reconstruction microscopy (dSTORM)— at nuclear speckles and NLIs where PIP2 was found in close proximity with the subset of RNAPII [56]. Furthermore,

we showed that the PH domain-containing MPRIP protein binds PIP2 in vitro and thus suggest the importance of PIP2 for its activity. These data suggest that MPRIP is a nuclear protein whose nuclear localization presumably depends on the PIP2.

Our immunoprecipitation experiments determined the unconventional myosin- MYO1C and the active RNAPII as the nuclear interactors of MPRIP (Figure4). MYO1C possess a C-terminal, PH-like domain which enables its binding to PIP2 [11,57,58]. An isoform of MYO1C termed NM1 was previously shown to be important for RNAPI and RNAPII mediated transcription [12,37,59]. Moreover, NM1 was defined as a transcription factor with the capacity to bind nuclear actin; a component of RNAPII pre-initiation complex and an important RNAPI regulator [59,60]. These data indicate a potential function for MPRIP in transcription regulation.

The overexpression of MPRIP induces the formation of granular nucleoplasmic foci and the spherical condensates depending on the time after transfection (Figure5A,B,D). The 1,6-hexandiol treatment showed that the condensates are formed by the phase separation (Figure6) and that these condensates display liquid-like properties (Figure7A and video S1) [24,43]. Further, we observed the formation of MPRIP fibers in the cell nucleus (Figure5C). We monitored these fibers for several hours and observed reformation of spherical condensates when fibers disassembled (Figure7B, Video S1). To the best of our knowledge, this is a novel behavior for phase-separated proteins that shows liquid-like properties even when bound to a fibrous structures (Figure9). Our FRAP data determined high mobility for MPRIP molecules within both structures—condensates and fibers (Figure8) . MPRIP condensates showed time-dependent solidification, as another intrinsic property of phase-separating proteins [24,61]. Moreover, the FRAP experiments showed that fibers contain a larger immobile fraction compare to spherical condensates. We assume that this immobile fraction indeed represents the MPRIP molecules bound to nuclear F-actin (Figure9).

The N-terminus of MPRIP contains the F-acting binding domain that covers one of the PH domains, the NLS region and the short IDR region interspaced between both PH domains [8]. In Figure10, we showed that the N-terminus region is responsible for MPRIP protein localization to the nucleus but not for its capacity to phase separate (Figure S1). Due to the overlap of PH and acting binding domains, we hypothesized that the binding of actin to MPRIP regulate PIP2-binding capacity and thus affects its nuclear localization. The impact of cytosolic/nuclear actin concentration equilibrium onto the MPRIP function remains elusive.

We showed that the C-terminal part of MPRIP is responsible for its phase separation. Interestingly, this fragment also showed to localize to cytosolic F-actin (Figure S5). This is contrary to in vitro observations of other authors showing that the C-terminal region is not responsible for a direct F-actin binding. However, it was shown to interact with actin regulators such as RhoA, MYPT1 and NUAK2 [2,3,6]. Therefore, we speculate that the C-terminal F-actin binding (Figure S5) and fiber formation (Figure10) is mediated indirectly through these factors.

Nuclear actin is an enigmatic factor which was identified as an interactor of a plethora of nuclear proteins such as transcriptional factors [11,62–65]. However, the nuclear F-actin formation is shown to be crucial for the relocalization of heterochromatin breaks and were associated with chromatin-modifying enzymes such as deacetylases, acetyltransferases and DNA repair factors [66,67]. Moreover, the formation of nuclear actin fibers is associated with defects in nuclear topology and RNAPII relocalization [68]. We observed the production of the nuclear MPRIP fibers when the formation of nuclear F-actin was stimulated by heat shock (Figure S6) [1]. Therefore, the formed nuclear F-actin might attract MPRIP and thus alter the RNAPII transcription.

In conclusion, we provided evidence for the presence of MPRIP, an actin regulatory protein, in cell nucleus. The MPRIP protein localizes to nuclear PIP2-rich sub-compartments and it was identified as a component of the RNAPII/NM1 complex. The expression of this protein leads to the formation of phase-separated condensates that are able to bind nuclear

F-actin fibers. We showed that this binding is reversible and the spherical condensates can reform when fibers disappear (summary in Figure11). These data suggest that the PIP2-associated RNAPII transcription might be regulated by phase separation that is dependent on nuclear actin polymerization.

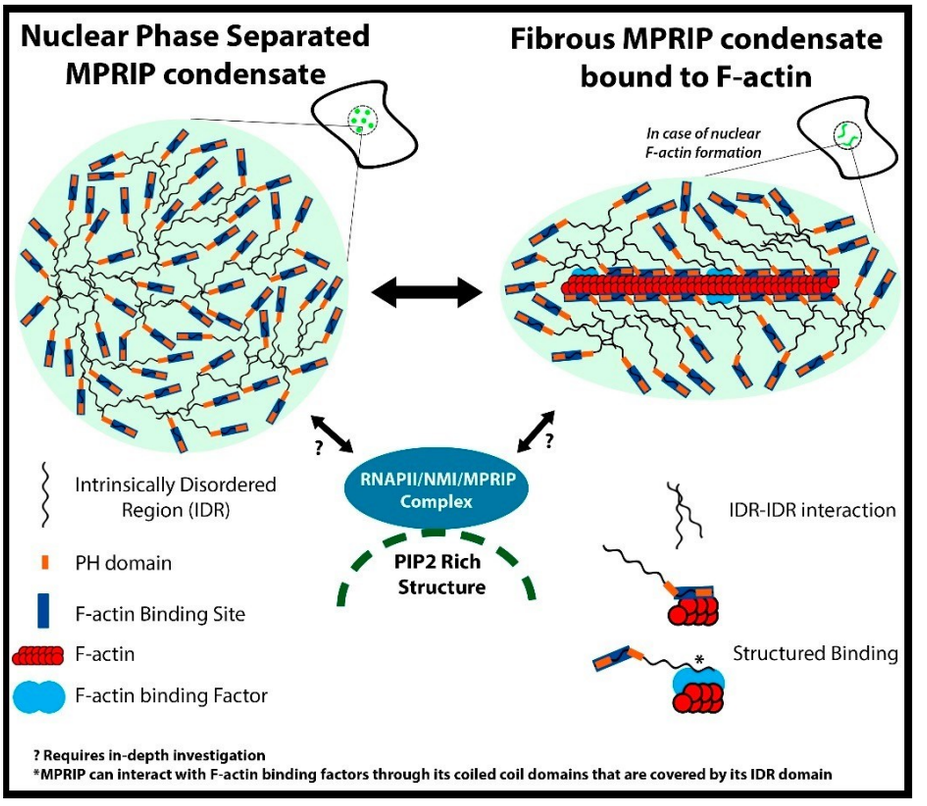

Figure 11. Illustration of the hypothetical model of interplay between MPRIP phase separation and its interactors. RNAPII/NMI/MPRIP complex localizes in the proximity of nuclear PIP2-rich structures. The MPRIP protein contains two PH domains, an F-actin binding site and C-terminal IDR. MPRIP is able to form phase-separated condensates through IDR interactions. These condensates can form fibers when associated with nuclear F-actin. (*) This association is mediated either by intrinsic MPRIP F-actin-binding site or by other F-actin binding factors. (?) It remains unclear how MPRIP/RNAPII/NM1/PIP2 complex formation depends on the phase separation, actin polymerization or association with PIP2-rich nuclear structures. It also needs further clarification as to how these processes orchestrate the MPRIP-mediated regulation of RNAPII activity and the consequent transcriptional output of the cell.

Supplementary Materials: The following are available online athttps://www.mdpi.com/article/10.3390/cells10040848/s1, Figure S1: Predicted NLS sequence of MPRIP protein. Figure S2: Clustal Omega test on eight mammalian MPRIP sequences, Figure S3: Structure Determination and IDR of MPRIP Human Isoform 3. Figure S4: Post translational modification sites of MPRIP Human Isoform 3. Figure S5: Fragment F2 of MPRIP localize to actin stress fibers, Figure S6: Heat Shock treatment of the stable cell line. Video s1: Live cell imaging of a cell overexpressing GFP-MPRIP.

Author Contributions: C.B. designed the research, performed all experiments, analyzed and interpreted the data, and wrote the manuscript; M.S. conceptualized the project, analyzed and interpreted the data; M.B. performed the FRAP analysis and interpreted the data; P.H. provided supervision and funding acquisition. All authors have read and approved the manuscript.

Funding: This study was supported by the Grant Agency of the Czech Republic (19-05608S, 18-19714S), the Czech Academy of Sciences (JSPS-20-06), by the institutional support (RVO: 68378050), European Regional Development Fund-Project (No. CZ.02.1.01/0.0/0.0/16_013/0001775), and by

the project "BIOCEV—Biotechnology and Biomedicine Centre of the Academy of Sciences and Charles University"; (CZ.1.05/1.1.00/02.0109), from the European Regional Development Fund. We acknowledge the Ministry of Education, Youth and Sports of the Czech Republic COST Inter-Excellence Internship (LTC19048 and LTC20024), EuroCellNet COST Action (CA15214) and the Microscopy Centre, Light/Electron Microscopy CF, IMG AS, Prague, Czech Republic, supported by MEYS CR (Large RI Project LM2018129 Czech-BioImaging).

Institutional Review Board Statement: Not applicable.

Informed Consent Statement: Not applicable.

Data Availability Statement: Data is contained within the article or Supplementary Materials.

Acknowledgments: We are very grateful to Tomi P. Mäkelä at THE University of Helsinki for providing us the pDEST53 GFP-MPRIP (Human Isoform 3 of MPRIP) plasmid. We thank Peter Gillespie and Piergiorgio Percipalle for providing the MYO1C antibody. We appreciate the relentless technical support provided by Pavel Krˇíž and for the support in cell culture; as well as Iva Jelínková. We are also grateful to Ivan Novotný for his technical support in super resolution microscopy and Martin Čapek for his help in analyzing the STED data.

Conflicts of Interest: The authors declare no conflict of interest.

References

1. Mulder, J.; Poland, M.; Gebbink, M.F.; Calafat, J.; Moolenaar, W.H.; Kranenburg, O. p116Rip is a novel filamentous actin-binding protein. *J. Biol. Chem.* **2003**, *278*, 27216–27223. [CrossRef]
2. Vallenius, T.; Vaahtomeri, K.; Kovac, B.; Osiceanu, A.M.; Viljanen, M.; Makela, T.P. An association between NUAK2 and MRIP reveals a novel mechanism for regulation of actin stress fibers. *J. Cell Sci.* **2011**, *124 Pt 3*, 384–393. [CrossRef]
3. Koga, Y.; Ikebe, M. p116Rip Decreases Myosin II Phosphorylation by Activating Myosin Light Chain Phosphatase and by Inactivating RhoA. *J. Biol. Chem.* **2005**, *280*, 4983–4991. [CrossRef]
4. Sztacho, M.; Salovska, B.; Cervenka, J.; Balaban, C.; Hoboth, P.; Hozak, P. Limited Proteolysis-Coupled Mass Spectrometry Identifies Phosphatidylinositol 4,5-Bisphosphate Effectors in Human Nuclear Proteome. *Cells* **2021**, *10*, 68. [CrossRef]
5. Mulder, J.; Ariaens, A.; van den Boomen, D.; Moolenaar, W.H. p116Rip targets myosin phosphatase to the actin cytoskeleton and is essential for RhoA/ROCK-regulated neuritogenesis. *Mol. Biol. Cell* **2004**, *15*, 5516–5527. [CrossRef] [PubMed]
6. Mulder, J.; Ariaens, A.; van Horck, F.P.G.; Moolenaar, W.H. Inhibition of RhoA-mediated SRF activation by p116Rip. *FEBS Lett.* **2005**, *579*, 6121–6127. [CrossRef]
7. Surks, H.K.; Riddick, N.; Ohtani, K. M-RIP Targets Myosin Phosphatase to Stress Fibers to Regulate Myosin Light Chain Phosphorylation in Vascular Smooth Muscle Cells. *J. Biol. Chem.* **2005**, *280*, 42543–42551. [CrossRef]
8. Surks, H.K.; Richards, C.T.; Mendelsohn, M.E. Myosin Phosphatase-Rho Interacting Protein a New Member of the Myosin Phosphatase Complex that Directly Binds RhoA. *J. Biol. Chem.* **2003**, *278*, 51484–51493. [CrossRef] [PubMed]
9. Yamamoto, E.; Kalli, A.C.; Yasuoka, K.; Sansom, M.S.P. Interactions of Pleckstrin Homology Domains with Membranes: Adding Back the Bilayer via High-Throughput Molecular Dynamics. *Structure* **2016**, *24*, 1421–1431. [CrossRef] [PubMed]
10. Almuzzaini, B.; Sarshad, A.A.; Farrants, A.K.; Percipalle, P. Nuclear myosin 1 contributes to a chromatin landscape compatible with RNA polymerase II transcription activation. *BMC Biol.* **2015**, *13*, 35. [CrossRef]
11. Nevzorov, I.; Sidorenko, E.; Wang, W.; Zhao, H.; Vartiainen, M.K. Myosin-1C uses a novel phosphoinositide-dependent pathway for nuclear localization. *EMBO Rep.* **2018**, *19*, 290–304. [CrossRef]
12. Sobol, M.; Krausova, A.; Yildirim, S.; Kalasova, I.; Faberova, V.; Vrkoslav, V.; Philimonenko, V.; Marasek, P.; Pastorek, L.; Capek, M.; et al. Nuclear phosphatidylinositol 4,5-bisphosphate islets contribute to efficient RNA polymerase II-dependent transcription. *J. Cell Sci.* **2018**, *131*. [CrossRef]
13. Castano, E.; Yildirim, S.; Fáberová, V.; Krausová, A.; Uličná, L.; Paprčková, D.; Sztacho, M.; Hozák, P. Nuclear Phosphoinositides—Versatile Regulators of Genome Functions. *Cells* **2019**, *8*, 649. [CrossRef]
14. Sztacho, M.; Sobol, M.; Balaban, C.; Escudeiro Lopes, S.E.; Hozak, P. Nuclear phosphoinositides and phase separation: Important players in nuclear compartmentalization. *Adv. Biol. Regul.* **2019**, *71*, 111–117. [CrossRef]
15. Boehning, M.; Dugast-Darzacq, C.; Rankovic, M.; Hansen, A.S.; Yu, T.; Marie-Nelly, H.; McSwiggen, D.T.; Kokic, G.; Dailey, G.M.; Cramer, P.; et al. RNA polymerase II clustering through carboxy-terminal domain phase separation. *Nat. Struct. Mol. Biol.* **2018**, *25*, 833–840. [CrossRef]
16. Cho, W.K.; Spille, J.H.; Hecht, M.; Lee, C.; Li, C.; Grube, V.; Cisse, I.I. Mediator and RNA polymerase II clusters associate in transcription-dependent condensates. *Science* **2018**, *361*, 412–415. [CrossRef]
17. Lu, H.; Yu, D.; Hansen, A.S.; Ganguly, S.; Liu, R.; Heckert, A.; Darzacq, X.; Zhou, Q. Phase-separation mechanism for C-terminal hyperphosphorylation of RNA polymerase II. *Nature* **2018**, *558*, 318–323. [CrossRef]
18. Banani, S.F.; Rice, A.M.; Peeples, W.B.; Lin, Y.; Jain, S.; Parker, R.; Rosen, M.K. Compositional Control of Phase-Separated Cellular Bodies. *Cell* **2016**, *166*, 651–663. [CrossRef] [PubMed]

19. Feric, M.; Vaidya, N.; Harmon, T.S.; Mitrea, D.M.; Zhu, L.; Richardson, T.M.; Kriwacki, R.W.; Pappu, R.V.; Brangwynne, C.P. Coexisting liquid phases underlie nucleolar sub-compartments. *Cell* **2016**, *165*, 1686–1697. [CrossRef] [PubMed]
20. Sawyer, I.A.; Bartek, J.; Dundr, M. Phase separated microenvironments inside the cell nucleus are linked to disease and regulate epigenetic state, transcription and RNA processing. *Semin. Cell Dev. Biol.* **2019**, *90*, 94–103. [CrossRef] [PubMed]
21. Strom, A.R.; Brangwynne, C.P. The liquid nucleome–phase transitions in the nucleus at a glance. *J. Cell Sci.* **2019**, *132*, jcs235093. [CrossRef]
22. Alberti, S.; Gladfelter, A.; Mittag, T. Considerations and challenges in studying liquid-liquid phase separation and biomolecular condensates. *Cell* **2019**, *176*, 419–434. [CrossRef]
23. Feng, Z.; Chen, X.; Wu, X.; Zhang, M. Formation of biological condensates via phase separation: Characteristics, analytical methods, and physiological implications. *J. Biol. Chem.* **2019**, *294*, 14823–14835. [CrossRef] [PubMed]
24. Wang, J.; Choi, J.-M.; Holehouse, A.S.; Lee, H.O.; Zhang, X.; Jahnel, M.; Maharana, S.; Lemaitre, R.; Pozniakovsky, A.; Drechsel, D.; et al. A Molecular Grammar Governing the Driving Forces for Phase Separation of Prion-like RNA Binding Proteins. *Cell* **2018**, *174*, 688–699.e16. [CrossRef]
25. Alberti, S. Phase separation in biology. *Curr. Biol.* **2017**, *27*, R1097–R1102. [CrossRef] [PubMed]
26. Hyman, A.A.; Weber, C.A.; Jülicher, F. Liquid-Liquid Phase Separation in Biology. *Annu. Rev. Cell Dev. Biol.* **2014**, *30*, 39–58. [CrossRef]
27. Nowak, G.; Pestic-Dragovich, L.; Hozak, P.; Philimonenko, A.; Simerly, C.; Schatten, G.; de Lanerolle, P. Evidence for the presence of myosin I in the nucleus. *J. Biol. Chem.* **1997**, *272*, 17176–17181. [CrossRef]
28. Pestic-Dragovich, L.; Stojiljkovic, L.; Philimonenko, A.A.; Nowak, G.; Ke, Y.; Settlage, R.E.; Shabanowitz, J.; Hunt, D.F.; Hozak, P.; de Lanerolle, P. A myosin I isoform in the nucleus. *Science* **2000**, *290*, 337–341. [CrossRef]
29. Dumont, R.A.; Zhao, Y.D.; Holt, J.R.; Bahler, M.; Gillespie, P.G. Myosin-I isozymes in neonatal rodent auditory and vestibular epithelia. *J. Assoc. Res. Otolaryngol.* **2002**, *3*, 375–389. [CrossRef]
30. Kosugi, S.; Hasebe, M.; Tomita, M.; Yanagawa, H. Systematic identification of cell cycle-dependent yeast nucleocytoplasmic shuttling proteins by prediction of composite motifs. *Proc. Natl. Acad. Sci. USA* **2009**, *106*, 10171–10176. [CrossRef]
31. Madeira, F.; Park, Y.M.; Lee, J.; Buso, N.; Gur, T.; Madhusoodanan, N.; Basutkar, P.; Tivey, A.R.N.; Potter, S.C.; Finn, R.D.; et al. The EMBL-EBI search and sequence analysis tools APIs in 2019. *Nucleic Acids Res.* **2019**, *47*, W636–W641. [CrossRef]
32. Oates, M.E.; Romero, P.; Ishida, T.; Ghalwash, M.; Mizianty, M.J.; Xue, B.; Dosztanyi, Z.; Uversky, V.N.; Obradovic, Z.; Kurgan, L.; et al. D(2)P(2): Database of disordered protein predictions. *Nucleic Acids Res.* **2013**, *41*, D508–D516. [CrossRef]
33. Dunn, K.W.; Kamocka, M.M.; McDonald, J.H. A practical guide to evaluating colocalization in biological microscopy. *Am. J. Physiol. Cell Physiol.* **2011**, *300*, C723–C742. [CrossRef]
34. Trinkle-Mulcahy, L.; Boulon, S.; Lam, Y.W.; Urcia, R.; Boisvert, F.M.; Vandermoere, F.; Morrice, N.A.; Swift, S.; Rothbauer, U.; Leonhardt, H.; et al. Identifying specific protein interaction partners using quantitative mass spectrometry and bead proteomes. *J. Cell Biol.* **2008**, *183*, 223–239. [CrossRef] [PubMed]
35. Hein, M.Y.; Hubner, N.C.; Poser, I.; Cox, J.; Nagaraj, N.; Toyoda, Y.; Gak, I.A.; Weisswange, I.; Mansfeld, J.; Buchholz, F.; et al. A human interactome in three quantitative dimensions organized by stoichiometries and abundances. *Cell* **2015**, *163*, 712–723.[CrossRef] [PubMed]
36. Shah, Z.H.; Jones, D.R.; Sommer, L.; Foulger, R.; Bultsma, Y.; D'Santos, C.; Divecha, N. Nuclear phosphoinositides and their impact on nuclear functions. *FEBS J.* **2013**, *280*, 6295–6310. [CrossRef]
37. Yildirim, S.; Castano, E.; Sobol, M.; Philimonenko, V.V.; Dzijak, R.; Venit, T.; Hozak, P. Involvement of phosphatidylinositol 4,5-bisphosphate in RNA polymerase I transcription. *J. Cell Sci.* **2013**, *126 Pt 12*, 2730–2739. [CrossRef]
38. Kroschwald, S.; Maharana, S.; Mateju, D.; Malinovska, L.; Nüske, E.; Poser, I.; Richter, D.; Alberti, S. Promiscuous interactions and protein disaggregases determine the material state of stress-inducible RNP granules. *eLife* **2015**, *4*, e06807. [CrossRef]
39. Patel, S.S.; Belmont, B.J.; Sante, J.M.; Rexach, M.F. Natively Unfolded Nucleoporins Gate Protein Diffusion across the Nuclear Pore Complex. *Cell* **2007**, *129*, 83–96. [CrossRef] [PubMed]
40. Kato, M.; McKnight, S.L. A Solid-State Conceptualization of Information Transfer from Gene to Message to Protein. *Annu. Rev. Biochem.* **2018**, *87*, 351–390. [CrossRef]
41. Nair, S.J.; Yang, L.; Meluzzi, D.; Oh, S.; Yang, F.; Friedman, M.J.; Wang, S.; Suter, T.; Alshareedah, I.; Gamliel, A.; et al. Phase separation of ligand-activated enhancers licenses cooperative chromosomal enhancer assembly. *Nat. Struct. Mol. Biol.* **2019**, *26*, 193–203. [CrossRef]
42. Lin, Y.; Mori, E.; Kato, M.; Xiang, S.; Wu, L.; Kwon, I.; McKnight, S.L. Toxic PR Poly-Dipeptides Encoded by the C9orf72 RepeatExpansion Target LC Domain Polymers. *Cell* **2016**, *167*, 789–802.e12. [CrossRef]
43. Brangwynne, C.P.; Eckmann, C.R.; Courson, D.S.; Rybarska, A.; Hoege, C.; Gharakhani, J.; Jülicher, F.; Hyman, A.A. Germline P Granules Are Liquid Droplets that Localize by Controlled Dissolution/Condensation. *Science* **2009**, *324*, 1729–1732. [CrossRef]
44. Yamamoto, M.; Hilgemann, D.H.; Feng, S.; Bito, H.; Ishihara, H.; Shibasaki, Y.; Yin, H.L. Phosphatidylinositol 4,5-bisphosphate induces actin stress-fiber formation and inhibits membrane ruffling in CV1 cells. *J. Cell Biol.* **2001**, *152*, 867–876. [CrossRef]
45. Shibasaki, Y.; Ishihara, H.; Kizuki, N.; Asano, T.; Oka, Y.; Yazaki, Y. Massive actin polymerization induced by phosphatidylinositol-4-phosphate 5-kinase in vivo. *J. Biol. Chem.* **1997**, *272*, 7578–7581. [CrossRef]

46. Chen, F.; Ma, L.; Parrini, M.C.; Mao, X.; Lopez, M.; Wu, C.; Marks, P.W.; Davidson, L.; Kwiatkowski, D.J.; Kirchhausen, T.; et al. Cdc42 is required for PIP(2)-induced actin polymerization and early development but not for cell viability. *Curr. Biol.* **2000**, *10*,758–765. [CrossRef]
47. Tsujita, K.; Itoh, T. Phosphoinositides in the regulation of actin cortex and cell migration. *Biochim. Biophys. Acta* **2015**, *1851*, 824–831. [CrossRef]
48. Riggi, M.; Niewola-Staszkowska, K.; Chiaruttini, N.; Colom, A.; Kusmider, B.; Mercier, V.; Soleimanpour, S.; Stahl, M.; Matile, S.; Roux, A.; et al. Decrease in plasma membrane tension triggers PtdIns(4,5)P2 phase separation to inactivate TORC2. *Nat. Cell Biol.* **2018**, *20*, 1043–1051. [CrossRef]
49. Sztacho, M.; Segeletz, S.; Sanchez-Fernandez, M.A.; Czupalla, C.; Niehage, C.; Hoflack, B. BAR Proteins PSTPIP1/2 Regulate Podosome Dynamics and the Resorption Activity of Osteoclasts. *PLoS ONE* **2016**, *11*, e0164829. [CrossRef]
50. Yamaguchi, H.; Shiraishi, M.; Fukami, K.; Tanabe, A.; Ikeda-Matsuo, Y.; Naito, Y.; Sasaki, Y. MARCKS regulates lamellipodia formation induced by IGF-I via association with PIP2 and beta-actin at membrane microdomains. *J. Cell. Physiol.* **2009**, *220*, 748–755. [CrossRef]
51. Sobol, M.; Yildirim, S.; Philimonenko, V.V.; Marášek, P.; Castaño, E.; Hozák, P. UBF complexes with phosphatidylinositol 4,5-bisphosphate in nucleolar organizer regions regardless of ongoing RNA polymerase I activity. *Nucleus* **2013**, *4*, 478–486. [CrossRef]
52. Ulicna, L.; Kalendova, A.; Kalasova, I.; Vacik, T.; Hozák, P. PIP2 epigenetically represses rRNA genes transcription interacting with PHF8. *Biochim. Biophys. Acta Mol. Cell Biol. Lipids* **2018**, *1863*, 266–275. [CrossRef] [PubMed]
53. Bavelloni, A.; Faenza, I.; Cioffi, G.; Piazzi, M.; Parisi, D.; Matic, I.; Maraldi, N.M.; Cocco, L. Proteomic-based analysis of nuclear signaling: PLCbeta1 affects the expression of the splicing factor SRp20 in Friend erythroleukemia cells. *Proteomics* **2006**, *6*, 5725–5734. [CrossRef]
54. Faenza, I.; Ramazzotti, G.; Bavelloni, A.; Fiume, R.; Gaboardi, G.C.; Follo, M.Y.; Gilmour, R.S.; Martelli, A.M.; Ravid, K.; Cocco, L. Inositide-dependent phospholipase C signaling mimics insulin in skeletal muscle differentiation by affecting specific regions of the cyclin D3 promoter. *Endocrinology* **2007**, *148*, 1108–1117. [CrossRef]
55. Lewis, A.E.; Sommer, L.; Arntzen, M.O.; Strahm, Y.; Morrice, N.A.; Divecha, N.; D'Santos, C.S. Identification of nuclear phosphatidylinositol 4,5-bisphosphate-interacting proteins by neomycin extraction. *Mol. Cell Proteomics* **2011**, *10*, M110.003376. [CrossRef]
56. Hoboth, P.; Sztacho, M.; Sebesta, O.; Schatz, M.; Castano, E.; Hozak, P. Nanoscale mapping of nuclear phosphatidylinositol phosphate landscape by dual-color dSTORM. *Biochim. Biophys. Acta Mol. Cell Biol. Lipids* **2021**, 158890. [CrossRef]
57. Hokanson, D.E.; Laakso, J.M.; Lin, T.; Sept, D.; Ostap, E.M. Myo1c binds phosphoinositides through a putative pleckstrin homology domain. *Mol. Biol. Cell* **2006**, *17*, 4856–4865. [CrossRef]
58. Hokanson, D.E.; Ostap, E.M. Myo1c binds tightly and specifically to phosphatidylinositol 4,5-bisphosphate and inositol 1,4,5-trisphosphate. *Proc. Nat. Acad. Sci. USA* **2006**, *103*, 3118–3123. [CrossRef]
59. Philimonenko, V.V.; Zhao, J.; Iben, S.; Dingova, H.; Kysela, K.; Kahle, M.; Zentgraf, H.; Hofmann, W.A.; de Lanerolle, P.; Hozak, P.; et al. Nuclear actin and myosin I are required for RNA polymerase I transcription. *Nat. Cell Biol.* **2004**, *6*, 1165–1172. [CrossRef]
60. Ye, J.; Zhao, J.; Hoffmann-Rohrer, U.; Grummt, I. Nuclear myosin I acts in concert with polymeric actin to drive RNA polymerase I transcription. *Genes Dev.* **2008**, *22*, 322–330. [CrossRef]
61. Yu, Y.; Reed, R. FUS functions in coupling transcription to splicing by mediating an interaction between RNAP II and U1 snRNP. *Proc. Nat. Acad. Sci. USA* **2015**, *112*, 8608–8613. [CrossRef]
62. Kristo, I.; Bajusz, C.; Borsos, B.N.; Pankotai, T.; Dopie, J.; Jankovics, F.; Vartiainen, M.K.; Erdelyi, M.; Vilmos, P. The actin binding cytoskeletal protein Moesin is involved in nuclear mRNA export. *Biochim. Biophys. Acta Mol. Cell Res.* **2017**, *1864*, 1589–1604.[CrossRef] [PubMed]
63. Sokolova, M.; Moore, H.M.; Prajapati, B.; Dopie, J.; Merilainen, L.; Honkanen, M.; Matos, R.C.; Poukkula, M.; Hietakangas, V.; Vartiainen, M.K. Nuclear Actin Is Required for Transcription during Drosophila Oogenesis. *iScience* **2018**, *9*, 63–70. [CrossRef]
64. Viita, T.; Kyheroinen, S.; Prajapati, B.; Virtanen, J.; Frilander, M.J.; Varjosalo, M.; Vartiainen, M.K. Nuclear actin interactome analysis links actin to KAT14 histone acetyl transferase and mRNA splicing. *J. Cell Sci.* **2019**, *132*. [CrossRef] [PubMed]
65. Venit, T.; Semesta, K.; Farrukh, S.; Endara-Coll, M.; Havalda, R.; Hozak, P.; Percipalle, P. Nuclear myosin 1 activates p21 gene transcription in response to DNA damage through a chromatin-based mechanism. *Commun. Biol.* **2020**, *3*, 115. [CrossRef] [PubMed]
66. Caridi, C.P.; D'Agostino, C.; Ryu, T.; Zapotoczny, G.; Delabaere, L.; Li, X.; Khodaverdian, V.Y.; Amaral, N.; Lin, E.; Rau, A.R.; et al. Nuclear F-actin and myosins drive relocalization of heterochromatic breaks. *Nature* **2018**, *559*, 54–60. [CrossRef]
67. Hurst, V.; Shimada, K.; Gasser, S.M. Nuclear Actin and Actin-Binding Proteins in DNA Repair. *Trends Cell Biol.* **2019**, *29*, 462–476. [CrossRef]
68. Serebryannyy, L.A.; Parilla, M.; Annibale, P.; Cruz, C.M.; Laster, K.; Gratton, E.; Kudryashov, D.; Kosak, S.T.; Gottardi, C.J.; de Lanerolle, P. Persistent nuclear actin filaments inhibit transcription by RNA polymerase II. *J. Cell Sci.* **2016**, *129*, 3412–3425. [CrossRef]

cells

MDPI

Supplementary Information

The F-Actin-Binding MPRIP Forms Phase-Separated Condensates and Associates with PI(4,5)P2 and Active RNA Polymerase II in the Cell Nucleus

Can Balaban[1], Martin Sztacho[1], Michaela Blažíková [2] and Pavel Hozák [1,2,*]

[1] Department of Biology of the Cell Nucleus, Institute of Molecular Genetics of the Czech Academy of Sciences, v.v.i., 142 20, Prague, Czech Republic
[2] Microscopy Centre, Institute of Molecular Genetics of the Czech Academy of Sciences, v.v.i., 142 20, Prague, Czech Republic
***** Correspondence: hozak@img.cas.cz; Received:

date; Accepted: date; Published: date

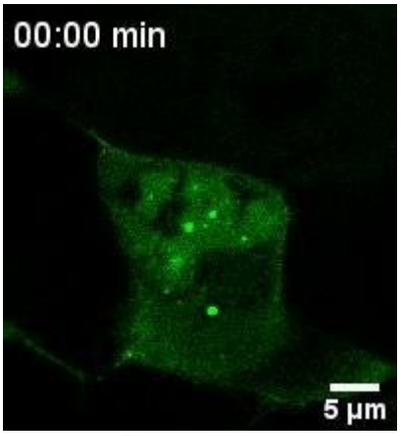

Video S1: **Live cell imaging of a cell overexpressing GFP-MPRIP**. The video was recorded approximately for 8 hours, imaging one frame per 5 minutes (for details, see MM). The cell shows many GFP-MPRIP condensates in nucleus and a few in cytoplasm. These condensates change their shape to fibers at the 4th hour of the video, which corresponds to 14th hour after transfection. Bar shows 5 µm. The frame rate of the video is 5 frame per second.

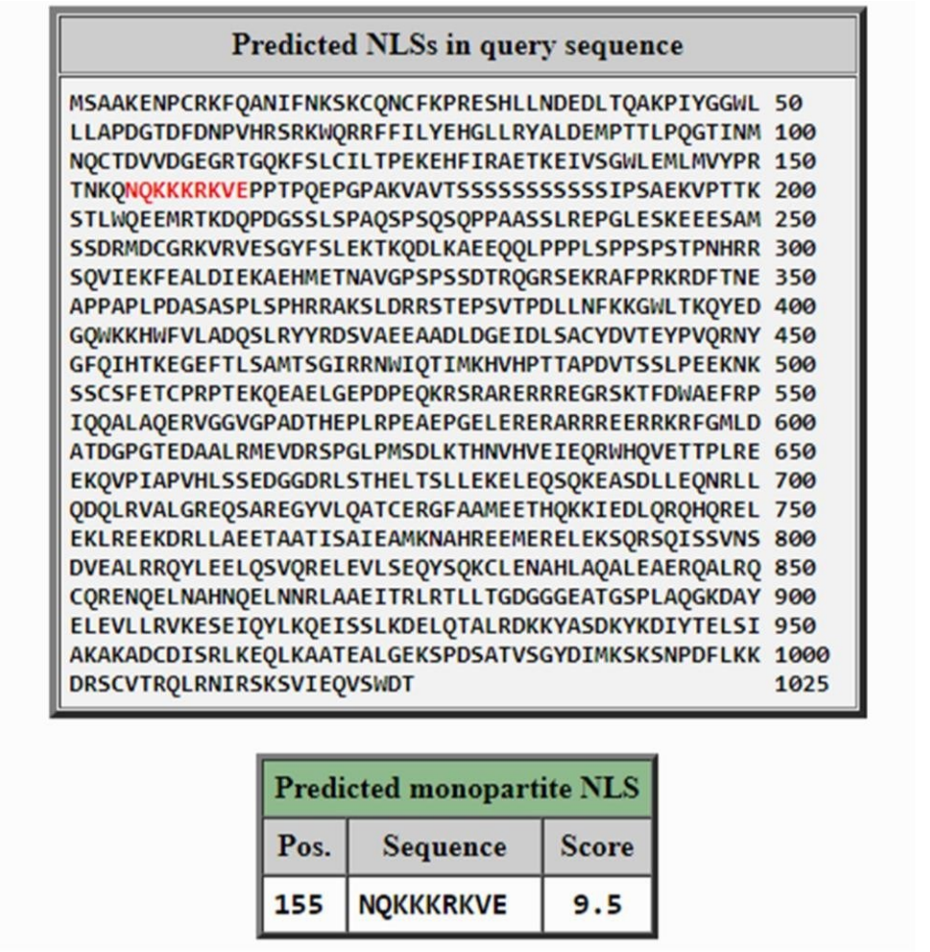

Predicted NLSs in query sequence

```
MSAAKENPCRKFQANIFNKSKCQNCFKPRESHLLNDEDLTQAKPIYGGWL  50
LLAPDGTDFDNPVHRSRKWQRRFFILYEHGLLRYALDEMPTTLPQGTINM 100
NQCTDVVDGEGRTGQKFSLCILTPEKEHFIRAETKEIVSGWLEMLMVYPR 150
TNKQNQKKKRKVEPPTPQEPGPAKVAVTSSSSSSSSSSIPSAEKVPTTK 200
STLWQEEMRTKDQPDGSSLSPAQSPSQSQPPAASSLREPGLESKEEESAM 250
SSDRMDCGRKVRVESGYFSLEKTKQDLKAEEQQLPPPLSPPSPSTPNHRR 300
SQVIEKFEALDIEKAEHMETNAVGPSPSSDTRQGRSEKRAFPRKRDFTNE 350
APPAPLPDASASPLSPHRRAKSLDRRSTEPSVTPDLLNFKKGWLTKQYED 400
GQWKKHWFVLADQSLRYYRDSVAEEAADLDGEIDLSACYDVTEYPVQRNY 450
GFQIHTKEGEFTLSAMTSGIRRNWIQTIMKHVHPTTAPDVTSSLPEEKNK 500
SSCSFETCPRPTEKQEAELGEPDPEQKRSRARERRREGRSKTFDWAEFRP 550
IQQALAQERVGGVGPADTHEPLRPEAEPGELERERARRREERRKRFGMLD 600
ATDGPGTEDAALRMEVDRSPGLPMSDLKTHNVHVEIEQRWHQVETTPLRE 650
EKQVPIAPVHLSSEDGGDRLSTHELTSLLEKELEQSQKEASDLLEQNRLL 700
QDQLRVALGREQSAREGYVLQATCERGFAAMEETHQKKIEDLQRQHQREL 750
EKLREEKDRLLAEETAATISAIEAMKNAHREEMERELEKSQRSQISSVNS 800
DVEALRRQYLEELQSVQRELEVLSEQYSQKCLENAHLAQALEAERQALRQ 850
CQRENQELNAHNQELNNRLAAEITRLRTLLTGDGGGEATGSPLAQGKDAY 900
ELEVLLRVKESEIQYLKQEISSLKDELQTALRDKKYASDKYKDIYTELSI 950
AKAKADCDISRLKEQLKAATEALGEKSPDSATVSGYDIMKSKSNPDFLKK 1000
DRSCVTRQLRNIRSKSVIEQVSWDT                           1025
```

Predicted monopartite NLS

Pos.	Sequence	Score
155	NQKKKRKVE	9.5

Figure S1: Predicted NLS sequence of MPRIP protein. The cNLS Mapper prediction tool shows a monopartite NLS sequence covering amino acids in position 155 to 164. The strength of the prediction is: 9.5/10.

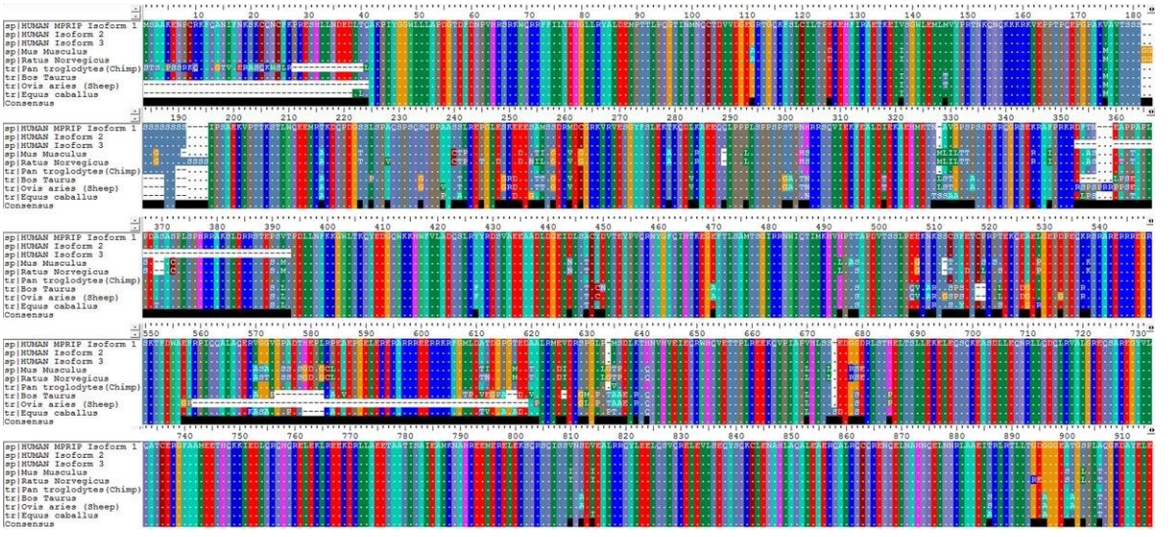

Figure S2: Clustal Omega test on eight mammalian MPRIP sequences. The first three sequences are the human isofroms of MPRIP, followed by orthologues from Mus Musculus (House mouse), Ratus Norvegicus (Brown Rat), Pan troglodytes (Chimpanzee), Bos Taurus

(Bovine), Ovis aries (Sheep) and Equus caballus (Horse). The last sequence is the consensus generated by pairwise sequence alignment provided by EMBL-EBI servers. Each amino acid is color coded where identical amino acids are shown as "." and missing amino acid in a sequence were indicated with a "- ". Missing or different amino acid in any of the eight mammalian sequences result a dark gap in the consensus sequence.

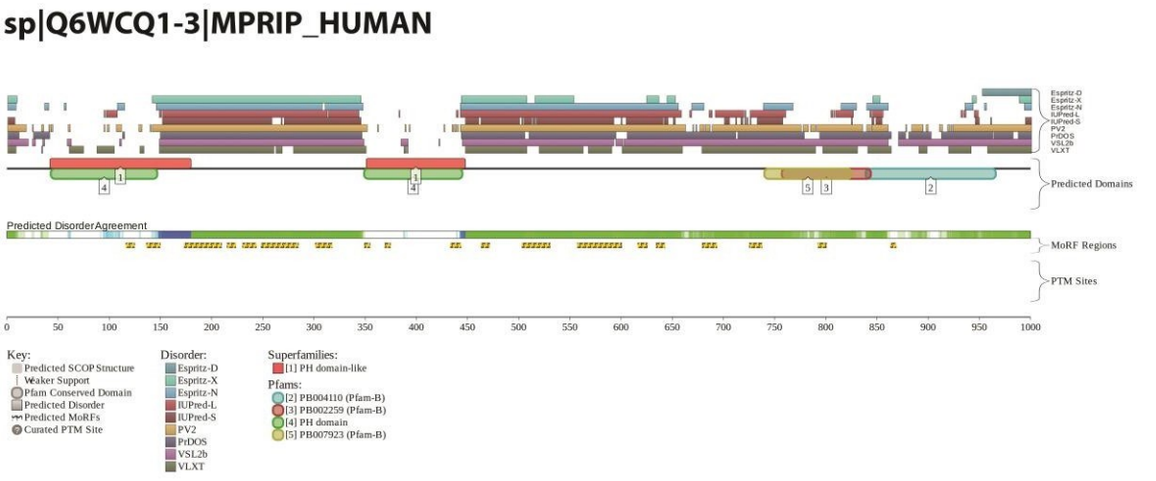

Figure S3: **Structure Determination and IDR of MPRIP Human Isoform 3.** Above, the schematic presentation of MPRIP shows the two PH domains and three coiled-coil (Pfam B) domains. The IDR prediction is generated by D2P2 database of disordered protein predictions that run a battery of disorder predictors: VL-XT, VSL2b, PrDOS, PV2, Espritz and IUPred.

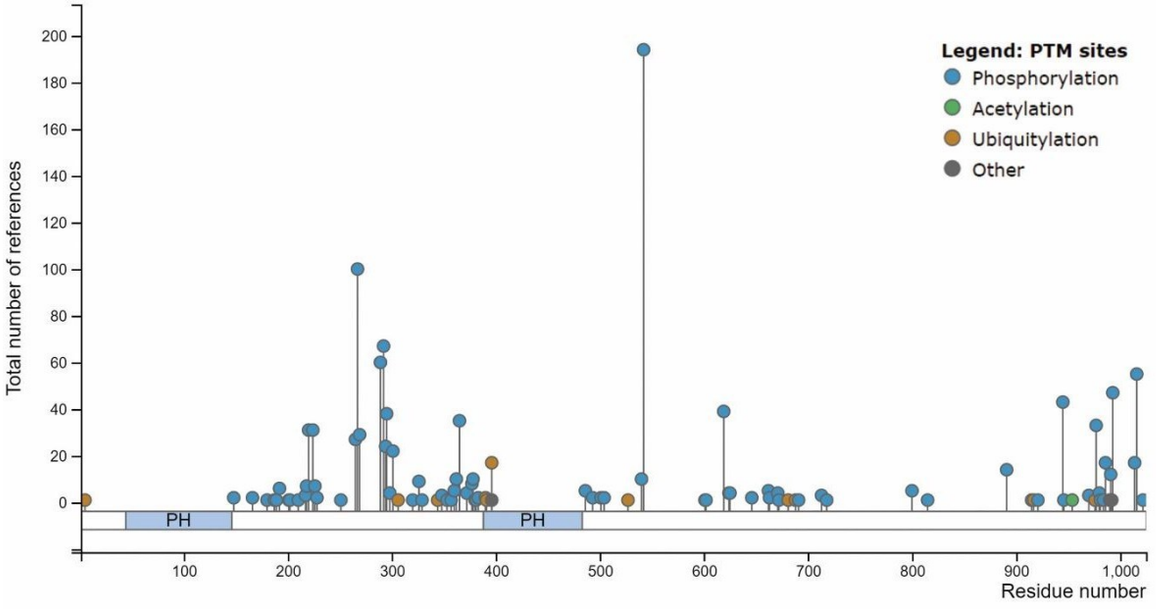

Figure S4: Post-translational modification sites of MPRIP Human Isoform 3. Image obtained from PhosphoSitePlus® shows the amino acid residues which are determined to be post-translationally modified by High Throughput papers. The length of the lollipop plot indicates the number of references published for that residue.

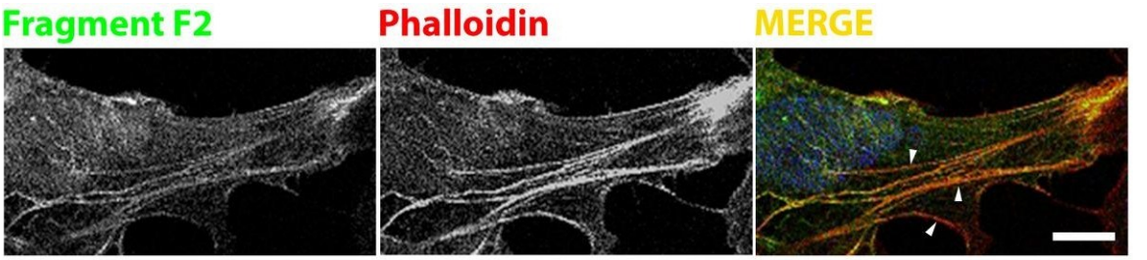

Figure S5: Fragment F2 of MPRIP localize to actin stress fibers. Confocal microscopy images show the cellular localization of the overexpressed fragment F2. Arrow heads point to the stress fibers and cortical actin Blue is DAPI, green is GFP-MPRIP and red is the phalloidin staining. Scale bar represent 10 μm.

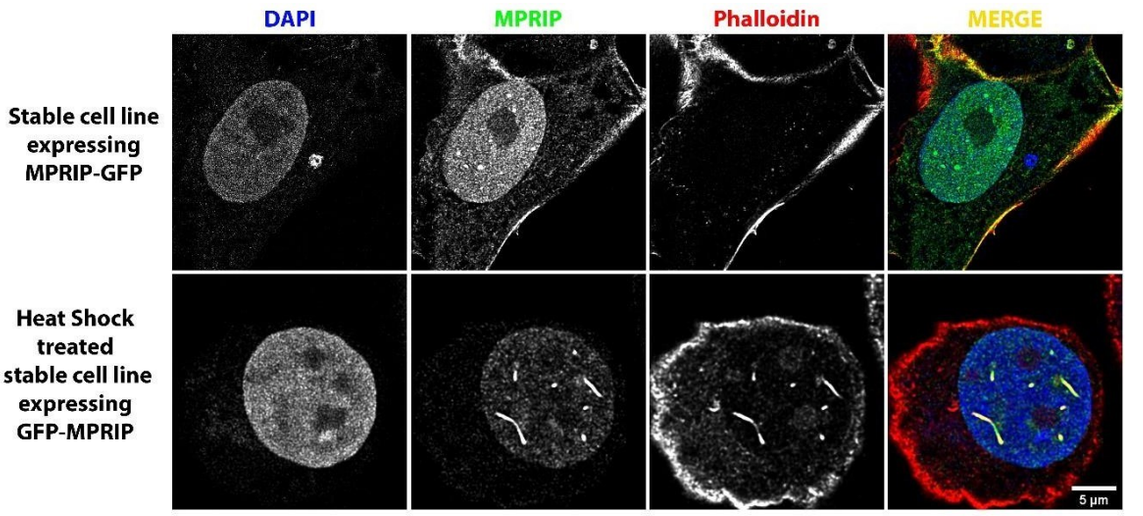

Figure S6: Heat Shock treatment of the stable cell line. Immunofluorescence experiment on the stable cell line expressing GFP-MPRIP. First row shows untreated cell as a control for heat shock. The cell at the second row is subjected to heat shock for 1 hour at 41°C (for more details,see Methods). Due to the high fluorescence of the fibers, the 488 laser intensity lowered in the heat shock imaging and therefore, DAPI staining looks more intense in the merge image. DAPIin blue, MPRIP in green, Phalloidin in red. Scale bar corresponds to 5 μm. Reproduced three times.

7.3. RNA Polymerase II Condensation and Transcription is Regulated by the Association of the Transcription Complex with PI(4,5)P2

Can Balaban, Martin Sztacho and Pavel Hozák

Manuscript

C.B. designed and performed all of the experiments (Confocal and STED microscopy, transfections, cellular fractionation, pull-down assays, western blotting and data analysis), wrote and revised the manuscript.

RNA Polymerase II Condensation and Transcription is Regulated by the Association between the Transcription Complex and PI(4,5)P2

Can Balaban[1], Martin Sztacho[1*], and Pavel Hozák[1*]

Department of Biology of the Cell Nucleus, Institute of Molecular Genetics of the Czech Academy of Sciences, v.v.i., 142 20 Prague, Czech Republic; can.balaban@img.cas.cz (C.B.); martin.sztacho@img.cas.cz (M.S.)

***** Correspondence: hozak@img.cas.cz

Abstract

The specific post-translational modifications of the C-terminal domain (CTD) of Rpb1 subunit of RNA polymerase II (RNAPII) correlates with different stages of transcription. The phosphorylation of the Ser5 residues of this domain associates with the initiation condensates which are formed through liquid–liquid phase separation (LLPS). The subsequent Tyr1 phosphorylation of the CTD occurs during the promoter-proximal pausing and marks the release of the RNAPII from the initiation condensate. We have previously reported that the nuclear Phosphatidylinositol 4,5-bisphosphate (PIP2) associates with the Ser5-phosphorylated-RNAPII complex and facilitates the RNAPII transcription. With this study, we identify an F-actin binding protein, as a novel regulator of the RNAPII transcription that determines the transcriptional output. This regulatory action of Myosin Phosphatase Rho-Interacting Protein (MPRIP) provides molecular insights into PIP2-associated RNAPII transcription mechanism. Our findings indicate a role for MPRIP in regulating the pause-release of RNAPII where nuclear actin polymerization might have an impact. Altogether, we demonstrate that MPRIP regulates RNAPII condensation and transcription by providing the association between the transcription complex and PIP2.

Introduction

The mammalian C-terminal domain (CTD) of the RPB1 subunit of RNA polymerase II (RNAPII) comprises a 52-heptad repeat, with the consensus sequence of Tyr1-Ser2-Pro3-Thr4-Ser5-Pro6-Ser7 (Eick and Geyer, 2013). The differential phosphorylation of this domain correlates with the stages of the RNAPII transcription and coins the term "CTD code" (Harlen and Churchman, 2017). Throughout transcription, RNAPII interacts with kinases and phosphatases that establish two major regulatory points, which limit the rate of the transcription; the initiation (RNAPII recruitment to promoter) and pause-release (Bartman et al, 2019).

During initiation, RNAPII is recruited to the promoter region by general transcription factors (TFs) that recognize specific promoter sequences and mediate the assembly of the pre-initiation complex (PIC) (Chen et al., 2021). The transcription factor Nuclear Myosin I (NMI) is an essential component of the initiation complex that is required for the formation of the first phosphodiester bond of the transcript (Hofmann et al., 2004). The RNAPII initiation complex is primarily phosphorylated at its Ser5 residues of the RPB1-CTD (CTD) which is mediated by both CDK7 of TFIIH (Lu et al., 2018) and the Positive Elongation Factor (P-TEFb) (Czudnochowski et al., 2012, Mayfield et al., 2019; Gibbs et al., 2017). Upon Ser5 phosphorylation, RNAPII escapes from promoter and pauses at the promoter-proximal region (+20 to +60) (Core and Adelman, 2019). The pausing of RNAPII provides a vital window to facilitate the integration of multiple cellular signals that determines the transcriptional output (Adelman and Lis, 2012). At this stage, RNAPII associates with macromolecular condensates that are formed through liquid–liquid phase separation (LLPS) (Lu et al., 2018; Pancholi et al., 2021). These condensates are enriched in coactivators such as CDK9, providing a platform to initiate the elongation (Lu et al, 2018; Guo et al, 2019). The Tyr1 phosphorylation of the CTD peaks near the promoter region and controls pausing of RNAPII, while lower levels of Tyr1 phosphorylations were maintained for efficient termination of the transcription (Harlen and Churchman, 2017; Collin et al., 2019; Shah et al., 2018). The Tyr1 phosphorylation of the CTD at promoter-proximal region was shown to alter the specificity of P-TEFb from Ser5 to Ser2 (Mayfield et al., 2019), enabling the release RNAPII from the condensate. This process is essential to trigger the release of RNAPII, as Ser2 phosphorylation of the CTD abolishes the affinity of RNAPII for the initiation condensate (Lu et al, 2018). The released RNAPII proceeds to elongation and relocates toward nuclear speckles where it interacts with the splicing machinery (Guo et al, 2019; Herzel et al., 2017).

The Phosphatidylinositol 4,5-bisphosphate (PIP2) is the most abundant PIP in nucleus and it determines the nuclear architecture by regulating processes such as chromatin remodeling, DNA-damage response and gene expression (Castano et al., 2021). PIP2 localizes to nuclear speckles, nucleoli and nucleoplasm which was determined by electron, light and super-resolution microscopy (Sobol et al., 2013, 2018; Hoboth et al., 2021a,b; Osborne et al., 2001). In nuclear speckles, PIP2 is associated with the small nuclear ribonucleoproteins, U1-U6 snRNAs, and the hyper-phosphorylated form of RNAPII (Osborne et al., 2001). In nucleolus, PIP2 interacts with many proteins including UBF and fibrillarin, and it participates to the rDNA transcription (Yıldırım et al., 2013; Sobol et al., 2018; Guillen-Chable et al., 2021). In a previous study, we have defined a nucleoplasmic pool of PIP2 (referred as Nucleoplasmic Lipid Islets; NLIs) which was observed as 40 to 100 nm foci (Sobol et al., 2018). The nascent transcripts were visualized at the periphery of NLIs and RNA was shown to be essential for their integrity. These structures were determined to interact with Ser5-phosphorylated CTD and NMI, suggesting a role in the transcription initiation (Sobol et al., 2018; Hofmann et al.,

2004). Therefore, we hypothesize that NLIs might serve as scaffolding platforms which facilitate the formation of the initiation condensates, enabling RNAPII-dependent transcription (Sobol et al., 2018).

Recently, we have identified the PIP2-nuclear interactome and defined the processes that are associated with PIP2-effectors (Sztacho et al., 2021). The Myosin Phosphatase Rho-Interacting Protein (MPRIP) was revealed as a promising candidate protein from the group of actin regulators, and it was identified in the complex with RNAPII and NMI (Sztacho et al., 2021; Balaban et al., 2021). MPRIP contains two PH-domains for PIP2 interaction and it localizes to the nuclear speckles and NLIs. The overexpression experiments showed that GFP-MPRIP forms LLPS condensates that are able to bind nuclear actin fibers (Balaban et al., 2021).

Actin is a transcription regulator that is required for the formation of the pre-initiation complex (PIC) (Hofmann et al., 2004; Obrdlik et al., 2008). It binds to the RPABC2 and RPABC3 subunits of all three RNA polymerases and interacts with the CTD of RNAPII (Hu et al., 2004; Kukalev et al., 2005). Moreover, the activity of the CDK9 depends on actin to trigger the promoter-proximal escape by Ser2 phosphorylation of the CTD. After the promoter-proximal escape actin remains bound to the hyper-phosphorylated CTD and interacts with heterogeneous nuclear ribonucleoproteins to regulate transcription elongation, through histone acetylation, and mRNA processing (Percipalle et al., 2001, 2002, 2003; Viita et al. 2019).

The polymerization of nuclear actin disrupts the interaction of monomeric actin with RNAPII that reduces transcription levels and inhibits cell proliferation (Serebryannyy et al., 2016). Serum stimulation was shown to induce the nuclear actin polymerization which affects formation of RNAPII condensates (Plessner et al., 2015; Cho et al., 2016). Furthermore, serum stimulation was determined to induce N-WASP and Arp2/3-dependent polymerization of short actin filaments which facilitate the formation of discrete RNAPII condensates (Wei et al., 2020). Similarly, many other actin cytoskeleton regulator proteins are known to translocate to nucleus and regulate nuclear actin dynamics, however, the intrinsic mechanisms showing how they regulate nuclear actin-polymerization and consequently, the RNAPII transcription, remains elusive (Ulferts et al., 2021).

With this study, we report the evidence of a novel transcription regulator that recruits Tyr1-phosphorylated RNAPII complex to PIP2-containing nuclear structures. We show that MPRIP regulates transcription through determining the association of the initiation complex with PIP2. The depletion of MPRIP increases the association of the Ser5 phosphorylated RNAPII complex with PIP2 and promotes the formation of the RNAPII condensates. Our data indicate that the transcription might be impaired due to a defect at promoter-proximal pause release. We suggest that MPRIP plays a key role in mediating RNAPII and PIP2 association while preserving its actin-binding capacity, which might offer a role in nuclear actin inducible transcription.

Material and Methods

1. Cell cultures and transfections

Human osteosarcoma (U2OS, ATCC no. HTB96) cells were grown in Dulbecco's modified Eagle's medium (DMEM, D6429, Merck, NJ, US) with 10% FBS at 37 °C in a humidified 5% CO2 atmosphere.

The 5-Fluorouridine (5-FU; F5130, Merck, NJ, USA), that was used for nascent transcript labelling, was initially diluted in water to 100 mM and the aliquots were kept in-20°C as stock solutions. Then, the stock solutions were diluted in DMEM with 10% FBS to a final concentration of 2mM. The cells were incubated for 20 minutes in the media with 2mM 5-FU.

For transfections of the GFP-tagged fragments, Lipofectamine 3000 (L3000015, Invitrogen, MA, USA) was used according to the manufacturer's protocol. Stable cell lines were established by single cell sorting of the transiently transfected cells which were further kept in selective media G418 (G8168, Merck, NJ, USA) with a final concentration of 0.5 mg/ml, for at least three weeks. The cells were evaluated by Western blot and fluorescence light microscopy (Balaban et al. 2021; Figure S6).

MISSION esiRNA (EHU141181, Merck, NJ, USA) was used to perform post-transcriptional silencing of the human MPRIP gene. This product is composed of a pool of hundreds of siRNA (21 bp each) that cover a region of 300 – 600 bp of the target mRNA. Each individual siRNA has around 50pM concentration in the pool which lowers the off-target effect significantly. MISSION siRNA Universal Negative Control #1 (SIC001, Merck, NJ, USA) was used as the negative control of the MPRIP depletions.

For transfections of the siRNAs, U2OS cells were plated 24 hours *a priori*. siRNAs were transfected using RNAiMax according to the manufacturer's instructions (13778075, Invitrogen, MA, USA). The media was replenished 6 hours after transfection and the cells were further incubated for 48 h. Knock-down efficiency was confirmed by western-blotting (WB).

2. Constructs and Antibodies

pDEST53-GFP-MPRIP (Human Isoform 3 of MPRIP) plasmid was used for the over-expression of MPRIP in U2OS cells (Figure S6). The N-terminal (1—450th amino acid) and the C-terminal (450-1000th amino acid) regions of MPRIP were amplified by PCR using pDest53-GFP-MPRIP as template. The N-terminal region was inserted in pEGFP-N1, while the C-terminal region was inserted in pEGFP-C1. For the detailed structure of the fragment, please see Balaban et al. 2021 Figure S3. The stable cell lines expressing the constructs were examined for their localization and features (Balaban et al. 2021).

Primary Antibodies (Final concentrations were achieved according to the manufacturer's instructions):
Anti-MPRIP antibodies; HPA022901 (Sigma, MO, USA) and sc-515720 (Santa Cruz, TX, USA)
Anti-RNAPII CTD Phospho S5 antibodies; ab5131 and ab5408 (Abcam, Cambridge, UK)
Anti-RNAPII CTD Phospho Tyr1 antibodies; 61383 and 91219 (Active Motif, CA, USA)
Anti-RNAPII CTD Phospho S2 antibody; ab5095 (Abcam, Cambridge, UK)
Anti-BrdU antibody; ab152095 (Abcam, Cambridge, UK)
Anti-PI(4,5)P2 antibody; Z-A045, clone 2C11 (Echelon Biosciences Inc., UT, USA)
Anti-beta Actin antibody; ab8227 (Abcam, Cambridge, UK)
Anti-MYO1C antibody; HPA001768 (Merck, NJ, USA)

Anti-GFP antibody; ab6556 (Abcam, Cambridge, UK)

Secondary Antibodies for Immunofluorescence labelling (Used at 1:400 dilution):
Goat anti-Mouse IgM (Heavy chain) Cross-Adsorbed, Alexa Fluor 568, A-21043 (Invitrogen, MA, USA)
Goat anti-Mouse IgG (H+L) Highly Cross-Adsorbed, Alexa Fluor 488, A-11029 (Invitrogen, MA, USA)
Goat anti-Mouse IgG (H+L) Highly Cross-Adsorbed, Alexa Fluor 568, A-11031 (Invitrogen, MA, USA)
Goat anti-Rabbit IgG (H+L) Cross-Adsorbed, Alexa Fluor 568, A-11011 (Invitrogen, MA, USA)
Goat anti-Rabbit IgG (H+L) Highly Cross-Adsorbed, Alexa Fluor 488, A-11034 (Invitrogen, MA, USA)
Goat anti-Rat IgG (H+L) Cross-Adsorbed, Alexa Fluor 488, A-11006 (Invitrogen, MA, USA)

Secondary Antibodies for WB (Used at 1:10.000 dilution):
IRDye 680RD Donkey anti-Mouse IgG, 926-68072 (LI-COR Biosciences, NE, USA)
IRDye 800CW Donkey anti-Mouse IgG, 926-32212 (LI-COR Biosciences, NE, USA)
IRDye 800CW Donkey anti-Rabbit IgG, 925-32213 (LICOR Biosciences, NE, USA)
IRDye 680RD Donkey anti-Rabbit IgG, 926-68073 (LI-COR Biosciences, NE, USA)
IRDye 800CW Goat anti-Rat IgG, 926-32219 (LI-COR Biosciences, NE, USA)

3. Immunofluorescence labelling

U2OS cells were grown on high-performance cover glasses of diameter 12 mm with restricted thickness-related tolerance (depth = 0.17 mm ± 0.005 mm) and the refractive index = 1.5255 ± 0.0015 (Marienfeld 0107222). After three washes with PBS, the cells were fixed with 2% formaldehyde for 20 minutes and permeabilized with 0.1% Triton X-100 for 5 minutes at room-temperature (RT). Non-specific binding was blocked by 5% bovine serum albumin (BSA) for 20 minutes at RT. All solutions were diluted in PBS. The cells were incubated 1 hour at RT with the corresponding primary antibodies. After several washes with PBS for 15 minutes (3 x 5 minutes) the cells were incubated for 45 minutes with the secondary antibodies at RT. Following another round of 15 minute PBS washing, the cells were mounted with 90% glycerol with 4% N-Propyl Gallate (NPG). For the super-resolution microscopy the cells were washed with purified water for 10minutes and then dried for 5 minutes at RT before mounting.

4. Confocal and Stimulated emission depletion (STED) microscopy

For confocal imaging, Leica TCS SP8 confocal microscope was employed with a Leica HC PL APO 63x/1.40 oil CS2 objective. The images of one technical repetition were acquired at the same resolution format and the zoom value for accurate image analysis.

STED imaging was performed with a Leica TCS SP8 STED 3× microscope, equipped with a Leica DFC365 FX digital camera with a STED white CS 100×1.40 NA oil objective for optimized overlay of excitation and a STED beam (Leica Mikrosysteme Vertrieb GmbH, Wetzlar, Germany). Image capturing was performed using the Leica LAS ×64-bit software package. The resolution format of the images is 1024x1024 and the corresponding pixel sizes are both 18 nm in x and y. The acquired images were deconvolved using Huygens Professional software version 19.04 (Scientific Volume Imaging, The Netherlands, http://svi.nl), using the CMLE algorithm, with SNR:07 and 20 iterations.

5. Image analysis

The image analysis was carried out using the Coloc2 function of the Fiji software. The significance of each statistical analysis was determined by the paired and two tailed Student's t-tests. Each data set was normalized to the average and the standard deviation of the all three repetitions. The randomized images were obtained by rotating one of the two channels 90 degrees (Dunn et al., 2011).

To determine the number of Ser5P clusters per cell, we have processed the confocal images as described by Cho et al. First, to minimalize the inter-batch variations of the staining densities, the median of the image was filtered (radius 8 pixel) and subtracted from the raw data. Then, the image was smoothed with a 1-pixel radius Gaussian blur for accurate counting of the clusters. Finally, find maxima was applied to count the number of clusters which were above the defined threshold within a cell nucleus. The nuclear outlines were segmented manually (Cho et al., 2018).

The segmentation of the nuclear PIP2 signals was performed on two channel confocal images where the nucleolar regions of each cell nucleus were subtracted manually from each channel by the distinctive staining of PIP2 at the nucleolar region (Yıldrım et al., 2013). Then, the PIP2 channel was smoothed by Gaussian blur (Sigma 3) to identify the broad areas of the dense signals that relates to large PIP2-rich structures (the nuclear speckles). This blurred image was further used as a mask for both channels: The region that overlapped with the blurred structures resulted in the image showing only the broad areas of the nuclear speckles, whereas the subtraction of the blurred structures resulted in the image showing only the nucleoplasmic PIP2 signal. Finally, the Coloc2 function of the FIJI software was applied to the images to detect the variations that occur on different PIP2-rich nuclear structures.

6. Pull-Down Assays

Cells were grown in 15cm dishes to 90% confluency. The cells are washed three times with ice-cold PBS and harvested by scrapping in 1xLysis Buffer (50 mM Tris-HCl, pH 7.2, 150mM NaCl, 0.1% NP-40). PhosStop (La Roche Ltd., Basel, Switzerland 4906837001) and protease inhibitors (La Roche Ltd., Basel, Switzerland, 05056489001) were added fresh to the lysis buffer on the day of the experiment. The homogenate was incubated 20 minutes on ice and then sonicated with Soniprep 150 (MSE) bench top sonicator (1 sec on, 1 s off for 30 cycles at power 10 amplitude microns). Sonicated lysate was spun down at 13,000× g for 30 min at 4°C. The supernatant was collected as the total cell extract. Protein concentrations were determined by Pierce™ BCA Protein Assay (Thermo Scientific, 23227) according to the manufacturer's protocol and determined to be 1,5mg/ml per sample.

Three types of beads were used in pull-down assays;

- Control beads for PIP2 pull-downs, P-B000 (Echelon Biosciences Inc., UT, USA)
- PI(4,5)P2 covered beads, P-B045A (Echelon Biosciences Inc., UT, USA)
- Anti-GFP mAb-Magnetic Beads, MAD153-11 (MBL International, MO, USA)

Thirty µl of slurry beads were used per condition. The beads were washed three times with 1 mL of ice-cold lysis buffer and then incubated overnight in the total cell extracts. The supernatant was discarded and the beads were washed five times with 1 mL of ice-cold lysis buffer and boiled in 40µl of 2x Laemmli buffer for 10 minutes. The beads were spun down and the supernatant was loaded to the SDS gel. After trans-blotting, the membranes were blocked with 5%BSA for 30 minutes at 4°C. The washes of the membranes were done by using PBS-Tween for 15 minutes at 4◦C. The dilutions of the primary antibodies were prepared in 5% BSA-PBS with sodium azide following each manufacturer's instructions. The incubation with primary antibodies were done at 4◦C with a duration ranging from 4 hours to overnight. The incubation with the secondary antibodies was 30 minutes at 4◦C. For scanning the membranes, LiCor Odyssey Infrared Imaging System 9120 (LI-COR Biosciences, NE, USA) was used.

Results

1. Nuclear MPRIP localization correlates with the phosphorylated forms of RNAPII

MPRIP localizes to the mammalian cell nucleus (Balaban et al. 2021). We have determined MPRIP in the same complex with active-RNAPII and NM1 which suggests a role in the transcription process (Balaban et al. 2021). To clarify the nuclear localization of MPRIP, we visualized endogenous MPRIP in respect to three different phosphorylated forms of RNAPII CTD, which mark the initiation (Ser5P), the transition to elongation (also called, initiation-release; Tyr1P) and the elongation (Ser2P) stages of the transcription (Harlen and Churchman, 2017; Mayfield et al., 2019; Descostes et al., 2014).

We performed three indirect immunofluorescence (IF) labeling experiments on U2OS cells with MPRIP- and Ser5P, Tyr1P and Ser2P-specific RNAPII-CTD antibodies (Figure 1A-I) and visualized by Stimulated emission depletion microscopy (STED). The spatial distributions of nuclear MPRIP and RNAPII forms were statistically evaluated and the analysis determined significant correlations between MPRIP and RNAPII forms (Figure 1J-L). The MPRIP localization in respect to Tyr1P-CTD shows the highest significance. These data indicate that MPRIP might be involved in the transition stage of the transcription wherein RNAPII is released from the promoter-proximal pause.

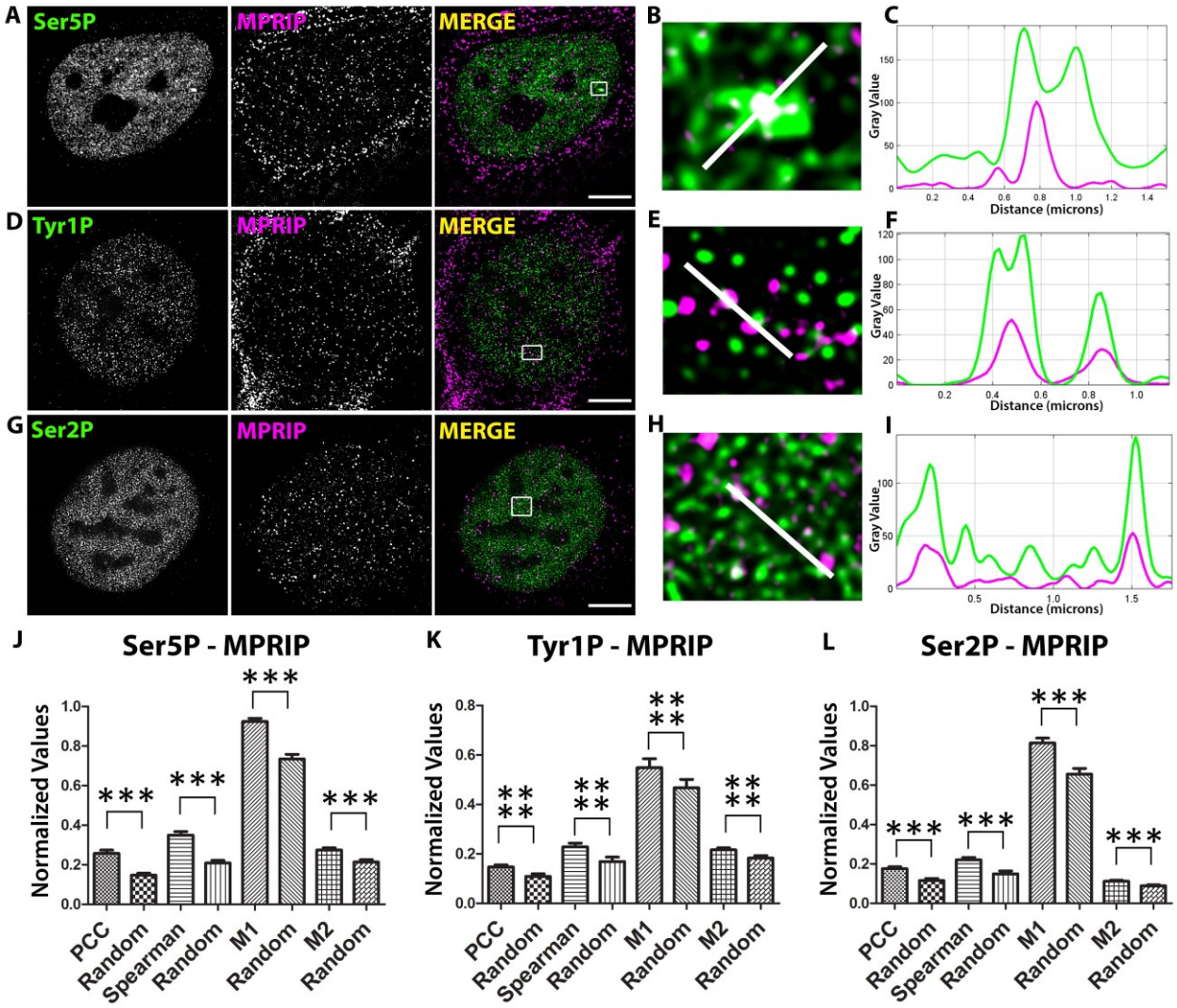

Figure 1: Mutual distribution of MPRIP and phosphorylated forms of RNAPII-CTD in the cell nucleus. *(A,D,G) Immunofluorescence labeling experiment showing the localization of endogenous MPRIP with Ser5, Tyr1 and Ser2 phosphorylated forms of RNAPII-CTD in U2OS nucleus. Scale bar represents 5 µm. (B,E,F) Zoomed views of the regions that are marked by a white rectangle in the "Merge" images. The white lines on the zoomed views represent the regions for the intensity plots on (C,F,I). (J,K,L) The bar graphs show the statistical coefficients of Pearson, Spearman and Manders of MPRIP and phosphorylated RNAPII signal. Manders 1 (M1) analysis: MPRIP over RNAPII channel, and Manders 2 (M2) analysis: RNAPII over MPRIP channel. Bars that are marked as `Random` were obtained by analyzing randomized images (see M.M.). The triple asterisk "***"corresponds to a significance level of p ≤ 0.001 and the quadruple asterisks "****" to p ≤ 0.0001. n=3, 15 cells/condition for each immunofluorescence experiment.*

2. MPRIP regulates transcriptional output and the number of the RNAPII condensates

The defects during the promoter-proximal pause of RNAPII are associated with decreased transcriptional output (Gressel et al., 2017). If MPRIP is involved in the regulation of RNAPII transcription, we expect a reduction in the transcriptional output when the cells are MPRIP depleted. Therefore, we compared the levels of the nascent RNAs in control and MPRIP depleted cells. We used siRNA-mediated depletion of the endogenous MPRIP and determined the signal of the incorporated 5-Fluorouridine (5-FU) in nascent RNA transcripts (Jao and Salic, 2008; Wissink et al., 2019 ;van't Sant et al., 2021) (Figure 2). This method enabled us to visualize the location and the amount of nascent RNAs and quantify the variation caused by MPRIP depletion. We found lower 5-FU signal in MPRIP depleted cells. The level of PIP2 signal remained unchanged in MPRIP depleted cells compare to the control cells (Figure 2B).

We have previously shown that MPRIP binds specifically to PIP2 *in vitro* and localizes to nuclear PIP2-rich structures in the cell nucleus; Nuclear Speckles and Nucleoplasmic Lipid Islets (NLIs) (Balaban et al., 2021). Both of these structures are involved in different stages of RNAPII transcription. The NLIs associate with the initiation of the RNAPII transcription, whereas nuclear speckles associate with the elongation stage (Sobol et al., 2018; Galganski et al., 2017). We have determined a significant decrease in the 5-FU signal at nucleoplasm (NP) and nuclear speckles (NS) (Figure 2C). This implies that upon MPRIP depletion, the transcription is affected from the initiation stage. Moreover, the Spearman coefficient indicates that the decrease in the transcriptional output upon MPRIP depletion is correlated with the PIP2 signal, which strengthens the importance of PIP2 in RNAPII transcription.

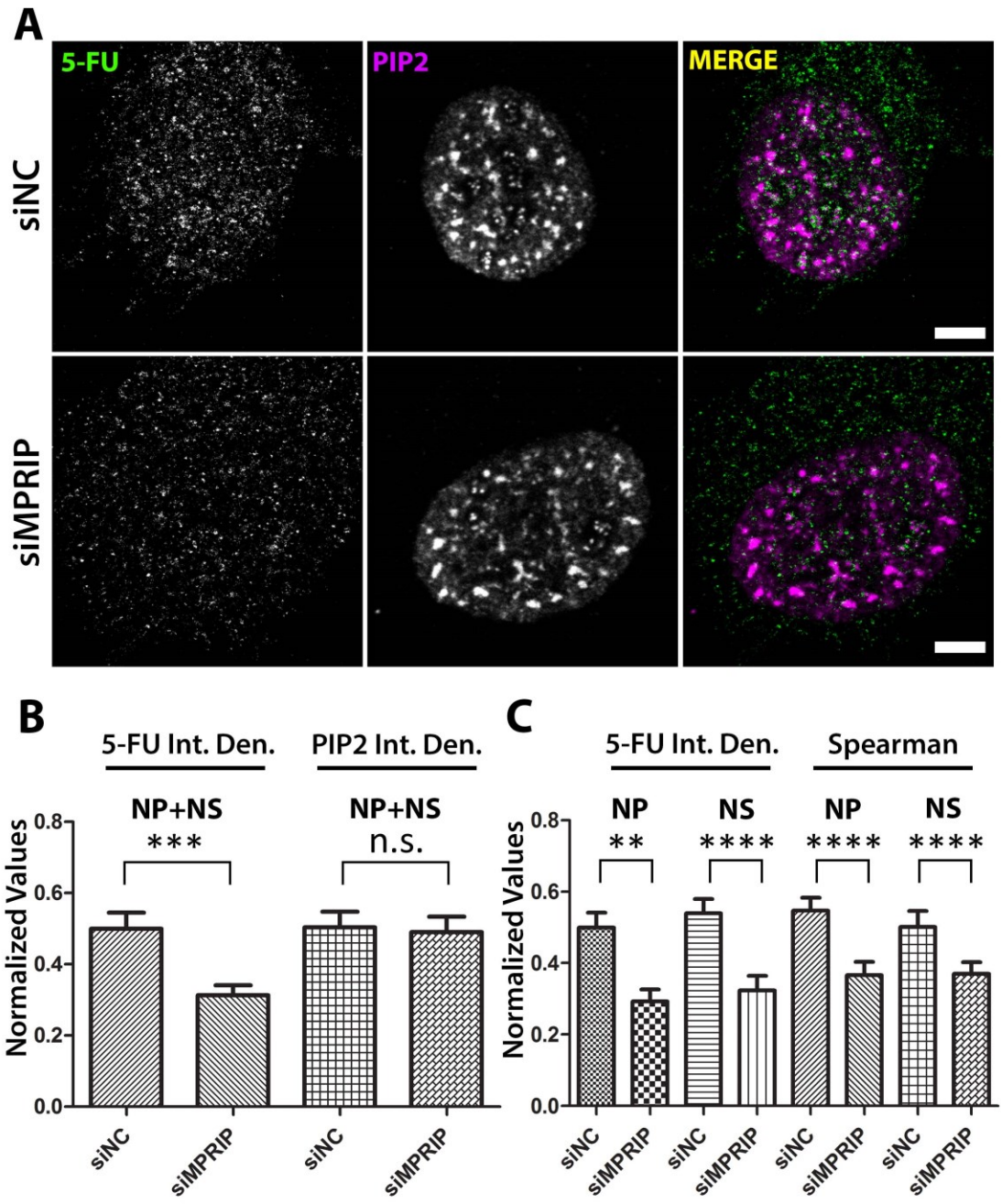

Figure 2: Nascent RNA profiling shows decreased transcriptional output in MPRIP depleted cells. *(A) Indirect immunofluorescence experiment on U2OS cells showing the 5-FU and PIP2 labeling in control (siNC) and siMPRIP nuclei. Scale bar represents 5 µm. (B) The integrated densities of 5-FU and PIP2 signals are normalized and reflected as a bar graph in siNC and siMPRIP conditions. (C) The bar graph shows normalized coefficients of Spearman and the integral densities of 5-FU signals that are observed in different PIP2-rich nuclear compartments. NP-Nucleoplasmic, NS-Nuclear Speckles. Not significant (n.s.). The double asterisk "**" corresponds to a significance level of p ≤ 0.01, the triple asterisk "***" corresponds to a significance level of p ≤ 0.001 and the quadruple asterisks "****" to p ≤ 0.0001. n=3, 10 cells/condition.*

We have previously reported that nuclear PIP2 associates with the initiation stage of the RNAPII transcription (Sobol et al., 2018). During the initiation stage, the RNAPII-CTD is phosphorylated at Ser5 residues and participates to macromolecular condensates that are formed through liquid-liquid phase separation (LLPS) (Guo et al., 2019; Hilbert et al., 2021). Several studies suggest that the defects in the promoter-proximal pause of transcription inhibit new transcription initiation with an accumulation of Ser5P-CTD at the promoter-proximal region of the gene (Shao and Zeitlinger, 2017; Gressel et al., 2019; Steurer et al., 2018; Core and Adelman, 2019). Therefore, we investigated the phenotype of the transcription initiation marker, the Ser5P-CTD, in MPRIP depleted cells. The confocal microscopy revealed that the number of the Ser5P-CTD clusters, which mark the initiation-condensates, is significantly increased upon MRPIP depletion (Figure 3) (Pancholi et al., 2021; Steurer et al., 2018). Therefore, these results indicate that MPRIP affects the formation and/or dissolution of the RNAPII initiation condensates. If the increased number condensates are indeed due to a defect during pausing of RNAPII, then it might also provide an explanation for the decreased transcriptional output in MPRIP depletion (Figure 2, 3).

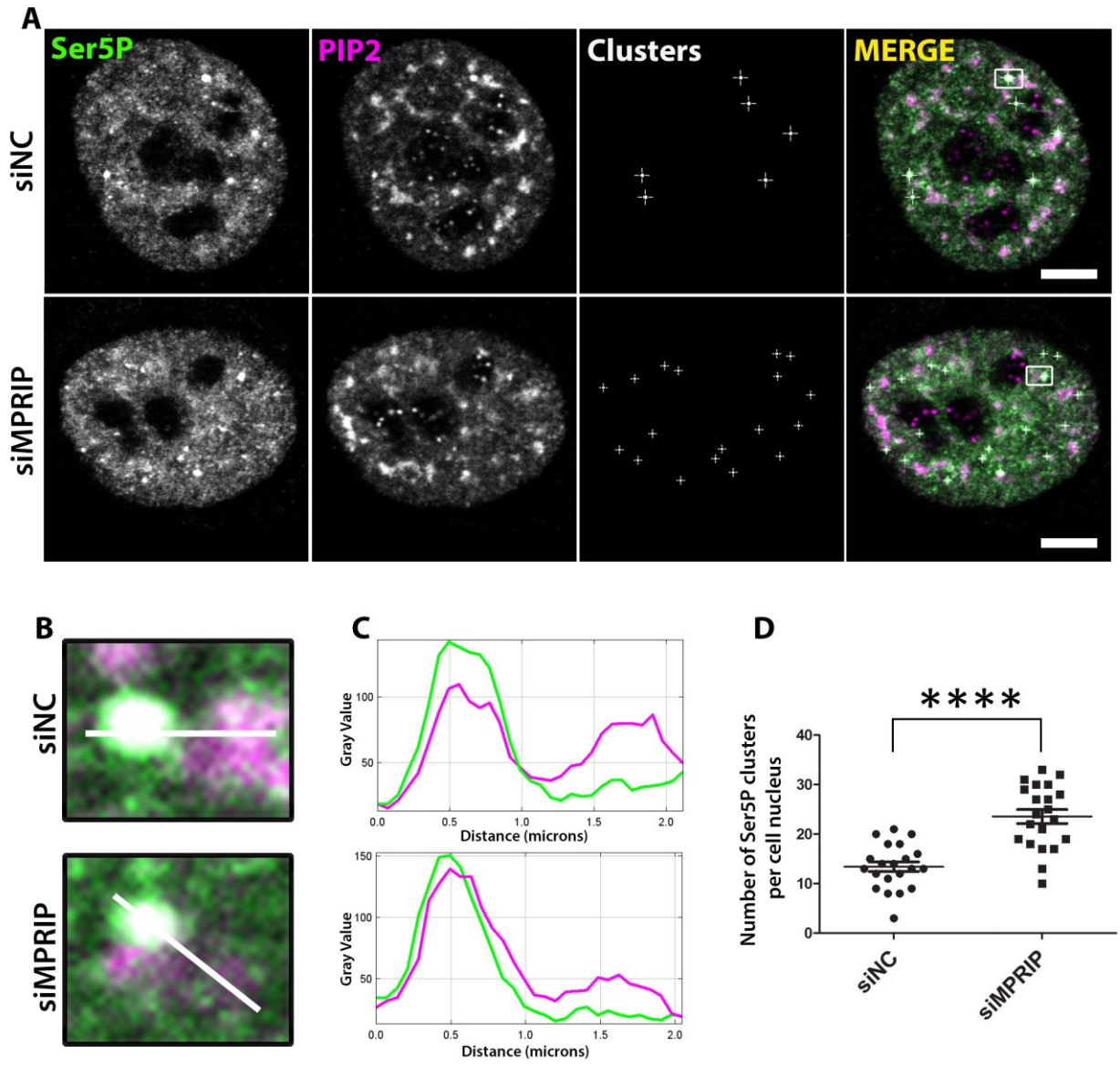

Figure 3: Ser5P-CTD clusters increase in MPRIP depletion. *(*A) Immunofluorescence labeling experiment on U2OS cells showing the *Ser5P*-CTD clusters in control (siNC) and MPRIP depleted (siMPRIP) nuclei. Scale bar represents 5 µm. (B) Zoomed views of clusters that are marked by a white rectangle in the "Merge" images. The white lines on the zoomed views represent the regions for the intensity plots on (C) where *the upper plot corresponds to the intensities of siNC and lower, to siMPRIP. (D) The dot plot shows the number of Ser5P-CTD clusters per cell nucleus of siNC and siMPRIP. The quadriple asterisk "****"corresponds to a significance level of p ≤ 0.0001. n=3.*

3. MPRIP affects the association of RNAPII complex with PIP2

The microscopy experiments indicate that the MPRIP depletion has an impact on RNAPII transcription in regard to the NLIs and nuclear speckles (Figure 2, 3). We have previously shown that the RNAPII associates with PIP2 (Sobol et al., 2018). Therefore, we sought to assess whether MPRIP affects the recruitment of RNAPII to PIP2 in different stages of transcription. To that end, we measured the association of Ser5P-, Tyr1P-, and Ser2P-CTD with PIP2-conjugated beads in pull–down experiments (Figure 4). The Ser5P-CTD shows increased association with PIP2 upon MPRIP depletion (Figure 4). This suggests that the increased number of Ser5P-CTD clusters upon MPRIP depletion (Figure 3) might be formed due to the increased affinity of RNAPII complex to PIP2 during the initiation stage. This is in accordance with the proposed role of PIP2 in the RNAPII initiation (Sobol et al., 2018). In MPRIP depleted cells, the markers of later stages of RNAPII transcription (Tyr1P and Ser2P) pulled-down by PIP2 beads were lower compared to control cells. This suggests that the RNAPII activity, which succeeds the initiation, is abrogated by the depletion of MPRIP (Figure 4). The overall levels of the CTD phosphorylations do not change significantly upon MPRIP depletion, indicating that MPRIP affects solely the association of RNAPII with PIP2.

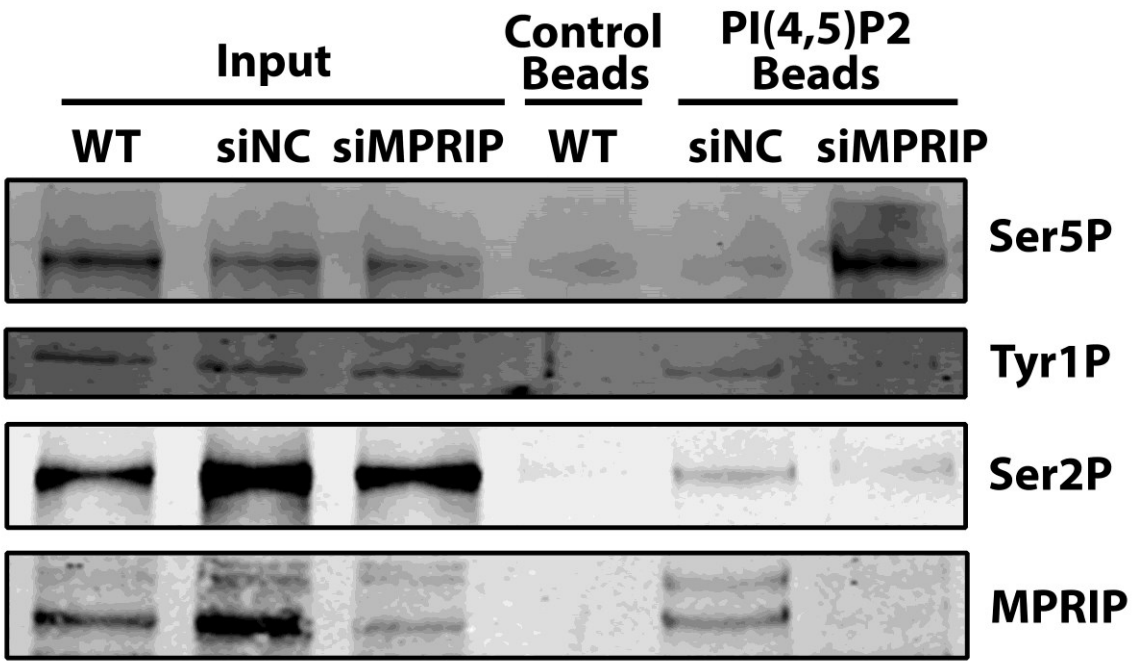

Figure 4: MPRIP regulates the association between RNAPII-CTD and PIP2. *PIP2-coated agarose beads were used as bait to pull-down interacting proteins from U2OS cell lysates. The membrane was blotted with anti-Ser5P, Tyr1P, Ser2P RNAPII-CTD and anti-MPRIP antibodies Empty agarose beads (control beads) were used as a control for unspecific binding. Input is 1%, WT-Wild Type U2OS cells, cKD- Control Knock–Down by siRNA, KD- Knock-Down of MPRIP by siRNA. n=3.*

The data presented in Balaban et al., identified MPRIP as a component of the RNAPII complex. Here, we showed the spatial co-distribution of MPRIP with three different phosphorylated forms of RNAPII-CTD (Figure 1). Therefore, to determine the stage of RNAPII transcription that involves MPRIP, we sought to clarify the predominant RNAPII form that associates with MPRIP and the region of MPRIP that is responsible for this association. In order to do so, we utilized the GFP-tagged MPRIP constructs coding for full-length (FL), N-terminal region (f1) comprising two PH domains and an actin-binding region, and C- terminal (f2) region, containing intrinsically disordered region (IDR) that promotes LLPS (Balaban et al., 2021). The Tyr1P-CTD was revealed as the predominant phosphorylated form that associates with the N-terminal region of MPRIP (Figure 5). Furthermore, transcription factors, NMI, and actin, were determined at this region. These results suggest that MPRIP possesses the ability to bind to RNAPII complex, presumably at the initiation-release where it affects the affinity of RNAPII complex to PIP2.

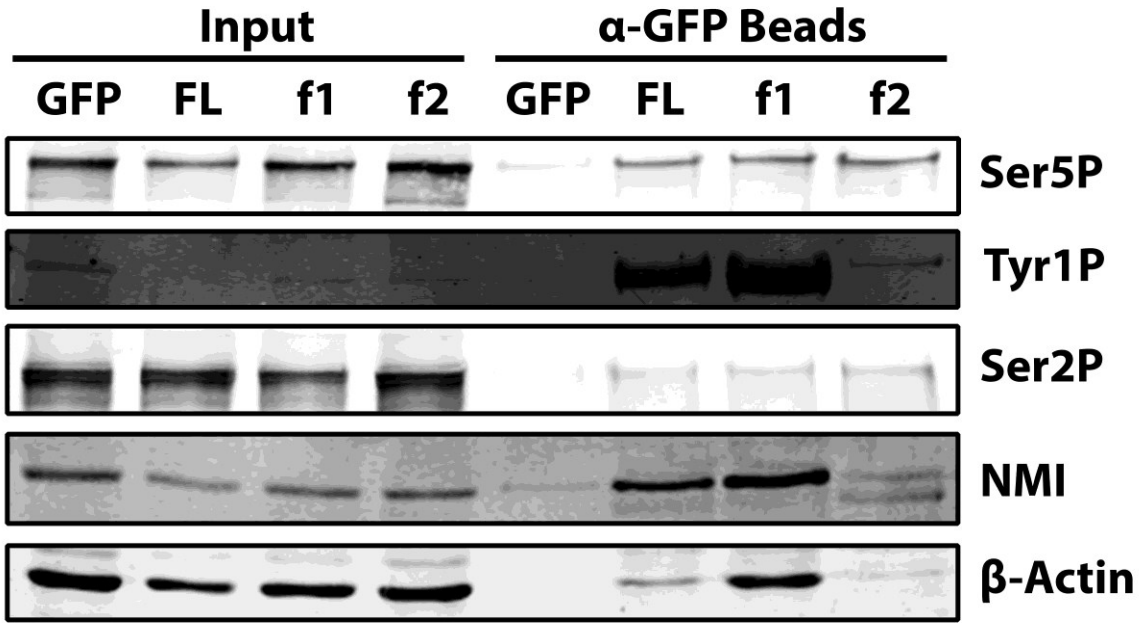

Figure 5: GFP-trap experiment showing the interacting partners of each fragment of MPRIP. *Anti-GFP coated magnetic beads were used as bait to pull-down interacting proteins from U2OS cell lysates that were overexpressing GFP, GFP-tagged full length (FL) MPRIP, and GFP-tagged N- and C-terminal MPRIP fragments (f1 and f2, respectively). The membrane was blotted with anti-Ser5P, Tyr1P, Ser2P RNAPII, MYO1C and β-actin antibodies. Only GFP expressing cells were used as a control for unspecific binding. Input is 1%. n=3.*

Recent data suggest that Tyr1 phosphorylation of CTD marks the promoter-proximal pause of RNAPII (Mayfield et al., 2019, Collin et al., 2019; Descostes et al., 2014). Our data shows that MPRIP affects the number of Ser5P-CTD clusters (Figure 3), the transcriptional output (Figure 2) and the association of RNAPII with PIP2 (Figure 1, 5). Since nuclear PIP2 is also implicated in the RNAPII transcription (Sobol et al., 2018; Galganski et al., 2017), it was necessary to elucidate whether MPRIP mediates the association between Tyr1P-CTD and PIP2. In order to address this, we overexpressed GFP-MPRIP constructs in U2OS cells and performed the pull-down experiments to detect if any phosphorylated form of RNAPII complex shows a change in its association with PIP2. The result in figure 6 shows that the full-length and particularly, N-terminus of MPRIP promotes the association between the Tyr1P-CTD and PIP2. Even though the presence of the PH domains and the F-actin binding region is evidently crucial for this interaction, the lack of C-terminal domain disrupted the association between PIP2 and MPRIP. This result points out that MPRIP mediates the PIP2-RNAPII association.

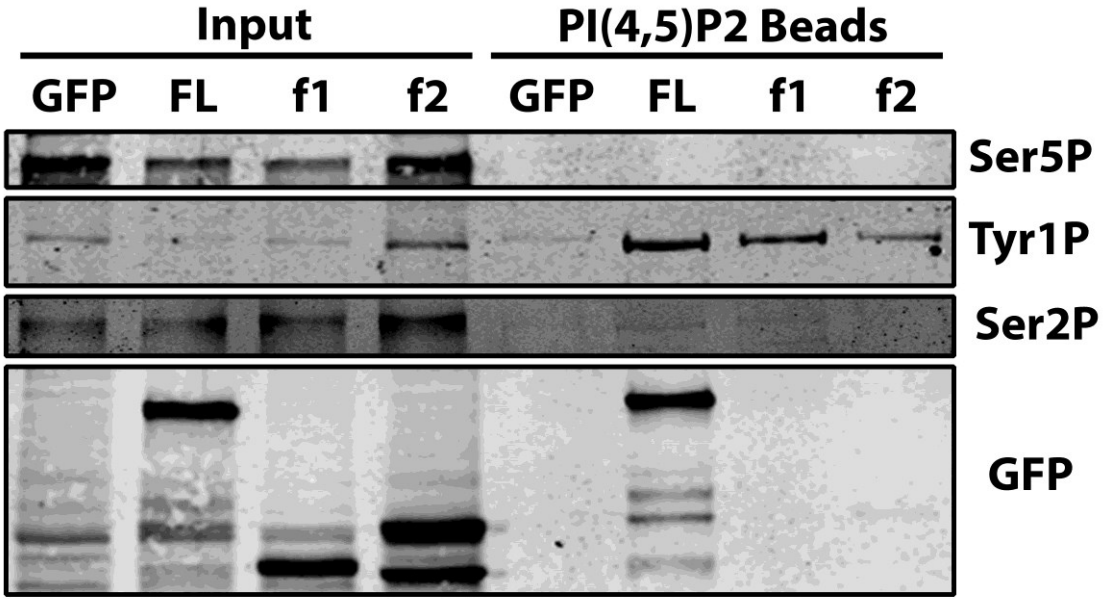

Figure 6: MPRIP promotes the recruitment of Tyr1 phosphorylated CTD to PIP2*. PIP2-coated agarose beads were used as a bait to pull-down interacting proteins from U2OS cell lysates that were overexpressing GFP, GFP-tagged full length (FL) MPRIP, and GFP-tagged N- and C-terminal MPRIP fragments (f1 and f2, respectively). The membrane was blotted with anti- Ser5P, Tyr1P, Ser2P-CTD specific RNAPII and anti-GFP antibodies. Only GFP-expressing cells were used as a control for unspecific interactions of GFP tagged overexpressing proteins. Input is 1%. n=3.*

So far, our results indicate that MPRIP affects the association of PIP2 with RNAPII complex *in vitro*. We further tested whether MPRIP depletion affects the localization of Tyr1P-CTD compare to the nuclear PIP2-containing structures. The Pearson's and Spearman analysis of the microscopy images show decreased colocalization between Tyr1P-CTD and nuclear PIP2-containing structures upon MPRIP depletion (Figure 7D). This effect is more prominent at NLIs compare to the nuclear speckles, pointing out to the initiation of transcription. In accordance with our *in vitro* data, the signal intensity levels of Tyr1P-CTD and PIP2 remained unchanged upon MPRIP depletion (Figure 7E). Overall, our results confirm the importance of MPRIP dependent regulatory axis that determines the association of Tyr1P-CTD with PIP2 as an important factor in defining the native transcription levels of RNAPII.

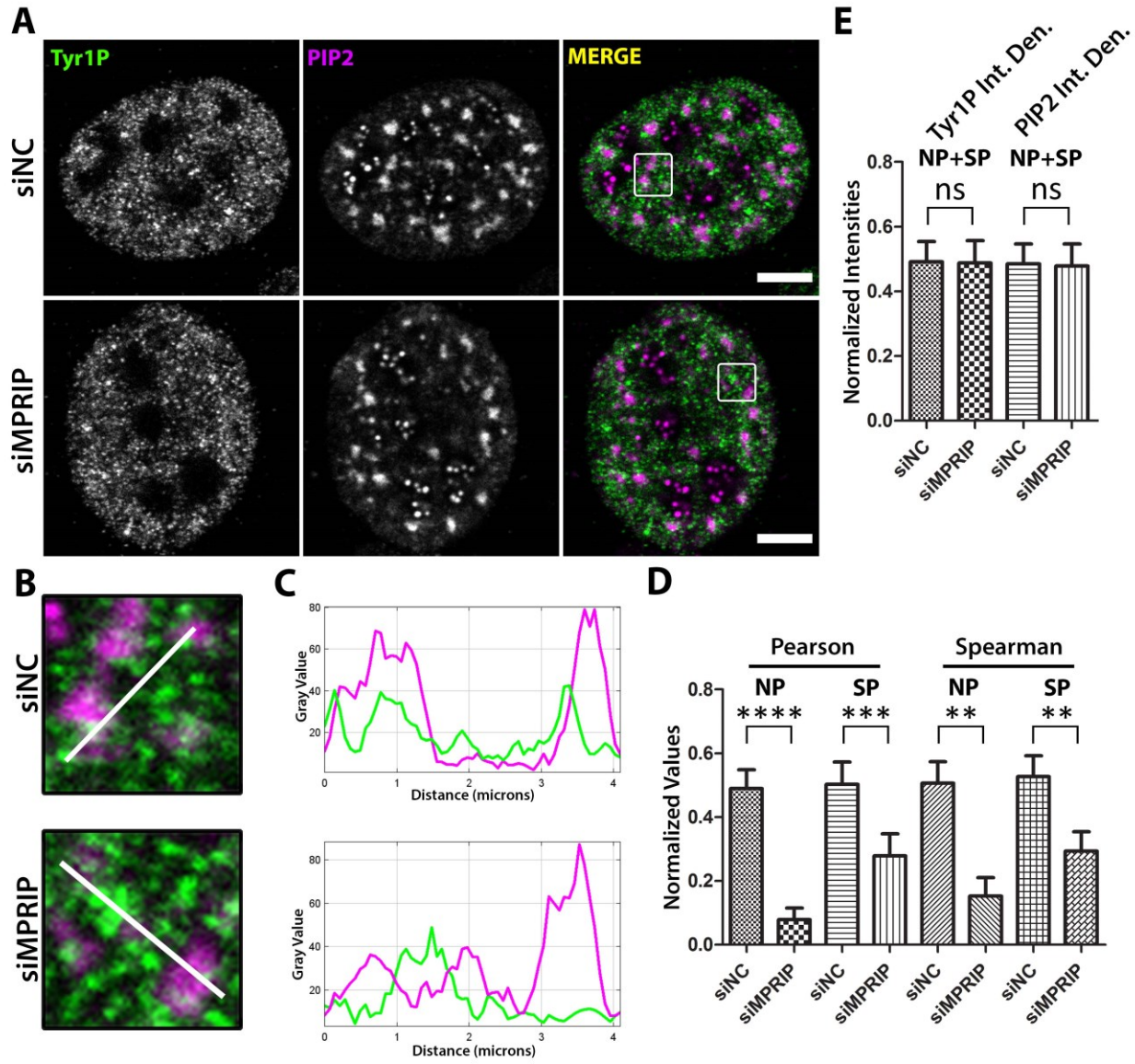

Figure 7: MPRIP depletion leads to* the decreased association of Tyr1 phosphorylated CTD to PIP2.** Immunofluorescence experiment showing the mutual distribution of PIP2 and Tyr1P-CTD in control and MPRIP depleted U2OS nucleus. Scale bar represents 5 µm. (B) Zoomed views of the regions that are marked by a white rectangle in the "Merge" images. The white lines on the zoomed views represent the regions of the intensity plots (C) where the upper plot corresponds to the intensities of siNC and lower, to siMPRIP. (D) The bar graph shows normalized coefficients of Spearman's and Pearson's that are observed in different PIP2-rich nuclear compartments. (E) The integrated densities of Tyr1P-CTD and PIP2 signals are normalized and reflected as a bar graph in siNC and siMPRIP conditions. NP-Nucleoplasmic, SP-Speckles. (ns) Not significant. The double asterisk "**"corresponds to a significance level of $p \leq 0.01$, the triple asterisk ""corresponds to a significance level of $p \leq 0.001$ and the quadruple asterisks "****" to $p \leq 0.0001$. n=2, 10 cells/condition.

Discussion

We have previously reported that MPRIP is not only a cytoplasmic protein that regulates actin stress fibers but also a component of the RNAPII transcription complex, localizing to PIP2-containing nuclear structures (Surks et al., 2003; Balaban et al., 2021). The overexpression of GFP-MPRIP showed the ability of this protein to form LLPS condensates, while preserving its capacity to bind nuclear actin filaments (Balaban et al., 2021). The growing body of evidence over the past decade emphasize the importance of nuclear actin regulators in the transcription process (Dopie et al., 2015; Hyrskyluoto and Vartiainen, 2020; Ulferts et al., 2021). The identification of an actin regulatory protein in nucleus, that associates with RNAPII complex paved the way for us to determine its' nuclear function. Here, we uncover the basics of the molecular mechanism of how nuclear MPRIP affects the RNAPII-mediated transcription.

Several studies have mapped the CTD phosphorylations during RNAPII activity and identified a correlation with different stages of the transcription (Harlen and Churchman, 2017). MPRIP localizes to close vicinity of three phosphorylated forms of CTD, which are associated with initiation (Ser5P-CTD), pause-release (Tyr1P-CTD), and elongation (Ser2P-CTD) stages (Mayfield et al., 2019; Descostes et al., 2014). From all three phosphorylated CTD forms, the statistical analysis of the super-resolution microscopy images revealed Tyr1P-CTD to have the most significant correlation with MPRIP (Figure 1). These data support the notion that MPRIP is linked to the RNAPII-mediated transcription, presumably acting on the paused RNAPII.

The transition to elongation which is labelled by Tyr1P-CTD, is a critical regulatory stage in transcription that determines the transcriptional output (Bartman et al., 2019; Mayfield et al., 2019). The studies show decreased transcription levels due to the defects during the pausing of RNAPII which inhibits new transcription initiation (Gressel et al., 2017, 2019; Shao and Zeitlinger, 2017). Similarly, the MPRIP depleted cells show lower transcriptional output, signaling a defect in the transcription machinery (Figure 2). Moreover, the Spearman coefficients which determine the correlation between PIP2 and nascent RNA transcripts, show decreased values in depletion of MPRIP. This points out that the transcription is impaired mainly, but not exclusively, at PIP2-containig nuclear structures (Figure 2). Considering nucleoplasmic-PIP2 (NLIs) is involved in initiation of the transcription (Sobol et al., 2018), this analysis indicates that the transcription is altered from the initiation stage when MPRIP is depleted.

Our previous study showed that MPRIP associates with NMI and PIP2, which are both factors linked to transcription initiation (Balaban et al., 2021; Hofmann et al., 2004; Sobol et al., 2018). The initiation stage of transcription is characterized by the increasing amounts of Ser5 phosphorylation of the CTD that associates with the macromolecular condensates with liquid-like properties (Pancholi et al., 2021; Steurer et al., 2018). Several studies documented the accumulation of Ser5P-CTD at promoter-proximal region due to the lack of factors that are involved in pause-release (Shao and Zeitlinger, 2017; Mayfield et al., 2019; Gressel et al., 2017; Gressel et al., 2019). Our findings show that MPRIP affects the number of initiation condensates (Figure 3), presumably by regulating the pause-release of RNAPII.

The factors such as the negative elongation factor (NELF), DRB sensitivity-inducing factor (DSIF) and polymerase-associated factor 1 (Paf1) are known to govern the pausing of the RNAPII while its release requires the kinase activity P-TEFb (Rawat et al., 2021; Vos et al., 2018; Yu et al., 2015; Lu et al., 2016). Our results show that MPRIP depletion abolishes the recruitment of Tyr1P-CTD to PIP2 (Figure 4). This outcome suggests that MPRIP might regulate the pause-release of RNAPII through modulating the affinity of RNAPII complex to PIP2 (Figure 4). In addition, this experiment also shows

increased association between Ser5P-CTD and PIP2 in MPRIP depleted cells. This might also provide an explanation to the increased number of Ser5P-CTD clusters in MPRIP depletion, where the increased PIP2 affinity of Ser5P-CTD might reduce the dissolution of the initiation condensate (Figure 3, 4). We suggest that the association between RNAPII and PIP2 determines the transcriptional output through regulating the pausing of RNAPII. Taken together we propose that MPRIP is necessary for release of RNAPII from the initiation condensate by reducing the affinity to PIP2.

The Tyr1P-CTD was revealed as the predominant form of RNAPII that associates with MPRIP. The N-terminal region that is responsible for this association, also showed interaction with NMI and actin (Figure 5). The nuclear myosin I (NMI), being an initiation factor, associates with the transcription complex through polymerase-associated actin to form the first phosphodiester bond of the transcript and maintain the active RNAPII transcription (Sarshad and Percipalle, 2014; Pestic-Dragovich et al., 2000; Hofmann et al., 2004). This suggests that MPRIP associates with the RNAPII-initiation complex. Furthermore, our results show that MPRIP provides the association between Tyr1P-CTD and PIP2 (Figure 6). This outcome shows that MPRIP is a mediator that promotes the recruitment of Tyr1P-CTD to PIP2. Given the importance of Tyr1 phosphorylation of the CTD in pause-release, it seems that MPRIP defines the susceptibility of RNAPII complex to leave the initiation condensate through determining the association of Tyr1P-CTD with PIP2. In accordance with this, our microscopy experiments show decreased Tyr1P-CTD colocalization with both NLIs and nuclear speckles in MPRIP depletion (Figure 7). Overall, our results indicate that through MPRIP, PIP2 represents an important factor in RNAPII condensation and transcription.

In contrary to full-length MPRIP, we observed a lack of interaction between the PH-domain-containing N-terminal region of MPRIP and PIP2 (Figure 6). This can be explained by the recent study which demonstrates that PH-domain-containing proteins lose their specificity and bind to other PIPs in comparison to their full-length counterparts (Singh et al., 2021). Alternative explanation can be provided by the conformation of the mutant, which seems to favor the interaction with actin instead of PIP2 (Figure 6). Since PIP2 and F-actin binding regions of MPRIP overlaps (Surks et al., 2003), the binding to F-actin might hide the PH-domains of the mutant hindering the interaction with PIP2.

The nuclear actin concentration is an important regulator of the RNAPII transcription (Huet et al., 2012). The F-actin formations, that sequesters the monomeric actin, play a crucial role in regulating the transcription (Plessner and Grosse, 2019). These formations can be induced upon serum-stimulation and affect the nuclear actin concentration. The fluctuations in the concentration of an initiation factor such as actin, can determine the transcription activity. Indeed, studies has documented that the F-actin formations can both activate and repress the expression of different genes (Hyrskyluoto and Vartiainen, 2020; Yamazaki et al., 2020). For example, persistent nuclear F-actin formations were shown to disrupt actin–RNAPII interaction and impaired RNAPII localization, reducing transcription levels and cell proliferation (Serebryannyy et al., 2016). In addition, through the activity of actin-binding proteins (N-WASP and Arp2/3), the serum-induced nuclear actin polymerization was shown to facilitate the formation of discrete RNAPII condensates (Wei et al., 2020). Since MPRIP is a negative F-actin regulator, it is tempting to speculate that the nuclear F-actin structures can occupy the PIP2-binding region of MPRIP which abolishes the association between Tyr1P-CTD and PIP2, leading to an increased number of the initiation condensates. However, it is clear that further research is required to elucidate the exact role of actin underlying in the regulatory axis of PIP2 and MPRIP-associated RNAPII machinery.

In summary, we show that MPRIP represents a novel regulator of RNAPII transcription that defines the number of initiation-condensates and the transcriptional output. This regulatory action of MPRIP provides molecular insights into PIP2-associated RNAPII transcription mechanism. We determine that MPRIP interacts with Tyr1P-CTD and mediates its association with PIP2. Our immunofluorescence experiment supports this data, providing an *in situ* evidence for the nuclear function of MPRIP. Considering the literature on Tyr1P-CTD, several indications point that MPRIP is involved in the regulation of pause-release of RNAPII. Finally, we suggest that MPRIP might be involved in F-actin associated regulation of RNAPII transcription. Taken together, we demonstrate that MPRIP regulates RNAPII condensation and transcription by providing the association between the initiation complex and nuclear PIP2.

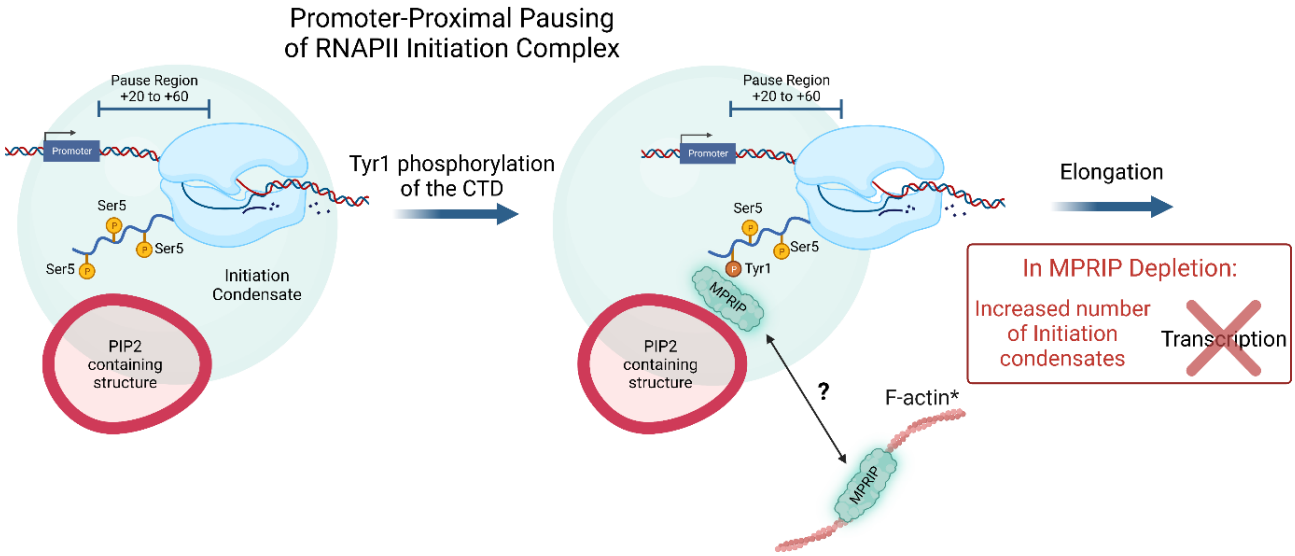

Figure 8: Model depicting proposed mechanism for the MPRIP mediated PIP2 association with Tyr1-phosphorylated-RNAPII complex facilitating the release of RNAPII from the promoter-proximal pausing.
*The Ser5-phosphorylated RNAPII complex pauses at the promoter-proximal region (+20 to +60). PIP2-containing structures associate with the initiation condensate (Sobol et al., 2018; Hoboth et al., 2021). Following the Tyr1 phosphorylation of the Rpb1 CTD, MPRIP mediates the interaction between the RNAPII complex and PIP2-containing structures. By regulating the affinity of RNAPII complex to the PIP2-containing structures, MPRIP regulates the release of RNAPII complex from the initiation condensate. In case of MPRIP depletion, due to increased association between Ser5P-CTD with PIP2, the RNAPII is not released from the initiation condensate thereby inhibiting transcription and increasing the number of the condensates in cell nucleus. * MPRIP shows binding to nuclear F-actin (Balaban et al., 2021). The nuclear actin polymerization might reflect a state similar to MPRIP depletion -by relocating MPRIP from transcription complex to the nuclear F-actin- and thus, causing a defect in promoter-proximal pause and decreasing transcriptional output.*

References

Balaban, C., Sztacho, M., Blažíková, M., Hozák, P., **2021**. The F-Actin-Binding MPRIP Forms Phase-Separated Condensates and Associates with PI(4,5)P2 and Active RNA Polymerase II in the Cell Nucleus. Cells 10. https://doi.org/10.3390/cells10040848

Bartman, C.R., Hamagami, N., Keller, C.A., Giardine, B., Hardison, R.C., Blobel, G.A., Raj, A., **2019**. Transcriptional Burst Initiation and Polymerase Pause Release Are Key Control Points of Transcriptional Regulation. Mol Cell 73, 519-532.e4. https://doi.org/10.1016/j.molcel.2018.11.004

Castano, E., Yildirim, S., Fáberová, V., Krausová, A., Uličná, L., Paprčková, D., Sztacho, M., Hozák, P., **2019**. Nuclear Phosphoinositides—Versatile Regulators of Genome Functions. Cells 8, 649. https://doi.org/10.3390/cells8070649

Cho, W.-K., Jayanth, N., English, B.P., Inoue, T., Andrews, J.O., Conway, W., Grimm, J.B., Spille, J.-H., Lavis, L.D., Lionnet, T., Cisse, I.I., **2016**. RNA Polymerase II cluster dynamics predict mRNA output in living cells. eLife 5, e13617. https://doi.org/10.7554/eLife.13617

Cisse, I.I., Izeddin, I., Causse, S.Z., Boudarene, L., Senecal, A., Muresan, L., Dugast-Darzacq, C., Hajj, B., Dahan, M., Darzacq, X., **2013**. Real-time dynamics of RNA polymerase II clustering in live human cells. Science 341, 664–667. https://doi.org/10.1126/science.1239053

Core, L., Adelman, K., **2019**. Promoter-proximal pausing of RNA polymerase II: a nexus of gene regulation. Genes Dev 33, 960–982. https://doi.org/10.1101/gad.325142.119

Czudnochowski, N., Bösken, C.A., Geyer, M., **2012**. Serine-7 but not serine-5 phosphorylation primes RNA polymerase II CTD for P-TEFb recognition. Nat Commun 3, 842. https://doi.org/10.1038/ncomms1846

Descostes, N., Heidemann, M., Spinelli, L., Schüller, R., Maqbool, M.A., Fenouil, R., Koch, F., Innocenti, C., Gut, M., Gut, I., Eick, D., Andrau, J.-C., **2014**. Tyrosine phosphorylation of RNA polymerase II CTD is associated with antisense promoter transcription and active enhancers in mammalian cells. eLife 3, e02105. https://doi.org/10.7554/eLife.02105

Dopie, J., Skarp, K.-P., Rajakylä, E.K., Tanhuanpää, K., Vartiainen, M.K., **2012.** Active maintenance of nuclear actin by importin 9 supports transcription. Proc Natl Acad Sci U S A 109, E544-552. https://doi.org/10.1073/pnas.1118880109

Dunn, K.W., Kamocka, M.M., McDonald, J.H., **2011**. A practical guide to evaluating colocalization in biological microscopy. Am J Physiol Cell Physiol 300, C723-742. https://doi.org/10.1152/ajpcell.00462.2010

Eick, D., Geyer, M., **2013**. The RNA polymerase II carboxy-terminal domain (CTD) code. Chem Rev 113, 8456–8490. https://doi.org/10.1021/cr400071f

Galganski, L., Urbanek, M.O., Krzyzosiak, W.J., **2017**. Nuclear speckles: molecular organization, biological function and role in disease. Nucleic Acids Res 45, 10350–10368. https://doi.org/10.1093/nar/gkx759

Gressel, S., Schwalb, B., Cramer, P., **2019**. The pause-initiation limit restricts transcription activation in human cells. Nat Commun 10, 3603. https://doi.org/10.1038/s41467-019-11536-8

Gressel, S., Schwalb, B., Decker, T.M., Qin, W., Leonhardt, H., Eick, D., Cramer, P., **2017**. CDK9-dependent RNA polymerase II pausing controls transcription initiation. eLife 6, e29736. https://doi.org/10.7554/eLife.29736

Guillen-Chable, F., Bayona, A., Rodríguez-Zapata, L.C., Castano, E., **2021**. Phase Separation of Intrinsically Disordered Nucleolar Proteins Relate to Localization and Function. Int J Mol Sci 22, 13095. https://doi.org/10.3390/ijms222313095

Guo, Y.E., Manteiga, J.C., Henninger, J.E., Sabari, B.R., Dall'Agnese, A., Hannett, N.M., Spille, J.-H., Afeyan, L.K., Zamudio, A.V., Shrinivas, K., Abraham, B.J., Boija, A., Decker, T.-M., Rimel, J.K., Fant, C.B., Lee, T.I., Cisse, I.I., Sharp, P.A., Taatjes, D.J., Young, R.A., **2019**. Pol II phosphorylation

regulates a switch between transcriptional and splicing condensates. Nature 572, 543–548. https://doi.org/10.1038/s41586-019-1464-0

Harlen, K.M., Churchman, L.S., **2017**. The code and beyond: transcription regulation by the RNA polymerase II carboxy-terminal domain. Nat Rev Mol Cell Biol 18, 263–273. https://doi.org/10.1038/nrm.2017.10

Herzel, L., Ottoz, D.S.M., Alpert, T., Neugebauer, K.M., **2017**. Splicing and transcription touch base: co-transcriptional spliceosome assembly and function. Nat Rev Mol Cell Biol 18, 637–650. https://doi.org/10.1038/nrm.2017.63

Hilbert, L., Sato, Y., Kuznetsova, K., Bianucci, T., Kimura, H., Jülicher, F., Honigmann, A., Zaburdaev, V., Vastenhouw, N.L., **2021**. Transcription organizes euchromatin via microphase separation. Nat Commun 12, 1360. https://doi.org/10.1038/s41467-021-21589-3

Hoboth, P., Šebesta, O., Hozák, P., **2021a**. How Single-Molecule Localization Microscopy Expanded Our Mechanistic Understanding of RNA Polymerase II Transcription. Int J Mol Sci 22, 6694. https://doi.org/10.3390/ijms22136694

Hoboth, P., Šebesta, O., Sztacho, M., Castano, E., Hozák, P., **2021b**. Dual-color dSTORM imaging and ThunderSTORM image reconstruction and analysis to study the spatial organization of the nuclear phosphatidylinositol phosphates. MethodsX 8, 101372. https://doi.org/10.1016/j.mex.2021.101372

Hofmann, W.A., Stojiljkovic, L., Fuchsova, B., Vargas, G.M., Mavrommatis, E., Philimonenko, V., Kysela, K., Goodrich, J.A., Lessard, J.L., Hope, T.J., Hozak, P., de Lanerolle, P., **2004**. Actin is part of pre-initiation complexes and is necessary for transcription by RNA polymerase II. Nat Cell Biol 6, 1094–1101. https://doi.org/10.1038/ncb1182

Hyrskyluoto, A., Vartiainen, M.K., 2020. Regulation of nuclear actin dynamics in development and disease. Curr Opin Cell Biol 64, 18–24. https://doi.org/10.1016/j.ceb.2020.01.012

Hu, P., Wu, S., Hernandez, N., **2004**. A role for β-actin in RNA polymerase III transcription. Genes Dev 18, 3010–3015. https://doi.org/10.1101/gad.1250804

Huet, G., Skarp, K.-P., Vartiainen, M.K., **2012**. Nuclear actin levels as an important transcriptional switch. Transcription 3, 226–230. https://doi.org/10.4161/trns.21062

Jao, C.Y., Salic, A., **2008**. Exploring RNA transcription and turnover in vivo by using click chemistry. Proc Natl Acad Sci U S A 105, 15779–15784. https://doi.org/10.1073/pnas.0808480105

Kukalev, A., Nord, Y., Palmberg, C., Bergman, T., Percipalle, P., **2005**. Actin and hnRNP U cooperate for productive transcription by RNA polymerase II. Nat Struct Mol Biol 12, 238–244. https://doi.org/10.1038/nsmb904

Lu, H., Yu, D., Hansen, A.S., Ganguly, S., Liu, R., Heckert, A., Darzacq, X., Zhou, Q., **2018**. Phase-separation mechanism for C-terminal hyperphosphorylation of RNA polymerase II. Nature 558, 318–323. https://doi.org/10.1038/s41586-018-0174-3

Lu, X., Zhu, X., Li, Y., Liu, M., Yu, B., Wang, Yu, Rao, M., Yang, H., Zhou, K., Wang, Yao, Chen, Y., Chen, M., Zhuang, S., Chen, L.-F., Liu, R., Chen, R., **2016**. Multiple P-TEFbs cooperatively regulate the release of promoter-proximally paused RNA polymerase II. Nucleic Acids Res 44, 6853–6867. https://doi.org/10.1093/nar/gkw571

Mayfield, J.E., Irani, S., Escobar, E.E., Zhang, Z., Burkholder, N.T., Robinson, M.R., Mehaffey, M.R., Sipe, S.N., Yang, W., Prescott, N.A., Kathuria, K.R., Liu, Z., Brodbelt, J.S., Zhang, Y., **2019**. Tyr1 phosphorylation promotes phosphorylation of Ser2 on the C-terminal domain of eukaryotic RNA polymerase II by P-TEFb. eLife 8, e48725. https://doi.org/10.7554/eLife.48725

Obrdlik, A., Percipalle, P., **2011**. The F-actin severing protein cofilin-1 is required for RNA polymerase II transcription elongation. Nucleus 2, 72–79. https://doi.org/10.4161/nucl.2.1.14508

Osborne, S.L., Thomas, C.L., Gschmeissner, S., Schiavo, G., **2001**. Nuclear PtdIns(4,5)P2 assembles in a mitotically regulated particle involved in pre-mRNA splicing. J Cell Sci 114, 2501–2511. https://doi.org/10.1242/jcs.114.13.2501

Pancholi, A., Klingberg, T., Zhang, W., Prizak, R., Mamontova, I., Noa, A., Sobucki, M., Kobitski, A.Y., Nienhaus, G.U., Zaburdaev, V., Hilbert, L., **2021**. RNA polymerase II clusters form in line with surface condensation on regulatory chromatin. Mol Syst Biol 17, e10272. https://doi.org/10.15252/msb.202110272

Percipalle, P., Jonsson, A., Nashchekin, D., Karlsson, C., Bergman, T., Guialis, A., Daneholt, B., **2002**. Nuclear actin is associated with a specific subset of hnRNP A/B-type proteins. Nucleic Acids Res 30, 1725–1734. https://doi.org/10.1093/nar/30.8.1725

Percipalle, P., Zhao, J., Pope, B., Weeds, A., Lindberg, U., Daneholt, B., **2001**. Actin Bound to the Heterogeneous Nuclear Ribonucleoprotein Hrp36 Is Associated with Balbiani Ring mRNA from the Gene to Polysomes. J Cell Biol 153, 229–236.

Pestic-Dragovich, L., Stojiljkovic, L., Philimonenko, A.A., Nowak, G., Ke, Y., Settlage, R.E., Shabanowitz, J., Hunt, D.F., Hozak, P., de Lanerolle, P., **2000**. A myosin I isoform in the nucleus. Science 290, 337–341. https://doi.org/10.1126/science.290.5490.337

Plessner, M., Grosse, R., **2019**. Dynamizing nuclear actin filaments. Curr Opin Cell Biol 56, 1–6. https://doi.org/10.1016/j.ceb.2018.08.005

Rawat, P., Boehning, M., Hummel, B., Aprile-Garcia, F., Pandit, A.S., Eisenhardt, N., Khavaran, A., Niskanen, E., Vos, S.M., Palvimo, J.J., Pichler, A., Cramer, P., Sawarkar, R., **2021**. Stress-induced nuclear condensation of NELF drives transcriptional downregulation. Molecular Cell 81, 1013-1026.e11. https://doi.org/10.1016/j.molcel.2021.01.016

Sarshad, A.A., Percipalle, P., **2014**. New insight into role of myosin motors for activation of RNA polymerases. Int Rev Cell Mol Biol 311, 183–230. https://doi.org/10.1016/B978-0-12-800179-0.00004-0

Serebryannyy, L.A., Parilla, M., Annibale, P., Cruz, C.M., Laster, K., Gratton, E., Kudryashov, D., Kosak, S.T., Gottardi, C.J., de Lanerolle, P., **2016**. Persistent nuclear actin filaments inhibit transcription by RNA polymerase II. J Cell Sci 129, 3412–3425. https://doi.org/10.1242/jcs.195867

Shah, S., Takei, Y., Zhou, W., Lubeck, E., Yun, J., Eng, C.-H.L., Koulena, N., Cronin, C., Karp, C., Liaw, E.J., Amin, M., Cai, L., **2018**. Dynamics and Spatial Genomics of the Nascent Transcriptome by Intron seqFISH. Cell 174, 363-376.e16. https://doi.org/10.1016/j.cell.2018.05.035

Shao, W., Zeitlinger, J., **2017**. Paused RNA polymerase II inhibits new transcriptional initiation. Nat Genet 49, 1045–1051. https://doi.org/10.1038/ng.3867

Singh, N., Reyes-Ordoñez, A., Compagnone, M.A., Moreno, J.F., Leslie, B.J., Ha, T., Chen, J., **2021**. Redefining the specificity of phosphoinositide-binding by human PH domain-containing proteins. Nat Commun 12, 4339. https://doi.org/10.1038/s41467-021-24639-y

Sobol, M., Krausová, A., Yildirim, S., Kalasová, I., Fáberová, V., Vrkoslav, V., Philimonenko, V., Marášek, P., Pastorek, L., Čapek, M., Lubovská, Z., Uličná, L., Tsuji, T., Lísa, M., Cvačka, J., Fujimoto, T., Hozak, P., **2018**. Nuclear phosphatidylinositol 4,5-bisphosphate islets contribute to efficient RNA polymerase II-dependent transcription. Journal of Cell Science 131, jcs211094. https://doi.org/10.1242/jcs.211094

Sobol, M., Yildirim, S., Philimonenko, V.V., Marášek, P., Castaño, E., Hozák, P., **2013**. UBF complexes with phosphatidylinositol 4,5-bisphosphate in nucleolar organizer regions regardless of ongoing RNA polymerase I activity. Nucleus 4, 478–486. https://doi.org/10.4161/nucl.27154

Steurer, B., Janssens, R.C., Geverts, B., Geijer, M.E., Wienholz, F., Theil, A.F., Chang, J., Dealy, S., Pothof, J., van Cappellen, W.A., Houtsmuller, A.B., Marteijn, J.A., **2018**. Live-cell analysis of endogenous GFP-RPB1 uncovers rapid turnover of initiating and promoter-paused RNA Polymerase II. Proc Natl Acad Sci U S A 115, E4368–E4376. https://doi.org/10.1073/pnas.1717920115

Surks, H.K., Richards, C.T., Mendelsohn, M.E., **2003**. Myosin phosphatase-Rho interacting protein. A new member of the myosin phosphatase complex that directly binds RhoA. J Biol Chem 278, 51484–51493. https://doi.org/10.1074/jbc.M305622200

Sztacho, M., Šalovská, B., Červenka, J., Balaban, C., Hoboth, P., Hozák, P., **2021**. Limited Proteolysis-Coupled Mass Spectrometry Identifies Phosphatidylinositol 4,5-Bisphosphate Effectors in Human Nuclear Proteome. Cells 10, E68. https://doi.org/10.3390/cells10010068

Ulferts, S., Prajapati, B., Grosse, R., Vartiainen, M.K., **2021**. Emerging Properties and Functions of Actin and Actin Filaments Inside the Nucleus. Cold Spring Harb Perspect Biol 13, a040121. https://doi.org/10.1101/cshperspect.a040121

van't Sant, L.J., White, J.J., Hoeijmakers, J.H.J., Vermeij, W.P., Jaarsma, D., **2021**. In vivo 5-ethynyluridine (EU) labelling detects reduced transcription in Purkinje cell degeneration mouse mutants, but can itself induce neurodegeneration. Acta Neuropathologica Communications 9, 94. https://doi.org/10.1186/s40478-021-01200-y

Viita, T., Kyheröinen, S., Prajapati, B., Virtanen, J., Frilander, M.J., Varjosalo, M., Vartiainen, M.K., **2019**. Nuclear actin interactome analysis links actin to KAT14 histone acetyl transferase and mRNA splicing. Journal of Cell Science 132, jcs226852. https://doi.org/10.1242/jcs.226852

Vos, S.M., Farnung, L., Boehning, M., Wigge, C., Linden, A., Urlaub, H., Cramer, P., **2018**. Structure of activated transcription complex Pol II–DSIF–PAF–SPT6. Nature 560, 607–612. https://doi.org/10.1038/s41586-018-0440-4

Wei, M., Fan, X., Ding, M., Li, R., Shao, S., Hou, Y., Meng, S., Tang, F., Li, C., Sun, Y., **2020**. Nuclear actin regulates inducible transcription by enhancing RNA polymerase II clustering. Science Advances 6, eaay6515. https://doi.org/10.1126/sciadv.aay6515

Wissink, E.M., Vihervaara, A., Tippens, N.D., Lis, J.T., **2019**. Nascent RNA Analyses: Tracking Transcription and Its Regulation. Nat Rev Genet 20, 705–723. https://doi.org/10.1038/s41576-019-0159-6

Yildirim, S., Castano, E., Sobol, M., Philimonenko, V.V., Dzijak, R., Venit, T., Hozák, P., **2013**. Involvement of phosphatidylinositol 4,5-bisphosphate in RNA polymerase I transcription. J Cell Sci 126, 2730–2739. https://doi.org/10.1242/jcs.123661

Yu, M., Yang, W., Ni, T., Tang, Z., Nakadai, T., Zhu, J., Roeder, R.G., **2015**. RNA Polymerase II-associated factor 1 regulates the release and phosphorylation of paused RNA Polymerase II. Science 350, 1383–1386. https://doi.org/10.1126/science.aad2338

7.4. Nuclear Phosphoinositides and Phase Separation: Important Players in Nuclear Compartmentalization

Martin Sztacho, Margarita Sobol, Can Balaban, Sara Escudeiro Lopes, Pavel Hozák

Advances in Biological Regulation. doi:10.1016/j.jbior.2018.09.009

IF: 4.84 (2019)

C.B. wrote the section “Actin-NM1-PIP2 interactions in RNAPII transcription”

Contents lists available at ScienceDirect

Advances in Biological Regulation

journal homepage: www.elsevier.com/locate/jbior

Nuclear phosphoinositides and phase separation: Important players in nuclear compartmentalization

Martin Sztacho[a], Margarita Sobol[a], Can Balaban[a], Sara Eliana Escudeiro Lopes[a], Pavel Hozák[a,b,c,*]

[a] Department of Biology of the Cell Nucleus, Institute of Molecular Genetics of the Czech Academy of Sciences, v.v.i., 142 20, Prague, Czech Republic
[b] Department of Epigenetics of the Cell Nucleus, Institute of Molecular Genetics of the Czech Academy of Sciences, v.v.i., division BIOCEV, 25250, Vestec, Czech Republic
[c] Microscopy Centre, Institute of Molecular Genetics of the Czech Academy of Sciences, v.v.i., 142 20, Prague, Czech Republic

ARTICLE INFO

Keywords: Nucleus
Phosphoinositides
Phase separation
Nuclear architecture
Transcription

ABSTRACT

Nuclear phosphoinositides are recognized as regulators of many nuclear processes including chromatin remodeling, splicing, transcription, DNA repair and epigenetics. These processes are spatially organized in different nuclear compartments. Phase separation is involved in the formation of various nuclear compartments and molecular condensates separated from surrounding environment. The surface of such structures spatiotemporally coordinates formation of protein complexes. PI(4,5)P2 (PIP2) integration into phase-separated structures might provide an additional step in their spatial diversification by attracting certain proteins with affinity to PIP2. Our laboratory has recently identified novel membrane-free PIP2-containing structures, so called Nuclear Lipid Islets (NLIs). We provide an evidence that these structures are evolutionary conserved in different organisms. We hypothesize that NLIs serve as a scaffolding platform which facilitates the formation of transcription factories, thus participating in the formation of nuclear architecture competent for transcription. In this review we speculate on a possible role of NLIs in the integration of various processes linked to RNAPII transcription, chromatin remodeling, actin-myosin interaction, alternative splicing and lamin structures.

1. Introduction

Phosphatidylinositol phosphates (PIPs) are phospholipids which act as precursors for second messengers or participate in the formation of diverse protein complexes on the surface of various membranous organelles and vesicles (Berridge and Irvine, 1984; Shewan et al., 2011). PIPs play important roles in membrane architecture and cytoskeletal dynamics, vesicular trafficking, signal transduction and neurotransmission (Di Paolo and De Camilli, 2006; Raben and Barber, 2017). Their exact functions depend on their localization and phosphorylation state. PIPs can be phosphorylated by a number of phosphoinositide kinases and dephosphorylated by phosphatases at positions 3, 4, or 5 of the inositol ring giving rise to seven different phosphorylated forms (Shewan et al., 2011).

Abbreviations: ALS, Amyotrophic lateral sclerosis; ARP, actin-related protein; AS, alternative splicing; IEM, Immunogold electron microscopy; NLIs, nuclear lipid islets; NM1, nuclear myosin I; PIPs, Phosphatidylinositol phosphates; PIP2, Phosphatidylinositol 4,5-bisphosphate; RNAP, RNA polymerase; SRSF, Serine/Arginine rich splicing factors; SWI/SNF, SWItch/Sucrose Non-Fermentable; TF, transcription factor

* Corresponding author. Department of Biology of the Cell Nucleus, Institute of Molecular Genetics of the Czech Academy of Sciences, v.v.i., 142 20, Prague, Czech Republic.
E-mail address: hozak@img.cas.cz (P. Hozák).

https://doi.org/10.1016/j.jbior.2018.09.009
Received 31 August 2018; Received in revised form 14 September 2018; Accepted 15 September 2018

Many enzymes of PIPs metabolism were detected in the nucleus (Barlow et al., 2010). Even though PIPs were identified among the first phospholipids in the nucleus, their nuclear functions have not been described in such details as their cytoplasmic counterparts (Osborne et al., 2001; Shah et al., 2013). Due to the lack of membranous organelles within the nucleus, data describing the presence of nuclear phosphoinositides were considered as controversial. However, an increasing amount of evidences opened a new field in the study of the crucial nuclear processes such as cell cycle progression, cell differentiation and proliferation (Ratti et al., 2018). PIP2 is one of the most abundant phosphoinositides in the nucleus and therefore its possible functions have been extensively studied during the last two decades (Jungmichel et al., 2014). In this review we will focus on the possible role of PIP2 as a determinant of spatial and functional diversification of the nuclear architecture. Several localization studies using different specific tools and imaging ap- proaches showed that PIP2 is enriched in various nuclear compartments: at nuclear speckles, nucleoli, and in the nucleoplasm (Boronenkov et al., 1998; Kalasova et al., 2016; Mazzotti et al., 1995; Mortier et al., 2005; Osborne et al., 2001; Sobol et al., 2013; Ulicna et al., 2018a; Vann et al., 1997; Watt et al., 2002; Yildirim et al., 2013). The first detailed description of the nucleoplasmic PIP2 revealed that it is the major component of the newly discovered NLIs (Sobol et al., 2018). The question, how these aliphatic molecules can be distributed in the membrane-free nuclear environment, remains elusive. One possibility is that lipid acyl groups are bound into the protein hydrophobic cavities as documented by example of SF1 protein. SF1 uses its hydrophobic binding pocket to hide acyl chains of PIP2 and PI(3,4,5)P3 (Blind et al., 2012; Blind et al., 2014). Second possibility is that lipids aggregate and reorient their hydrophobic moieties inward the micellar structures, where they are not in contact with aqueous environment. Third, yet not well described complex RNA folds which might hypothetically participate in lipid aggregation (discussed below). In all these sce- narios, the hydrophilic inositol head with the phosphate group(s) remains exposed and accessible for proteins recognizing the ne- gative charge(s). The strong indication that PIP2 may have a role in nuclear processes comes from the work of Lewis et al. (2011), where the authors have identified more than 300 regulatory nuclear proteins which interact with PIP2. In accordance with these important findings, there is a growing number of studies showing that PIP2 is involved in regulation of nuclear pathways. PIP2 has both inducible and repressive functions in processes like pre-mRNA splicing and polyadenylation, rRNA processing, chromatin re- modeling, histone acetylation/deacetylation, regulation of RNAPs transcriptional activity (Shah et al., 2013; Ulicna et al., 2018b). These PIP2 functions are realized through the alterations of protein conformation and/or protein localization (Rando et al., 2002; Ulicna et al., 2018a; Yildirim et al., 2013). Hence, the spatial distribution of PIP2 in different parts of the nucleus may result from its binding to various nuclear proteins thus determining the function of PIP2 in the nuclear structures. These nuclear structures are membrane-less so might be formed by the phase separation (Mitrea and Kriwacki, 2016).

2. Formation of nuclear structures by phase separation

Cellular compartmentalization regulates kinetics of complex biochemical reactions by controlling the localization of reaction components (Levy et al., 2014). In the cytoplasm, it is achieved through the compartmentalization of membrane-delineated orga- nelles, molecular crowding, recruitment of proteins onto surfaces or formation of liquid-liquid phase separated boundaries (Hyman et al., 2014; Leake, 2018; Mitrea and Kriwacki, 2016; Stanek and Fox, 2017). Functional compartmentalization of membrane-free nuclear environment can be explained by association of scaffolding proteins and nucleic acids or lipids (Courchaine et al., 2016; Sawyer and Dundr, 2016). Phase separation is an entropy-driven mechanism by which molecules condense into dynamic liquid-like droplets, where concentration of particular molecules is higher than in the neighboring environment (Hyman et al., 2014). Therefore, the phase separation enables formation of surfaces, where the recruitment of proteins increases the probability of their interactions and thus efficiency of complex formation at the right place and right time (Hyman et al., 2014; Mitrea and Kriwacki, 2016; Stroberg and Schnell, 2018). Formation of such condensates depends on the multivalence of interactions among structural components. Typically, the interacting molecules might be the proteins with multiple interaction domains and/or intrinsically disordered regions (IDRs), nucleic acids with tandem repeats, and the lipids with hydrophobic acyl chains. IDRs lack the defined secondary and tertiary structure and therefore can adopt various conformations depending on a type and number of interacting partners. Thus, they can act as hubs for a crosstalk among different regulatory pathways (Mahmoudabadi et al., 2013; Protter et al., 2018). It is becoming more evident that multivalent base pairing in non-coding RNAs is involved in the condensation of phase separated nuclear structures, thus participating in nuclear compartmentalization (Saha and Hyman, 2017; Stanek and Fox, 2017). It is of a great interest that tandem repeats within RNA transcripts are linked to pathogenesis of disorders like Huntington disease, myotonic dystrophy, or ALS (Jain and Vale, 2017). These diseases are characterized by the accumulation of tandem repeats leading to the formation of RNA-containing foci within nucleus (Jain and Vale, 2017). Formation of such structures causes an imbalance in both physiological molecular distribution and a crosstalk of nuclear regulatory proteins (Sun et al., 2017). Interestingly, RNA seems to be an integral constituent of various nuclear structures containing PIP2 (Stanek and Fox, 2017). Could RNA be responsible for an integration of PIP2 hydrophobic tails into nuclear structures? RNA can adopt complex conformations enabling various interactions. It was shown that oligomerization is a key factor increasing the RNA affinity for phospholipid-containing membranes (Vlassov et al., 2001). Moreover, series of short helical regions

interspersed with non-canonical base pairing regions, multi-base contacts, or flips-out allow residues to adopt non-canonical tertiary conformations. This enables RNA molecules to pack together and produce unique architecture (Doudna and Doherty, 1997; Reiter et al., 2011). Indeed, several studies showed that RNA internal repeats and vertical base stacking contribute to formation of structures which interact with both hydrophobic and hydrophilic parts of lipids (Khvorova et al., 1999; Majerfeld and Yarus, 1994;Marty et al., 2009). The existence of multivalent RNA molecules as a structural component of nuclear structures leads us to a speculation that RNA might be crucial for the formation of hydrophobic cavities, where acyl chains of lipids might be buried. Inaccordance with that, RNA seems to be the crucial element for PIP2 nuclear localization, since RNA enzymatic digestion leads to substantial reduction of PIP2 signal within the nucleoplasm (Osborne et al., 2001; Sobol et al., 2018).

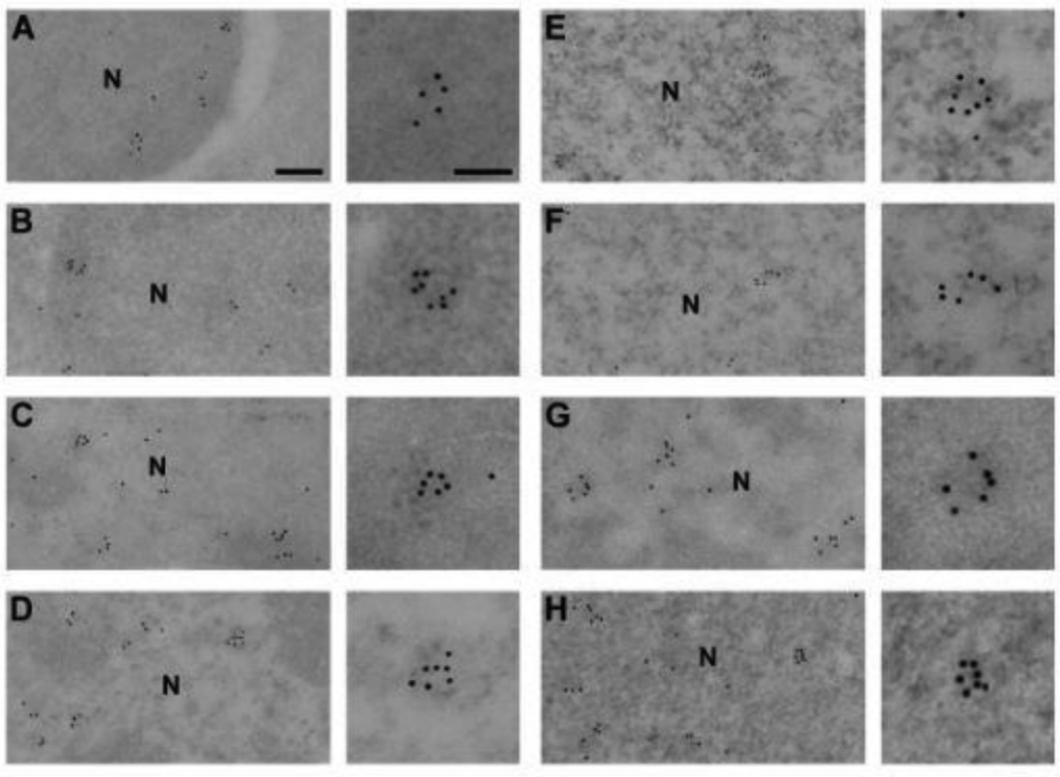

Fig. 1. NLIs are evolutionary conserved nuclear structures in different organisms. Immunogold electron microscopy (IEM) on ultrathin sec- tions shows that all studied organisms have similar PIP2-containing structures of 40–100 nm size visualized with anti-PIP2 antibody and secondary antibody conjugated to 12 nm gold particles. Yeast (*Saccharomyces cerevisiae* - A), protozoa (Giardia lamblia – B, Tetrahymena thermophila - C), beans (Vicia faba; germinated bean meristem cells - D), mice (*Mus musculus*; primary skin fibroblasts - E), humans (*Homo sapiens*: mesenchymal stem

cells – F, stimulated lymphocytes – G, cervical carcinoma cells – H) N – nucleus. General view: bar is 200 nm, magnified view: bar is 100 nm.

3. Discovery of PIP2-containing NLIs

We recently discovered a novel type of nuclear PIP2-enriched structures, which we termed NLIs (Sobol et al., 2018). The size ofthese structures varies from 40 to 100 nm and they have no detectable membrane (Fig. 1). The surface of NLIs contains PIP2, cholesterol and ceramide. Furthermore, the surface of NLIs is in the proximity to chromatin. About 73% of NLIs contain RNA at the surface. In accordance with this, the integrity of NLIs is dependent on the presence of RNA, since the treatment by RNase leads to lossof NLIs (Sobol et al., 2018). The NLIs contain proteins, lipids and RNA - the typical components of phase separated nuclear com- partment (Banani et al., 2017; Stanek and Fox, 2017; Weber and Brangwynne, 2012). Based on this we speculate that NLIs might represent a novel type of nuclear compartment formed by phase separation. To confirm whether NLIs are evolutionary conserved structures, we studied the distribution of PIP2 in the nuclei of different organisms (Fig. 1A–H). With the immunogold electron microscopy (IEM), we demonstrated that yeast, protozoa, beans, mice, and humans exhibit similar NLIs of 40–100 nm in diameter.

NLIs are therefore evolutionary conserved nuclear structures among different organisms. What is the function of such evolutionary conserved structures? Our recently published data indicate that about a half of nascent transcripts localize at the surface of NLIs implying their function in transcription (Sobol et al., 2018). The notion of active transcription clustered in nuclear foci was describedin many other studies (Cisse et al., 2013; Cho et al., 2016a, 2016b, 2018; Pombo et al., 1999). Recently published work shows that gene clusters and super-enhancers may form nuclear foci with liquid-like properties (Sabari et al., 2018). It is obvious that there is a certain degree of transcriptional compartmentalization in the nucleus. Our recent study suggests that NLIs may be involved in the association of active RNAPII complexes with the transcription factor NM1 in order to maintain the transcription (Sobol et al., 2018). NM1 contains PH domain with the capacity to bind specifically to PIP2. The NM1 mutation abolishing the PIP2 binding prevents the interaction of NM1 with RNAPII. Further, the overexpression of this mutated NM1 is insufficient to revert the transcription to thenormal level in NM1-deficient cells. The surface of NLIs attracts NM1 and other transcription factors (TFIID, TFIIE, and TFIIH) (Sobol et al., 2018). Therefore, we hypothesize that PIP2-enriched surface of NLIs serves as a scaffolding platform bringing in close proximity all the necessary components for efficient transcription.

4. Actin-NM1-PIP2 interactions in RNAPII transcription

It was shown that β-actin and NM1 complex is necessary for proper transcription of RNAPI and RNAPII (Almuzzaini et al., 2015;Castano et al., 2010; Hofmann et al., 2004; Kalendova et al., 2014; Philimonenko et al., 2004, 2010; Sobol et al., 2018). Moreover, NM1 was described as a part of B-WICH complex which positively regulates RNAPIII transcription by changing the chromatin structure (Vintermist et al., 2011). It seems that the transcription of active genes is enhanced by NM1-actin interaction. NM1 as a member of unconventional myosin family with only one motor head domain is probably not involved in movement along the longactin fibers, since long actin fibers are normally not present in the nucleus (Castano et al., 2010). Multiple single headed NM1 molecules present on the NLIs surface might produce a processive force enabling “tread-milling” of transcription machinery. Such possible phenomenon might also provide a force during chromosomal rearrangement. Involvement of PIP2 and actin in the recruitment of the chromatin remodeling SWI/SNF complex is previously documented (Rando et al., 2002; Zhao et al., 1998). Inter- estingly, some of the SWI/SNF subunits belong to actin related protein (ARP) family (Peterson et al., 1998). This is in accordance with our yet unpublished observations that SWI/SNF subunit together with several SRSF proteins regulating splicing site selection are enriched at NLIs. Therefore, PIP2-containing NLIs surface may connect transcription and chromosome remodeling pathways onto the same spatial units within nucleoplasm. Also transcriptional dynamics might be one of the regulatory mechanism for alternative splicing (AS). This presumption is interesting with regard to the previously observed effect of SWI/SNF on the alternative splicing of pre-mRNA (Batsche et al., 2006; Tyagi et al., 2009; Waldholm et al., 2011). Low transcription elongation rates favour the proximal splicing sites which are longer exposed to the splicing machinery, while fast RNAP rates increase the chance of use of the weeksplicing sites leading to AS (de la Mata et al., 2003; Kornblihtt, 2005; Tyagi et al., 2009). Thus, enhanced initiation rate would increase the incidence of AS. Enhancing RNAPII fidelity and spatial arrangement of chromatin might enable the more frequent use of weak splicing sites. Therefore, these indications might suggest that PIP2-associated actin-NM1 complex mediates formation of active RNAPII machinery together with the increasing chromatin accessibility. The accessibility of transcriptionally active chromatin is a one of the key factors determining the gene expression level. This might represent a possible mechanism, how spatial organization of regulatory elements on the NLIs PIP2-enriched surface regulates gene expression at the level of DNA accessibility, RNAP dynamicsand RNA processing.

5. Nucleoplasmic lamins and transcription

Here we would like to discuss another phenomenon, which could be in a close connection to above mentioned nuclear PIP2- dependent regulatory mechanism of intranuclear order. Lamins are the components of lamina forming a protein meshwork which acts as a scaffold for many structural and functional proteins underneath the inner nuclear membrane (Mattout-Drubezki and Gruenbaum, 2003). The nuclear lamina anchors chromatin at the nuclear periphery and is linked to a gene repression (Dechat et al., 2009; Reddy et al., 2008; Verstraeten et al., 2007). Electron microscopy studies described the existence of nucleoplasmic lamin pool localizing throughout the nuclear interior (Hozak et al., 1995). This nucleoplasmic lamin is suggested to be a determinant of nuclear archi-tecture acting through chromosome positioning in the intranuclear space (Dechat et al., 2008; Dorner et al., 2007; Goldman et al., 2002; Naetar et al., 2017; Vlcek and Foisner, 2007a; b). Nucleoplasmic lamins were shown to play an important role in such processes as chromatin remodeling, DNA replication, DNA repair, and RNAPII transcription (Broers et al., 2006; Dechat et al., 2008; Guelen et al., 2008; Montes de Oca et al., 2009). It was also shown that nucleoplasmic lamin pool associates with transcriptionally active chromatin and is important for RNAPII-driven transcription (Gesson et al., 2016; Kolb et al., 2011). Indeed, disassembly of higher- order nucleoplasmic lamin structures impairs RNAPII transcription (Kumaran et al., 2002; Spann et al., 2002). Our yet unpublished data reveal a possible interaction between lamin A and PIP2 in the nucleoplasm (Escudeiro Lopes our unpublished data). Here we propose that the PIP2-enriched NLIs surface might serve as a scaffold for lamin function regulating gene expression in the nucleo- plasm. Lamins likely regulate transcription in several ways. On the one hand, lamins act by sequestering transcription factors into inactive areas at the inner membrane of nuclear envelope. On the other hand, lamins might provide the platform for gene expression in nucleoplasm. Mutations causing laminopathies induce alterations of such processes leading to tissue-specific pathogenic patterns in gene expression (Broers et al., 2006; Capanni et al., 2003, 2005; Cenni et al., 2005; Filesi et al., 2005; Goldman et al., 2004; Hutchison, 2002; Naetar and Foisner, 2009; Sabatelli et al., 2001; Sullivan et al., 1999). It will be very exciting to test whether mutations connected to diverse laminopathies are affecting the ability of lamins to interact with PIP2 directly or indirectly at the surface of NLIs. Further studies may bring valuable information about such aberrations in molecular mechanisms involved in NLIs- dependent gene expression.

6. Conclusion

Here, we discussed the nucleoplasmic functions of PIP2 linked to gene expression. PIP2 present on the surface of NLIs enables recruitment of RNAPII machinery together with the components involved in the regulation of the chromatin accessibility, RNA splicing as well as the structural proteins (NM1, actin, lamins). Newly discovered NLIs may enable spatial and temporal organization of particular protein complexes thus regulating crucial nuclear processes. It is important to understand the underlying molecular mechanisms, because the aberrations in these spatio-temporal regulations might affect the dynamic interplay on the surface of NLIs leading to the changes in transcriptional patterns and thus the development of such pathological states as laminopathies.

Conflict of interest disclosure

The authors declare no competing conflicts of interest to disclose.

Acknowledgments

This study was supported by the Grant Agency of the Czech Republic (16-03346S, 17-09103S); the Technology Agency of the Czech Republic (TE01020118); the European Regional Development Fund via the project 'BIOCEV-Biotechnology and Biomedicine Centre of the Academy of Sciences and Charles University' (CZ.1.05/1.1.00/02.0109) and the project 'Modernization and support of research activities of the national infrastructure for biological and medical imaging Czech-BioImaging' (CZ.02.1.01/0.0/0.0/16_013/ 0001775); the Czech Academy of Sciences (JSPS-18-18/748934); the Institute of Molecular Genetics (IMG) of the CAS
(RVO:68378050). We thank the Light Microscopy Core Facility, IMG of the CAS, Prague, Czech Republic, supported by the Ministry of Education, Youth and Sports of the Czech Republic (LM2015062); the Operational Program Prague – Competitiveness (CZ.2.16/ 3.1.00/21547) co-financed by the European Regional Development Fund; the National Programme of Sustainability I (LO1419) from the Ministry of Education, Youth and Sports of the Czech Republic. We thank the Electron Microscopy Core Facility, IMG of the CAS, Prague, Czech Republic, supported by the Ministry of Education, Youth and Sports of the Czech Republic (LM2015062 Czech-BioImaging).

References

Almuzzaini, B., Sarshad, A.A., Farrants, A.K., Percipalle, P., 2015. Nuclear myosin 1 contributes to a chromatin landscape compatible with RNA polymerase IItranscription activation. BMC Biol. 13, 35.

Banani, S.F., Lee, H.O., Hyman, A.A., Rosen, M.K., 2017. Biomolecular condensates: organizers of cellular biochemistry. Nat. Rev. Mol. Cell Biol. 18, 285–298.

Barlow, C.A., Laishram, R.S., Anderson, R.A., 2010. Nuclear phosphoinositides: a signaling enigma wrapped in a compartmental conundrum. Trends Cell Biol. 20,25–35.

Batsche, E., Yaniv, M., Muchardt, C., 2006. The human SWI/SNF subunit Brm is a regulator of alternative splicing. Nat. Struct. Mol. Biol. 13, 22–29.

Berridge, M.J., Irvine, R.F., 1984. Inositol trisphosphate, a novel 2nd messenger in cellular signal transduction. Nature 312, 315–321.

Blind, R.D., Sablin, E.P., Kuchenbecker, K.M., Chiu, H.J., Deacon, A.M., Das, D., Fletterick, R.J., Ingraham, H.A., 2014. The signaling phospholipid PIP3 creates a newinteraction surface on the nuclear receptor SF-1. Proc. Natl. Acad. Sci. U. S. A. 111, 15054–15059.

Blind, R.D., Suzawa, M., Ingraham, H.A., 2012. Direct modification and activation of a nuclear receptor-PIP(2) complex by the inositol lipid kinase IPMK. Sci. Signal 5, ra44.

Boronenkov, I.V., Loijens, J.C., Umeda, M., Anderson, R.A., 1998. Phosphoinositide signaling pathways in nuclei are associated with nuclear speckles containing pre-mRNA processing factors. Mol. Biol. Cell 9, 3547–3560.

Broers, J.L., Ramaekers, F.C., Bonne, G., Yaou, R.B., Hutchison, C.J., 2006. Nuclear lamins: laminopathies and their role in premature ageing. Physiol. Rev. 86,967–1008.

Capanni, C., Cenni, V., Mattioli, E., Sabatelli, P., Ognibene, A., Columbaro, M., Parnaik, V.K., Wehnert, M., Maraldi, N.M., Squarzoni, S., et al., 2003. Failure of lamin A/C to functionally assemble in R482L mutated familial partial lipodystrophy fibroblasts: altered intermolecular interaction with emerin and implications for genetranscription. Exp. Cell Res. 291, 122–134.

Capanni, C., Mattioli, E., Columbaro, M., Lucarelli, E., Parnaik, V.K., Novelli, G., Wehnert, M., Cenni, V., Maraldi, N.M., Squarzoni, S., et al., 2005. Altered pre-lamin A processing is a common mechanism leading to lipodystrophy. Hum. Mol. Genet. 14, 1489–1502.

Castano, E., Philimonenko, V.V., Kahle, M., Fukalova, J., Kalendova, A., Yildirim, S., Dzijak, R., Dingova-Krasna, H., Hozak, P., 2010. Actin complexes in the cellnucleus: new stones in an old field. Histochem. Cell Biol. 133, 607–626.

Cenni, V., Sabatelli, P., Mattioli, E., Marmiroli, S., Capanni, C., Ognibene, A., Squarzoni, S., Maraldi, N.M., Bonne, G., Columbaro, M., et al., 2005. Lamin A N-terminal phosphorylation is associated with myoblast activation: impairment in Emery-Dreifuss muscular dystrophy. J. Med. Genet. 42, 214–220.

Cho, W.K., Jayanth, N., English, B.P., Inoue, T., Andrews, J.O., Conway, W., Grimm, J.B., Spille, J.H., Lavis, L.D., Lionnet, T., et al., 2016a. RNA Polymerase II clusterdynamics predict mRNA output in living cells. Elife 5.

Cho, W.K., Jayanth, N., Mullen, S., Tan, T.H., Jung, Y.J., Cisse II, , 2016b. Super-resolution imaging of fluorescently labeled, endogenous RNA Polymerase II in livingcells with CRISPR/Cas9-mediated gene editing. Sci. Rep. 6, 35949.

Cho, W.K., Spille, J.H., Hecht, M., Lee, C., Li, C., Grube, V., Cisse II, , 2018. Mediator and RNA polymerase II clusters associate in transcription-dependent condensates. Science 361, 412–415.

Cisse II, , Izeddin, I., Causse, S.Z., Boudarene, L., Senecal, A., Muresan, L., Dugast-Darzacq, C., Hajj, B., Dahan, M., Darzacq, X., 2013. Real-time dynamics of RNApolymerase II clustering in live human cells. Science 341, 664–667.

Courchaine, E.M., Lu, A., Neugebauer, K.M., 2016. Droplet organelles? EMBO J. 35, 1603–1612.

de la Mata, M., Alonso, C.R., Kadener, S., Fededa, J.P., Blaustein, M., Pelisch, F., Cramer, P., Bentley, D., Kornblihtt, A.R., 2003. A slow RNA polymerase II affectsalternative splicing in vivo. Mol. Cell 12, 525–532.

Dechat, T., Pfleghaar, K., Sengupta, K., Shimi, T., Shumaker, D.K., Solimando, L., Goldman, R.D., 2008. Nuclear lamins: major factors in the structural organization andfunction of the nucleus and chromatin. Genes Dev. 22, 832–853.

Dechat, T., Adam, S.A., Goldman, R.D., 2009. Nuclear lamins and chromatin: when structure meets function. Adv.

Enzym. Regul. 49, 157–166.Di Paolo, G., De Camilli, P., 2006. Phosphoinositides in cell regulation and membrane

dynamics. Nature 443, 651–657.

Dorner, D., Gotzmann, J., Foisner, R., 2007. Nucleoplasmic lamins and their interaction partners, LAP2alpha, Rb, and BAF, in transcriptional regulation. FEBS J. 274,1362–1373.

Doudna, J.A., Doherty, E.A., 1997. Emerging themes in RNA folding. Folding Des. 2, R65–R70.

Filesi, I., Gullotta, F., Lattanzi, G., D'Apice, M.R., Capanni, C., Nardone, A.M., Columbaro, M., Scarano, G., Mattioli, E., Sabatelli, P., et al., 2005. Alterations of nuclear envelope and chromatin organization in mandibuloacral dysplasia, a rare form of laminopathy. Physiol. Genom. 23, 150–158.

Gesson, K., Rescheneder, P., Skoruppa, M.P., von Haeseler, A., Dechat, T., Foisner, R., 2016. A-type lamins bind both hetero- and euchromatin, the latter beingregulated by lamina-associated polypeptide 2 alpha. Genome Res. 26, 462–473.

Goldman, R.D., Gruenbaum, Y., Moir, R.D., Shumaker, D.K., Spann, T.P., 2002. Nuclear lamins: building blocks of nuclear architecture. Genes Dev. 16, 533–547.

Goldman, R.D., Shumaker, D.K., Erdos, M.R., Eriksson, M., Goldman, A.E., Gordon, L.B., Gruenbaum, Y., Khuon, S., Mendez, M., Varga, R., et al., 2004. Accumulationof mutant lamin A causes progressive changes in nuclear architecture in Hutchinson-Gilford progeria syndrome. Proc. Natl. Acad. Sci. U. S. A. 101, 8963–8968.

Guelen, L., Pagie, L., Brasset, E., Meuleman, W., Faza, M.B., Talhout, W., Eussen, B.H., de Klein, A., Wessels, L., de Laat, W., et al., 2008. Domain organization of humanchromosomes revealed by mapping of nuclear lamina interactions. Nature 453, 948–951.

Hofmann, W.A., Stojiljkovic, L., Fuchsova, B., Vargas, G.M., Mavrommatis, E., Philimonenko, V., Kysela, K., Goodrich, J.A., Lessard, J.L., Hope, T.J., et al., 2004. Actin is part of pre-initiation complexes and is necessary for transcription by RNA polymerase II. Nat. Cell Biol. 6, 1094–1101.

Hozak, P., Sasseville, A.M., Raymond, Y., Cook, P.R., 1995. Lamin proteins form an internal nucleoskeleton as well as a peripheral lamina in human cells. J. Cell Sci. 108 (Pt 2), 635–644.

Hutchison, C.J., 2002. Lamins: building blocks or regulators of gene expression? Nat. Rev. Mol. Cell Biol. 3, 848–858. Hyman, A.A., Weber, C.A., Julicher, F., 2014. Liquid-liquid phase separation in biology. Annu. Rev. Cell Dev. Biol. 30, 39–58.Jain, A., Vale, R.D., 2017. RNA phase transitions in repeat expansion disorders. Nature 546, 243–247.

Jungmichel, S., Sylvestersen, K.B., Choudhary, C., Nguyen, S., Mann, M., Nielsen, M.L., 2014. Specificity and commonality of the phosphoinositide-binding proteomeanalyzed by quantitative mass spectrometry. Cell Rep. 6, 578–591.

Kalasova, I., Faberova, V., Kalendova, A., Yildirim, S., Ulicna, L., Venit, T., Hozak, P., 2016. Tools for visualization of phosphoinositides in the cell nucleus. Histochem. Cell Biol. 145, 485–496.

Kalendova, A., Kalasova, I., Yamazaki, S., Ulicna, L., Harata, M., Hozak, P., 2014. Nuclear actin filaments recruit cofilin and actin-related protein 3, and their formationis connected with a mitotic block. Histochem. Cell Biol. 142, 139–152.

Khvorova, A., Kwak, Y.G., Tamkun, M., Majerfeld, I., Yarus, M., 1999. RNAs that bind and change the permeability of phospholipid membranes. Proc. Natl. Acad. Sci. USA 96, 10649–10654.

Kolb, T., Maass, K., Hergt, M., Aebi, U., Herrmann, H., 2011. Lamin A and lamin C form homodimers and coexist in higher complex forms both in the nucleoplasmicfraction and in the lamina of cultured human cells. Nucleus 2, 425–433.
Kornblihtt, A.R., 2005. Promoter usage and alternative splicing. Curr. Opin. Cell Biol. 17, 262–268.
Kumaran, R.I., Muralikrishna, B., Parnaik, V.K., 2002. Lamin A/C speckles mediate spatial organization of splicing factor compartments and RNA polymerase IItranscription. J. Cell Biol. 159, 783–793.
Leake, M.C., 2018. Transcription factors in eukaryotic cells can functionally regulate gene expression by acting in oligomeric assemblies formed from an intrinsically disordered protein phase transition enabled by molecular crowding. Transcription 1–9.
Levy, E.D., Kowarzyk, J., Michnick, S.W., 2014. High-resolution mapping of protein concentration reveals principles of proteome architecture and adaptation. CellRep. 7, 1333–1340.
Lewis, A.E., Sommer, L., Arntzen, M.O., Strahm, Y., Morrice, N.A., Divecha, N., D'Santos, C.S., 2011. Identification of nuclear phosphatidylinositol 4,5-bisphosphate-interacting proteins by neomycin extraction. Mol. Cell. Proteomics 10 M110 003376.
Mahmoudabadi, G., Rajagopalan, K., Getzenberg, R.H., Hannenhalli, S., Rangarajan, G., Kulkarni, P., 2013. Intrinsically disordered proteins and conformational noise:implications in cancer. Cell Cycle 12, 26–31.
Majerfeld, I., Yarus, M., 1994. An RNA pocket for an aliphatic hydrophobe. Nat. Struct. Biol. 1, 287–292.
Marty, R., N'Soukpoe-Kossi, C.N., Charbonneau, D.M., Kreplak, L., Tajmir-Riahi, H.A., 2009. Structural characterization of cationic lipid-tRNA complexes. NucleicAcids Res. 37, 5197–5207.
Mattout-Drubezki, A., Gruenbaum, Y., 2003. Dynamic interactions of nuclear lamina proteins with chromatin and transcriptional machinery. Cell. Mol. Life Sci. 60,2053–2063.
Mazzotti, G., Zini, N., Rizzi, E., Rizzoli, R., Galanzi, A., Ognibene, A., Santi, S., Matteucci, A., Martelli, A.M., Maraldi, N.M., 1995. Immunocytochemical detection of phosphatidylinositol 4,5-bisphosphate localization sites within the nucleus. J. Histochem. Cytochem. 43, 181–191.
Mitrea, D.M., Kriwacki, R.W., 2016. Phase separation in biology; functional organization of a higher order. Cell Commun. Signal. 14, 1.
Montes de Oca, R., Shoemaker, C.J., Gucek, M., Cole, R.N., Wilson, K.L., 2009. Barrier-to-autointegration factor proteome reveals chromatin-regulatory partners. PLoSOne 4 e7050.
Mortier, E., Wuytens, G., Leenaerts, I., Hannes, F., Heung, M.Y., Degeest, G., David, G., Zimmermann, P., 2005. Nuclear speckles and nucleoli targeting by PIP2-PDZdomain interactions. EMBO J. 24, 2556–2565.
Naetar, N., Foisner, R., 2009. Lamin complexes in the nuclear interior control progenitor cell proliferation and tissue homeostasis. Cell Cycle 8, 1488–1493.
Naetar, N., Ferraioli, S., Foisner, R., 2017. Lamins in the nuclear interior - life outside the lamina. J. Cell Sci. 130, 2087–2096.
Osborne, S.L., Thomas, C.L., Gschmeissner, S., Schiavo, G., 2001. Nuclear PtdIns(4,5)P2 assembles in a mitotically regulated particle involved in pre-mRNA splicing. J.Cell Sci. 114, 2501–2511.
Peterson, C.L., Zhao, Y., Chait, B.T., 1998. Subunits of the yeast SWI/SNF complex are members of the actin-related protein (ARP) family. J. Biol. Chem. 273, 23641–23644.
Philimonenko, V.V., Zhao, J., Iben, S., Dingova, H., Kysela, K., Kahle, M., Zentgraf, H., Hofmann, W.A., de Lanerolle, P., Hozak, P., et al., 2004. Nuclear actin andmyosin I are required for RNA polymerase I transcription. Nat. Cell Biol. 6, 1165–1172.
Philimonenko, V.V., Janacek, J., Harata, M., Hozak, P., 2010. Transcription-dependent rearrangements of actin and nuclear myosin I in the nucleolus. Histochem. CellBiol. 134, 243–249.
Pombo, A., Jackson, D.A., Hollinshead, M., Wang, Z., Roeder, R.G., Cook, P.R., 1999. Regional specialization in human nuclei: visualization of discrete sites of transcription by RNA polymerase III. EMBO J. 18, 2241–2253.
Protter, D.S.W., Rao, B.S., Van Treeck, B., Lin, Y., Mizoue, L., Rosen, M.K., Parker, R., 2018. Intrinsically disordered regions can contribute promiscuous interactions toRNP granule assembly. Cell Rep. 22, 1401–1412.
Raben, D.M., Barber, C.N., 2017. Phosphatidic acid and neurotransmission. Adv Biol Regul 63, 15–21.
Rando, O.J., Zhao, K., Janmey, P., Crabtree, G.R., 2002. Phosphatidylinositol-dependent actin filament binding by the SWI/SNF-like BAF chromatin remodelingcomplex. Proc. Natl. Acad. Sci. U. S. A. 99, 2824–2829.
Ratti, S., Ramazzotti, G., Faenza, I., Fiume, R., Mongiorgi, S., Billi, A.M., McCubrey, J.A., Suh, P.G., Manzoli, L., Cocco, L., et al., 2018. Nuclear inositide signaling and cell cycle. Adv. Biol. Regul. 67, 1–6.
Reddy, K.L., Zullo, J.M., Bertolino, E., Singh, H., 2008. Transcriptional repression mediated by repositioning of genes to the nuclear lamina. Nature 452, 243–247.Reiter, N.J., Chan, C.W., Mondragon, A., 2011. Emerging structural themes in large RNA molecules. Curr. Opin. Struct. Biol. 21, 319–326.
Sabari, B.R., Dall'Agnese, A., Boija, A., Klein, I.A., Coffey, E.L., Shrinivas, K., Abraham, B.J., Hannett, N.M., Zamudio, A.V., Manteiga, J.C., et al., 2018. Coactivatorcondensation at super-enhancers links phase separation and gene control. Science 361.
Sabatelli, P., Lattanzi, G., Ognibene, A., Columbaro, M., Capanni, C., Merlini, L., Maraldi, N.M., Squarzoni, S., 2001. Nuclear alterations in autosomal-dominant Emery-Dreifuss muscular dystrophy. Muscle Nerve 24, 826–829.
Saha, S., Hyman, A.A., 2017. RNA gets in phase. J. Cell Biol. 216, 2235–2237.
Sawyer, I.A., Dundr, M., 2016. Nuclear bodies: built to boost. J. Cell Biol. 213, 509–511.
Shah, Z.H., Jones, D.R., Sommer, L., Foulger, R., Bultsma, Y., D'Santos, C., Divecha, N., 2013. Nuclear phosphoinositides and their impact on nuclear functions. FEBS J. 280, 6295–6310.
Shewan, A., Eastburn, D.J., Mostov, K., 2011. Phosphoinositides in cell architecture. Csh. Perspect. Biol. 3.
Sobol, M., Yildirim, S., Philimonenko, V.V., Marasek, P., Castano, E., Hozak, P., 2013. UBF complexes with phosphatidylinositol 4,5-bisphosphate in nucleolarorganizer regions regardless of ongoing RNA polymerase I activity. Nucleus 4, 478–486.
Sobol, M., Krausova, A., Yildirim, S., Kalasova, I., Faberova, V., Vrkoslav, V., Philimonenko, V., Marasek, P., Pastorek, L., Capek, M., et al., 2018. Nuclear phos-phatidylinositol 4,5-bisphosphate islets contribute to efficient RNA polymerase II-dependent transcription. J. Cell Sci. 131.
Spann, T.P., Goldman, A.E., Wang, C., Huang, S., Goldman, R.D., 2002. Alteration of nuclear lamin organization inhibits RNA polymerase II-dependent transcription. J.Cell Biol. 156, 603–608.
Stanek, D., Fox, A.H., 2017. Nuclear bodies: news insights into structure and function. Curr. Opin. Cell Biol. 46, 94–101.
Stroberg, W., Schnell, S., 2018. Do cellular condensates accelerate biochemical reactions? Lessons from microdroplet chemistry. Biophys. J. 115, 3–8.
Sullivan, T., Escalante-Alcalde, D., Bhatt, H., Anver, M., Bhat, N., Nagashima, K., Stewart, C.L., Burke, B., 1999. Loss of A-type lamin expression compromises nuclearenvelope integrity leading to muscular dystrophy. J. Cell Biol. 147, 913–920.
Sun, X.H., Ali, M.S.S.H., Moran, M., 2017. The role of interactions of long non-coding RNAs and heterogeneous nuclear ribonucleoproteins in regulating cellularfunctions. Biochem. J. 474, 2925–2935.
Tyagi, A., Ryme, J., Brodin, D., Ostlund Farrants, A.K., Visa, N., 2009. SWI/SNF associates with nascent pre-mRNPs and regulates alternative pre-mRNA processing. PLoS Genet. 5, e1000470.
Ulicna, L., Kalendova, A., Kalasova, I., Vacik, T., Hozak, P., 2018a. PIP2 epigenetically represses rRNA genes transcription interacting with PHF8. Biochim. Biophys. Acta 1863, 266–275.

Ulicna, L., Paprckova, D., Faberova, V., Hozak, P., 2018b. Phospholipids and inositol phosphates linked to the epigenome. Histochem. Cell Biol. 150, 245–253.

Vann, L.R., Wooding, F.B., Irvine, R.F., Divecha, N., 1997. Metabolism and possible compartmentalization of inositol lipids in isolated rat-liver nuclei. Biochem. J. 327(Pt 2), 569–576.

Verstraeten, V.L., Broers, J.L., Ramaekers, F.C., van Steensel, M.A., 2007. The nuclear envelope, a key structure in cellular integrity and gene expression. Curr. Med. Chem. 14, 1231–1248.

Vintermist, A., Bohm, S., Sadeghifar, F., Louvet, E., Mansen, A., Percipalle, P., Ostlund Farrants, A.K., 2011. The chromatin remodelling complex B-WICH changes thechromatin structure and recruits histone acetyl-transferases to active rRNA genes. PLoS One 6, e19184.

Vlassov, A., Khvorova, A., Yarus, M., 2001. Binding and disruption of phospholipid bilayers by supramolecular RNA complexes. Proc. Natl. Acad. Sci. U. S. A. 98,7706–7711.

Vlcek, S., Foisner, R., 2007a. Lamins and lamin-associated proteins in aging and disease. Curr. Opin. Cell Biol. 19, 298–304.

Vlcek, S., Foisner, R., 2007b. A-type lamin networks in light of laminopathic diseases. Biochim. Biophys. Acta 1773, 661–674.

Waldholm, J., Wang, Z., Brodin, D., Tyagi, A., Yu, S., Theopold, U., Farrants, A.K., Visa, N., 2011. SWI/SNF regulates the alternative processing of a specific subset ofpre-mRNAs in Drosophila melanogaster. BMC Mol. Biol. 12, 46.

Watt, S.A., Kular, G., Fleming, I.N., Downes, C.P., Lucocq, J.M., 2002. Subcellular localization of phosphatidylinositol 4,5-bisphosphate using the pleckstrin homologydomain of phospholipase C delta1. Biochem. J. 363, 657–666.

Weber, S.C., Brangwynne, C.P., 2012. Getting RNA and protein in phase. Cell 149, 1188–1191.

Yildirim, S., Castano, E., Sobol, M., Philimonenko, V.V., Dzijak, R., Venit, T., Hozak, P., 2013. Involvement of phosphatidylinositol 4,5-bisphosphate in RNA poly-merase I transcription. J. Cell Sci. 126, 2730–2739.

Zhao, K., Wang, W., Rando, O.J., Xue, Y., Swiderek, K., Kuo, A., Crabtree, G.R., 1998. Rapid and phosphoinositol-dependent binding of the SWI/SNF-like BAF complex to chromatin after T lymphocyte receptor signaling. Cell 95, 625–636.